PhD degree in Molecular Medicine (curriculum in Molecular Oncology)

European School of Molecular Medicine (SEMM),

University of Milan and University of Naples "Federico II"

Settore disciplinare: BIO/11

The role of ATM in the regulation of cell mechanics

Giulia Bastianello

IFOM, Milan

Matricola n. R10325

Supervisor: Prof. Marco Foiani

IFOM, Milan

Added Supervisor: Dr. Hiroshi Arakawa

IFOM, Milan

Anno accademico 2015-2016

TABLE OF CONTENTS

1. ABSTRACT 12

2. INTRODUCTION 13

2.1 Genome integrity and DNA damage response (DDR). 13

2.2 The DSB repair cascade: the canonical activation of ATM. 17

2.3 When ATM is defective: the Ataxia-telangiectasia disease. 22

2.4 Beyond the genomic challenge: alternative mechanisms of ATM activation and its role outside the nuclear envelope. 26

2.4.1 Non-canonical substrates of ATM activation. 26

2.4.2 Non-nuclear functions of ATM. 28

2.5 ATM as a member of the PIKK family. 31

2.6 PIKKs and mechanical stress. 35

2.7 A novel connection between DDR and cytoskeleton. 39

2.7.1 DNA damage and DDR factors influence the cytoskeleton. 39

2.7.2 Cytoskeleton influences the DNA damage response. 42

2.7.3 Role of cell mechanics in cell migration and tools to study the mechanical properties of cells. 44

3. MATERIALS AND METHODS 47

3.1 Plasmids and Reagents 47

3.2 Cell culture 48

3.3 Lipofectamine transfection 49

3.4 Lentiviral transduction 50

3.5 Cell lysate preparation for western blot 51

3.6 Western blotting 53

3.7 BCA protein quantification 54
3.8 Protein immunoprecipitation (IP) 55
3.9 Coomassie Blue protein gel staining 57
3.10 Mass spectrometry 58
3.11 Electron microscopy (EM) sample preparation 59
3.12 Preparation of micro-channel devices used for 3D migration analysis 61
3.13 Immunofluorescence (IF) 65
3.14 Fluorescence resonance energy transfer (FRET) analysis 67
3.15 Atomic force microscopy (AFM) 68
3.16 Nuclear isolation for AFM analysis 69
3.17 Analysis of single cell migration by manual tracking 70
4. RESULTS 71
4.1 ATM influences cell plasticity measured by Atomic Force Microscopy (AFM). 72
4.2 ATM depletion alters the nuclear shape. 77
4.3 ATM depletion does not affect the expression of lamins in our experimental conditions. 80
4.4 ATM influences cell stiffness independently of nuclear plasticity. 83
4.5 Analysis of the ultrastructure of ATM defective cells by electron microscopy. 85
4.6 ATM inhibition impairs the movement and survival of cells during interstitial migration. 92
4.7 ATM is activated in cells migrating across constrictions. 99
4.9 ATM deficiency reduces the migration speed of single cells. 107

4.10 ATM physically interacts with several proteins involved in membrane trafficking and cytoskeletal regulation. 109
5. DISCUSSION 115
5.1 ATM regulates cell plasticity. 115
5.2 ATM influences 2D locomotion and interstitial migration 121
7. REFERENCES 128
8. APPENDIX 151
8.1 ABSTRACT 151
8.2 INTRODUCTION 152
8.3 MATERIALS AND METHODS 157
8.3.1 Cell culture and reverse genetics 157
8.3.2 Vectors 157
8.3.3 Cell lines 158
8.3.4 Sorting, cloning, and sequencing 159
8.3.5 Oligonucleotides 160
8.3.6 Western blotting 161
8.4 RESULTS 162
8.4.1 GFP reporter to assay DSB-induced Ig reversion 162
8.4.2 Ig reversion induced by a DSB or SSB 164
8.4.3 Gene conversion induced by AID 167
8.4.4 Gene conversion induced by a DSB 171
8.4.5 Non-gene conversion pathways induced by a DSB 175
8.5 DISCUSSION 177
8.6 REFERENCES 186

ABBREVIATIONS

DDR: DNA damage response

ROS: reactive oxygen species

UV: ultraviolet

SSB: single-strand breaks

DSB: double-strand breaks

ATM: Ataxia telangiectasia mutated

ATR: Ataxia telangiectasia and Rad3 related

RPA: replication protein A

CHK1: Checkpoint kinase 1

CHK2: Checkpoint kinase 2

CDK: cyclin-dependend kinase

DNA-PK: DNA-dependent protein kinase catalytic

MRN: Mre11-Rad50- Nbs1 complex

A-T: Ataxia Telangiectasia

NSCs: neural stem cells

iPS: induced pluripotent stem

ATMIN: ATM interactor

mTOR: mechanistic target of rapamycin

BID: BH3-interacting domain death agonist

PIKKs: phosphatidylinositol 3-kinase-related kinases

TRRAP: transformation/transcription domain associated protein

hSMG-1: human SMG-1

HEAT repeats: Huntingtin, elongation factor 3, a subunit of protein phosphatase 2A, PI3 kinase target of rapamycin 1

FAT: FRAP, ATM ad TRRAPP

FATC: FAT at C-terminus

LINC: Linker of Nucleoskeleton and Cytoskeleton

NE: nuclear envelope

CDT: Cytolethal distending toxins

EMC: extracellular matrix

NHEJ: non-homologous end joining

AFM: Atomic Force Microscopy

FBS: fetal bovine serum

NEAA: non essential amino acids

shRNA: short hairpin RNA

EDTA: Ethylenediaminetetraacetic acid

PBS: phosphate-buffered saline

RT : room temperature

WB: western blot

IP: immunoprecipitation

BCA: bicinchoninic acid assay

EM: electron microscopy

IR: ionizing radiation

PDSM: here polydim-ethylsiloxane

IF: immunofluorescence

ON: overnight

BF: bright-field

FRET: fluorescence resonance energy transfer

CFP: cyan fluorescent protein

YFP: yellow fluorescent protein

GFP: green fluorescent protein

FT: flow-through

AID: activation-induced cytidine deaminase

Ig: Immunoglobulin

CDR1: complementarity determining region 1

Fc: fragment crystallizable region

FACS: fluorescence activated cell sorting

Dox: doxycycline

DIVAC: diversification activator

FIGURES INDEX

Figure 1. Recruitment of ATM at DSBs and formation of DNA repair foci. 21

Figure 2. The ATM interaction network. 27

Figure 3. The cytoplasmic functions of ATM. 30

Figure 5. Model for the ATM three-dimensional protein structure. 34

Figure 6. The transmission of mechanical forces from the extracellular matrix to the nucleus. 36

Figure 7. Example of a silicon wafer used to produce PDMS mold of micro-channels. 61

Figure 8. Example of PDMS mold bonded to chamber glass and structure of channels. 64

Figure 9. Atomic force microscopy (AFM) analysis of cell stiffness in ATM defective cells. 75

Figure 10. AFM measurements of primary fibroblasts derived from healthy individual and A-T patient. 76

Figure 11. Analysis of nuclear shape in shATM HeLa cells. 79

Figure 12. ATM inhibition or depletion does not significantly affect lamin B1 and lamin A/C protein levels in our conditions. 82

Figure 13. The increased stiffness observed in ATMi-treated cells and ATM KO cells is not due to the nucleus. 84

Figure 14a. EM analysis of the morphology of HeLa shATM cells. 88

Figure 14b. EM analysis of the morphology of U2OS shATM cells. 90

Figure 15. The EM cellular ultrastructure of A-T fibroblasts. 91

Figure 16. Accumulation of actin stress fibers in HeLa shATM and A-T fibroblasts. 91
Figure 17. Description of microchannel devices used for 3D migration analysis and cell seeding process. 94
Figure 18. Caffeine treatment impairs movement and survival of HeLa cells during interstitial migration. 95
Figure 19. ATM is required for cell movement and survival during interstitial migration. 98
Figure 20. Schematic representations of the cytoplasmic and H2B-fused ATM reporters (images adapted from Johnson et al., 2007). 100
Figure 21. ATM is activated during interstitial migration (H2B-fused ATM reporter). 102
Figure 22. ATM is activated during interstitial migration (Cytoplasmic ATM reporter). 103
Figure 23. ATMi-induced cell death during 3D migration is not associated to a specific cell cycle phase. 106
Figure 24. ATM depletion affects the 2D migration of single cells. 108
Figure 25. Description of the experimental conditions used for ATM immunoprecipitation and mass spectrometry analysis of ATM physical interactors. 111
Figure 26. Mass spectrometry analysis of ATM physical interactions in control and IR-treated HeLa cells. 112
Figure 28. Ig reversion assay to analyze DSB repair in the rearranged immunoglobulin light chain gene. 163

Figure 29. Plasmid maps of the Tet-On 3G expression vector and the Tet-inducible I-SceI expressing vector. 164
Figure 30. Analysis of Ig reversion induced by AID, DSB and SSB. 166
Figure 31. AID-induced gene conversion at the VJ-GFP reporter. 169
Figure 32. Sequence analysis of VJ-GFP reporter in AID knockout cells. 170
Figure 33. Summary of AID-induced DNA repair pathways. 170
Figure 34. DSB-induced gene conversion. 173
Figure 35. Sequence analysis of the rearranged Ig heavy chain locus. 174
Figure 36. Successive gene conversion events caused by a single DSB. 175
Figure 37. Non-gene conversion pathways induced by a DSB. 176
Figure 38. Summary of the DNA repair pathways triggered by AID or a DSB at the Ig light chain locus. 177
Figure 39. Models for successive immunoglobulin gene conversion and DSB induced gene conversion. 185

TABLES INDEX

Table 1. DDR mechanisms. (Adapted from S.P. Jackson and J.Bartek, 2009) 14
Table 2. Mutant ATM mouse models. 25
Table 3. ATM interactors involved in the regulation of cytoskeleton and cell structure. 114

1. ABSTRACT

The ATM (Ataxia-telangiectasia mutated) kinase is one of the major players of the DNA damage response and its mutation causes the development of the Ataxia-telangiectasia genetic disorder (A-T). ATM belongs to the family of phosphatidylinositol 3-kinase-related kinases, which also includes TRRAP, SMG1, ATR, DNA-PK and mTOR. ATM, ATR and DNA-PK collaborate to preserve genome integrity in the face of DNA double strand breaks (ATM, DNA-PK) and replication stress (ATR). Recent observations are expanding the roles of these kinases outside the nucleus. Accordingly, ATM and ATR are activated in the absence of DNA damage by multiple stress conditions. Our group previously showed that ATR is activated by mechanical stress and localizes to the nuclear envelope; moreover, recent unpublished observations in our lab suggest that ATR influences cell mechanics regulating nuclear plasticity. Here we investigate the function of ATM in relation to cell mechanics using a variety of techniques to study the mechanical properties of the cells and their ability to migrate across constrictions. We found that ATM depletion increases cell stiffness and impairs cell survival during interstitial migration. Moreover, ATM is activated in cells subjected to nuclear deformation during the squeezing across constrictions in 3D migration. By mass spectrometry analysis we identified a plethora of proteins involved in the regulation of cytoskeleton and cell structure that interact with ATM, many of which are subjected to future investigations. Altogether these observations suggest that ATM plays a role in the control of cell plasticity and migration, possibly through the regulation of cytoskeletal components.

2. INTRODUCTION

2.1 Genome integrity and DNA damage response (DDR).

The DNA damage response (DDR) is an intricate network of signaling cascades that cells evolved to protect their genome against endogenous and environmental agents, which constantly attack the DNA.

Cells of the human body have to deal with tens of thousands of DNA lesions on a daily basis mainly arising during physiological processes such as DNA replication, hydrolytic reactions, non-enzymatic DNA methylation and generation of reactive oxygen species (ROS). Moreover, several environmental factors contribute to genomic insults: UV light, ionizing radiation, exposure to natural or manmade radioisotopes, tobacco smoking (Jackson & Bartek, 2009; Lindahl & Barnes, 2000; Valko et al, 2006; Wogan et al, 2004).

The outcome of these damaging agents is the introduction of lesions in DNA molecules mainly in the form of single-strand breaks (SSB) or double-strand breaks (DSB). The DSBs are less frequent than other types of lesions but are the most dangerous and difficult to repair (Harper & Elledge, 2007; Khanna & Jackson, 2001). Cells exploit multiple repair systems to efficiently resolve different types of lesions comprehensively called the DDR, which are summarized in table1.

Table 1 DDR mechanisms and components

DDR mechanism	Prime lesions acted upon	Key protein components
Direct lesion reversal	O^6 alkylguanine	O^6-methylguanine methyltransferase
Mismatch repair	DNA mismatches and insertion/deletion loops arising from DNA replication	Sensors MSH 2–MSH 6 and MSH 2–MSH 3 plus MLH 1–PMS 2, MLH 1–PMS 1, PLH 1–MLH 3, EXO 1, polymerases d and e, PCNA, RFC, RPA, ligase I
Base excision repair and SSB repair	Abnormal DNA bases, simple base adducts, SSBs generated as base-excision repair intermediates by oxidative damage or by abortive topoisomerase I activity	DNA glycosylases (sensors), APE 1 endonuclease, DNA polymerases (b, d, e) and associated factors, flap endonuclease FEN1, ligase I or ligase III. SSB repair can also involve polymerase b lyase activity, XRCC 1, PARP 1, PARP 2, polynucleotide kinase and aprataxin.
Nucleotide excision repair (NER)	Lesions that disrupt the DNA double helix, such as bulky base adducts and ultraviolet photo-products	Sensors elongating RNA polymerase, XPC-HR 23B and DDB1/2, plus XPA, XPE, XPF/ERCC 1, XPG, CSA, CSB, TFIIH (containing helicases XPB and XPD), DNA polymerases including polymerase k and associated factors, PCNA, RPA, ligase I and III
Trans-lesion bypass mechanisms	Base damage blocking replication-fork progression	'Error-prone' DNA polymerases, including polymerases g, i, k, REV 3 and REV 1; plus associated factors
Non-homologous end-joining (NHEJ)	Radiation- or chemically-induced DSBs plus V(D)J and class-switch recombination intermediates	Sensors Ku and DNA-PKcs plus XRCC 4, XLF/Cernunnos and ligase IV. Can also use the MRE 11–RAD 50–NBS 1 complex, Artemis nuclease, polynucleotide kinase, aprataxin and polymerases mand l .
Homologous recombination (HR)	DSBs, stalled replication forks, inter-strand DNA crosslinks and sites of meiotic recombination and abortive topoisomerase II action	RAD 51, RAD 51-related proteins (XRCC 2, XRCC 3, RAD 51B, RAD 51C, RAD 51D, DMC 1), RAD 52, RAD 54, BRCA 2, RPA, FEN 1, DNA polymerase and associated factors. Promoted by MRN, CtIP, BRCA 1 and the ATM signalling pathway.
Fanconi anaemia (FANC) pathway	Inter-strand DNA crosslinks	FANCA, FANCC, FANCD 1/BRCA 2, FANCD 2, FANCE, FANCF, FANCG, FANCI, FANCJ, FANCL, FANCM, FANCN plus factors including PALB 2 and HR factors
ATM-mediated DDR signalling	DSBs	ATM, MRN and CHK 2. Promoted by mediator proteins such as MDC1, 53BP1 MCPH 1/BRIT 1, and by ubiquitin ligases RNF8, RNF 168/RIDDLIN and BRCA 1.
ATR-mediated DDR signalling	ssDNA, resected DSBs	Sensors ATR, ATRIP and RPA plus the RAD 9–RAD 1–HUS 1 (9-1-1) complex, RAD 17 (RFC 1-like) and CHK 1. Promoted by MRN, CtIP and mediator proteins such as TOPBP 1, Claspin, MCPH 1/BRIT 1 and BRCA 1.

Table 1. DDR mechanisms. (Adapted from S.P. Jackson and J.Bartek, 2009)

Two major players of the DDR are the ATM (Ataxia-Telangiectasia mutated) and ATR (Ataxia-Telangiectasia and Rad3 related) kinases. ATM is recruited to and activated by DSBs while ATR responds to replication protein A (RPA)-coated ssDNA lesions that arise during DNA replication stress or after DBSs resection (Andegeko et al, 2001; Awasthi et al, 2016; Canman & Lim, 1998; Cimprich & Cortez, 2008; Shiloh, 2003; Zou & Elledge, 2003).

These kinases act as upstream sensors of DNA damage and phosphorylate many targets including other protein kinases, causing amplification of the signal. Two of the most characterized targets of ATR/ATM are the CHK1 (Checkpoint kinase 1) and CHK2 (Checkpoint kinase 2) kinases (Bartek et al, 2001; Matsuoka et al, 2000; Zhao & Piwnica-Worms, 2001). As their name suggests, CHK1 and CHK2 collaborate with ATR/ATM in the control of "cell-cycle checkpoints" by

inhibiting the cyclin-dependent kinase (CDK) and therefore slowing-down or arrest the cell cycle progression while cells repair damaged DNA. According to the cell cycle phase in which the damage occurred, cells can arrest at G1-S transition, intra-S or G2-M transition. These checkpoints ensure that the cells have time to repair the lesions before entering into the next cell cycle phase (Kastan & Bartek, 2004).

In the meantime, ATM and ATR also phosphorylate a cascade of protein to facilitate the repair: induction of repair factors by transcriptional or post-transcriptional regulation, recruitment of repair factors to the damage, recruitment of chromatin remodeling proteins to facilitate the repair, stabilization of the replisome machinery and inhibition of origin firing in case of replication stress and intra-S checkpoint arrest (Huen & Chen, 2008; Matsuoka et al, 2007). When the damage cannot be repaired, the persistent activation of DDR results in apoptosis or senescence. Therefore, the DDR works to guarantee intact genomic information and to eliminate damaged cells that can become potential tumor cells.

Moreover the DDR pathways are involved in many physiological processes that naturally involve the formation of DNA lesions. These processes include the generation of immune-receptor diversities through V(D)J recombination, class-switch recombination and somatic hyper-mutation (Bassing & Alt, 2004); the meiotic recombination for the production of gametes (Richardson et al, 2004) the maintenance of telomere homeostasis (Longhese, 2008; Reaper et al, 2004) and the interactions between host DNA and viral pathogens (Lilley et al, 2007).

Therefore, it is not surprising that alterations in the DDR pathway are associated with multiple severe human diseases.

A defective DDR predisposes to cancer development contributing to the "mutator phenotype" and many DDR genes are mutated in human cancers (Halazonetis et al, 2008). Although recent pieces of evidence suggest that DDR proteins might have a tumor-promoting role in later stages of cancer development, they act as an anti-cancer barrier in a nascent tumor (Bartkova et al, 2005; Gorgoulis et al, 2005). Several immunodeficiency syndromes are related to mutations in DDR proteins (Ataxia-Telangiectasia (A-T), Nijmegen breakage syndrome (NBS)) together with infertility (Matzuk & Lamb, 2008) and metabolic syndrome (Kastan, 2008; Schneider et al, 2006). The accumulation of DNA damage is associated with aging, neurodegeneration, stem-cell dysfunction and cardiovascular diseases (Kulkarni et al, 2008; Mahmoudi et al, 2006; Schumacher et al, 2009; Sharpless & DePinho, 2007).

The strong impact of DDR on human health is the reason why researchers put so many efforts to understand its mechanisms of action, however, still many questions remain to be addressed especially considering the incredible amount of protein targets that DDR can regulate inside and outside the nucleus (Matsuoka et al, 2007). Recent studies showed how these kinases can affect several cellular processes in addition to those related to DNA repair, and a better understanding of such processes might open new possibilities of therapy for the patients suffering from diseases associated with defective DDR.

2.2 The DSB repair cascade: the canonical activation of ATM.

ATM is one of the key factors of the DDR and it regulates the cellular response to DSBs (together with DNA-PK). When a DSB occurs in a cell, several proteins including ATM are recruited to the site of damage within few minutes.

The recruitment of ATM at the site of damage requires the MRN complex (Mre11-Rad50- Nbs1) and is mediated by the physical interaction between ATM and NBS1 (Lee & Paull, 2005; Uziel et al, 2003; You et al, 2005).

In vitro studies demonstrated that MRN is necessary to stimulate the kinase activity of ATM in the presence of DNA (Lee & Paull, 2005).

The MRN complex is recruited to DSBs where MRE11 forms a hetero tetramer with RAD50 tethering the broken DNA ends (figure1). The association of RAD50 to MRE11 activates the 3'-5' exonuclease activity of MRE11 causing the processing of the break (Costanzo et al, 2004; de Jager et al, 2001; Jazayeri et al, 2008; Paull & Gellert, 1998).

Several studies have proposed that ATM is recruited to the DSB in the form of an inactive dimer; the complete activation of ATM requires auto-phosphorylation at multiple sites and dimer dissociation. This was first demonstrated from Bakkenist and Kastan in the work of 2003 where they reported the auto-phosphorylation of ATM at serine 1981 in response to ionizing radiation (IR).

Kozlov et al. validated this site and included additional sites of auto-phosphorylation that are important for ATM activation (S367, S1893, S2996)(Kozlov et al, 2003; Kozlov et al, 2006).

The relevance of auto-phosphorylation suggested that phosphatases might be

involved in the regulation of ATM. Indeed, Goodarzi and coworkers showed that PP2A is required to maintain ATM in an inactive conformation in the absence of DNA damage (figure 1) (Goodarzi et al, 2007). PP2A was found to interact with ATM in a yeast two-hybrid screening in unirradiated cells, while this interaction was lost upon irradiation.

Differently from PP2A, the phosphatase PP5 was also suggested to regulate ATM activity in a positive manner by stimulating ATM activation (Ali et al, 2004). The phosphatase WIP1 (Wild-type p53-induced phosphatase-1) has also an inhibitory effect on ATM in unirradiated cells (Shreeram et al, 2006). Other post-translational modifications like acetylation, poly(ADP-ribosyl)ation and methylation are involved in ATM activation and regulation of downstream factors, these are intensely reviewed in Guleria and Chandna, 2016 (Guleria & Chandna, 2016).

When ATM is recruited to the DSB it phosphorylates the histone variant H2AX at serine 139 (figure 1), this phosphorylated form, named γ-H2AX, accumulates at the break sites in few minutes (Rogakou et al, 1998). γ-H2AX serves for the recruitment of MDC1 (Mediator of DNA Damage Checkpoint Protein 1). MDC1 directly binds to the phosphorylated H2AX (Stucki et al, 2005), interacts with the MRN complex and helps to retain ATM at the DSB, this increases the phosphorylation of H2AX around the break (Savic et al, 2009; Stucki et al, 2005). H2AX and MDC1 work as scaffolds for the recruitment of several other proteins: RAP80-BRCA1, 53BP1, RNF8, UBC-13, RNF168, FANC2D and SMC1 (Doil et al, 2009; Kolas et al, 2007; Mailand et al, 2007; Plans et al, 2006).

These proteins form the DNA repair center surrounding the DSB and ATM phosphorylates most of these factors (figure 1).

ATM also phosphorylates other effector molecules involved in the cell-cycle checkpoints in order to arrest the cell cycle in the presence of DNA damage.

The G1-S checkpoint requires phosphorylation of CHK2 by ATM, CHK2 thus phosphorylates and inactivates the phosphatase Cdc25A (Mailand & Diffley, 2005). Cdc25A inhibition results in inactivation of the Cdk2/cyclin-E complex due to phosphorylation of Cdk2.

Cdk2/cyclin-E is responsible for the G1-S transition and its inhibition causes G1-S arrest. In later steps, a p53-dependent G1-S arrest is also induced by ATM, which in turn phosphorylates p53 at serine 15 (directly) and serine 20 (through CHK2) (Cheng et al, 2009; Hirao et al, 2000; Saito et al, 2002; Schiebe et al, 2000). These events cause the dissociation of the Mdm2-p53 complex, together with the phosphorylation of Mdm2 by ATM (Schon et al, 2002). P53 is stabilized and mediates the G1-S arrest through transcriptional regulation of several genes, including the overexpression of p21, an inhibitor of Cdk2.

When the damage occurs in S phase, ATM phosphorylates multiple substrates including BRCA1, FANC2D, NBS1 and SMC1, required for the S-phase arrest together with the already-described inactivation of Cdc25A by CHK2 (Kitagawa et al, 2004; Lim et al, 2000; Taniguchi et al, 2002; Xu et al, 2001).

The G2-M arrest mediated by ATM prevents entry in mitosis with unrepaired DNA.

This checkpoint involves BRCA1 at several levels (Xu et al, 2001; Yarden et al, 2002; Yu et al, 2006), p53, p21 (Flatt et al, 2000; Innocente et al, 1999), and CHK2. All these effectors are regulated by ATM through phosphorylation and cause the inhibition of Cdc25C (Melixetian et al, 2009). Cdc25C is the

phosphatase that in normal conditions activates Cdc2 by removing the inhibitory phosphate at tyrosine 15 and stimulates the formation of the Cdc2-cyclin B complex required to enter in mitosis.

The cell cycle arrest is maintained until the DNA damage is successfully repaired and the termination of the DDR response involves deubiquitination of the chromatin and the phosphatase WIP1, that de-phosphorylates γ-H2AX (Moon et al, 2010; Shao et al, 2009).

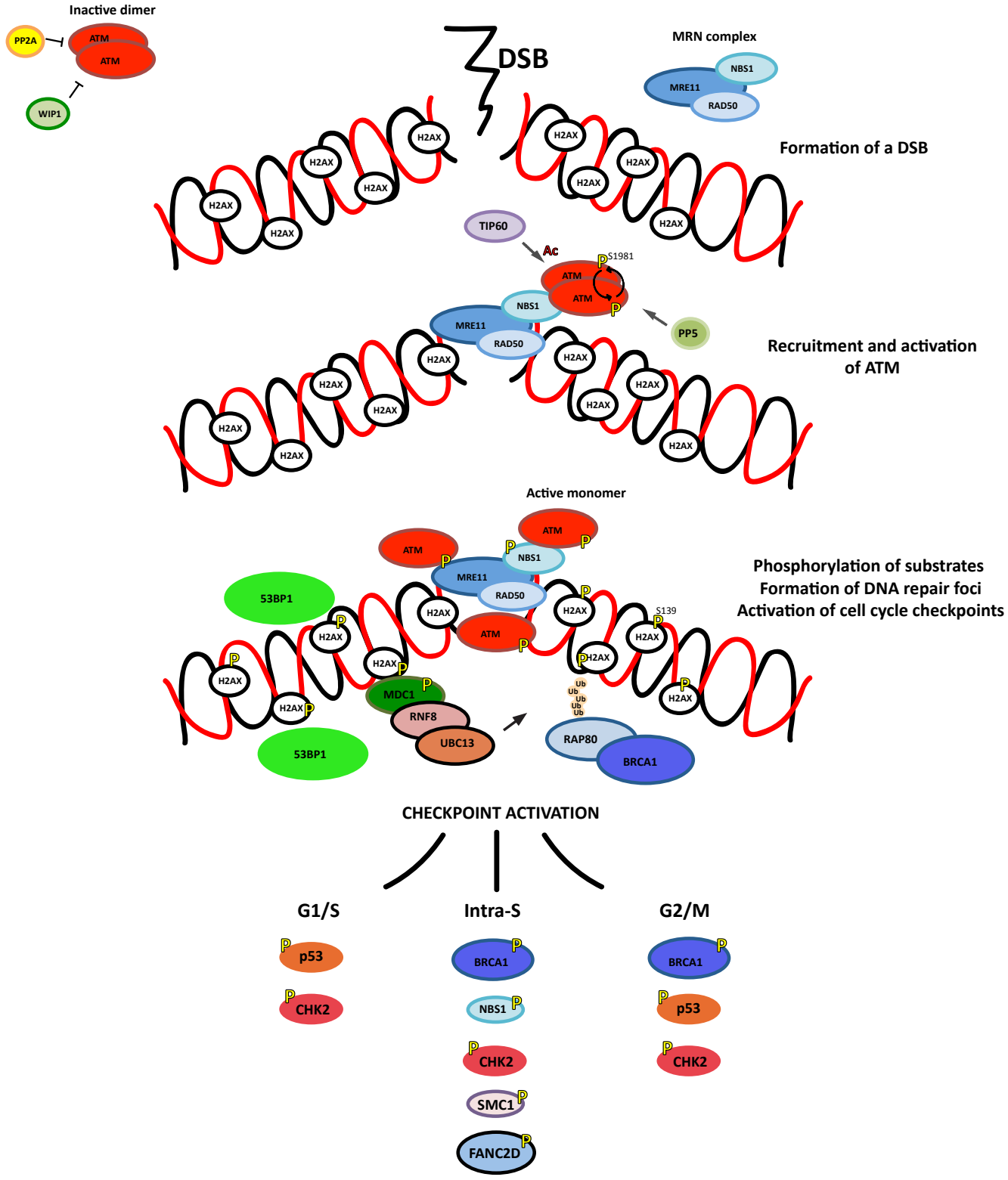


Figure 1. Recruitment of ATM at DSBs and formation of DNA repair foci.

2.3 When ATM is defective: the Ataxia-telangiectasia disease.

In 1995 the group of Yosef Shiloh identified ATM as the single gene product responsible for the onset of Ataxia-telangiectasia disease (A-T) (Savitsky et al, 1995).

Ataxia-telangiectasia is an autosomal recessive neurodegenerative disorder characterized by multisystem abnormalities that include progressive cerebellar ataxia, oculo-cutaneous telangiectasia, susceptibility to bronchopulmonary disease, and high incidence of lymphoid tumors.

Other clinical aspects of the disease include general immunodeficiency, thymic and gonadal degeneration, the progressive apraxia of eye movements, insulin-resistant diabetes, clinical and cellular radio-sensitivity, cell-cycle checkpoint defects and chromosomal instability (Lavin, 2008).

The first report of A-T dates back to 1926 (Syllaba et al., 1926) and only later in 1957 A-T was defined as a familial syndrome (Boder & Sedgwick, 1958).

The patients affected by A-T carry truncating mutations or splice-site mutations that give rise to shorter, unstable ATM proteins. A-T patients have a life span between 20 and 30 years (Crawford et al, 2006) and the major causes of death are lymphoreticular malignancies or recurrent sinopulmonary infections. The occurrence of the disease happens in between 1/4000 and 1/100000 persons worldwide. The absence of a functional DSB response and the inability to activate the cell cycle checkpoints is responsible for many defects found in A-T. Indeed, mutations in components of the MRE11-RAD50-NBS1 (MRN) complex, which is known to associate with ATM and cause its activation at DSB sites, cause the

Nijmegen breakage syndrome (NBS1 mutants) and the A-T-like disorder (MRE11 mutants), two genetic diseases that share similar phenotypes with A-T (Andegeko et al, 2001; Frappart et al, 2005; Stewart et al, 1999; Varon et al, 1998). The defect of DSB repair certainly explains the hypersensitivity to ionizing radiation, the cancer predisposition and chromosomal instability phenotypes of the patients (Gotoff et al, 1967; Stewart et al, 1999; Swift et al, 1991; Taylor et al, 1975). Moreover, ATM has been implicated in lymphocyte development at several levels.

ATM plays an important role in the resolution of physiological DSBs that arise during V(D)J recombination and class-switch recombination reactions that take place in differentiating B and T lymphocytes. ATM has been shown to accumulate at V(D)J- induced DSBs (Perkins et al, 2002) and to maintain the expression of T cell receptor during recombination (Matei et al, 2007). These data suggest that the defects of lymphocyte development found in A-T patients are also associated to the DSB repair function of ATM. As a consequence, A-T patients suffer from immunodeficiency, are susceptible to continuous infections and have a high probability of lymphomas.

Some of the patients affected by Ataxia-telangiectasia also suffer from insulin-resistant diabetes (Bar et al, 1978; Schalch et al, 1970).

This phenotype resembles the metabolic syndrome and ATM was indeed found to participate in insulin-mediated pathways (Halaby et al, 2008; Jeong et al, 2010; Viniegra et al, 2005; Yang & Kastan, 2000).

It was shown that activation of ATM by chloroquine treatment in ApoE-/- mice could improve their glucose tolerance. Furthermore, the deletion of ATM in these mice accentuated their phenotype (Schneider et al, 2006), supporting the

importance of ATM in the insulin pathway.

This aspect of the disease is less connected with the genome surveillance role of ATM pointing to an additional function of the kinase in control of cell homeostasis.

The most severe symptom of A-T is the cerebellar degeneration associated with the progressive loss of Purkinje cells that causes problems of movement coordination (Shiloh & Lederman, 2016). The cause of the neurodegeneration is however still being debated and over the past decades has been subject of intense research. Current hypotheses include the possibility that neurodegeneration might be linked to a defective response to DNA damage in pre- and post-mitotic neurons (Lee & Paull, 2007) and an alternative scenario where ATM involvement in cytoplasmic pathways could be the cause of cerebellar atrophy (Hoche et al, 2012). Supporting the second hypothesis, ATM was found to be predominantly cytoplasmic in neuronal cells (Barlow et al, 2000; Boehrs et al, 2007) where it interacts with synaptic proteins as VAMP2 and Synapsin-1 (Li et al, 2009). Recently this interaction has been proposed to regulate presynaptic vesicles in mouse neurons (Vail et al, 2016).

Additionally, increased ROS levels in A-T patients have been associated to neurodegeneration (Barzilai et al, 2008; Barzilai et al, 2002; Liu et al, 2005). More recently the nuclear accumulation of HDAC4 in ATM-deficient cells was proposed to lead to neurodegeneration by altering the expression of neuronal genes (Li et al, 2012).

In conclusion, several factors seem to contribute to A-T neurodegeneration and it is possible that both nuclear and cytoplasmic functions of ATM might be involved and therefore it is important to investigate in both localization-mediated roles of ATM.

The challenges in studying neurodegeneration of A-T are also due to the lack of an appropriate model system able to recapitulate the phenotype in vitro or in vivo. Most of the studies on A-T have been performed using human cell lines, patient-derived cell lines and ATM mutant mouse models (comprehensive listed in table 2) (Lavin, 2013).

GENETIC BACKGROUND	MUTANT	TUMORS	RADIO-SENSITIVITY	APOPTOSIS RESISTANCE	NEUROLOGICAL DEFECT	NEURO-DEGENERATION	REFERENCES
129SvEv/Bleck Swiss	Atm−/−	YES	YES	ND	YES	NO	Barlow et al., 1996
C57Bl.6	Atm−/−	YES	YES	thymocytes	ND	NO	Xu and Baltimore, 1996
C57Bl.6	Atm−/−	ND	ND	ND	ND	neurons	Kuljis et al., 1997
129/svj C57 Bl/6	Atm−/−	ND	YES	Developing CNS	ND	NO	Herzog et al., 1998
129SVEV/Black Swiss	Atm−/−	ND	YES	ND	ND	ND	Elson et al., 1996
129 SV/C57B6	Atmy/y	YES	ND	ND	YES	some pathogenic changes	Borghesani et al., 2000
129/svj B57 Bl/6	AtmSRI/SRI	YES	YES	ND	YES	NO	Spring et al., 2001

Table 2. Mutant ATM mouse models.

Although these models have provided a large amount of information about ATM function, localization and signaling, they failed to recapitulate the neurodegeneration phenotype completely. Neurological and neurobehavioural abnormalities were described in some of the models but most of them do not develop ataxia or neurodegeneration.

Recent advances in stem cell biology are providing an alternative solution to this problem. It is now possible to obtain genetically stable neural stem cells (NCSs)

derived from mammalian brain that can be later differentiated into neurons, astrocytes and oligodendrocytes. ATM depletion in human NCSs has been achieved (Carlessi et al, 2009). Moreover different groups have now succeeded to generate human induced pluripotent stem (iPS) cells by reprogramming fibroblasts and other somatic cells. This technique allows the direct reprogramming of A-T patient fibroblasts into iPS cells and finally neurons (Carlessi et al, 2013; Nayler et al, 2012).

These tools will offer the possibility to study the effect of ATM depletion in human neurons and will certainly help in understanding the function of ATM in neurons.

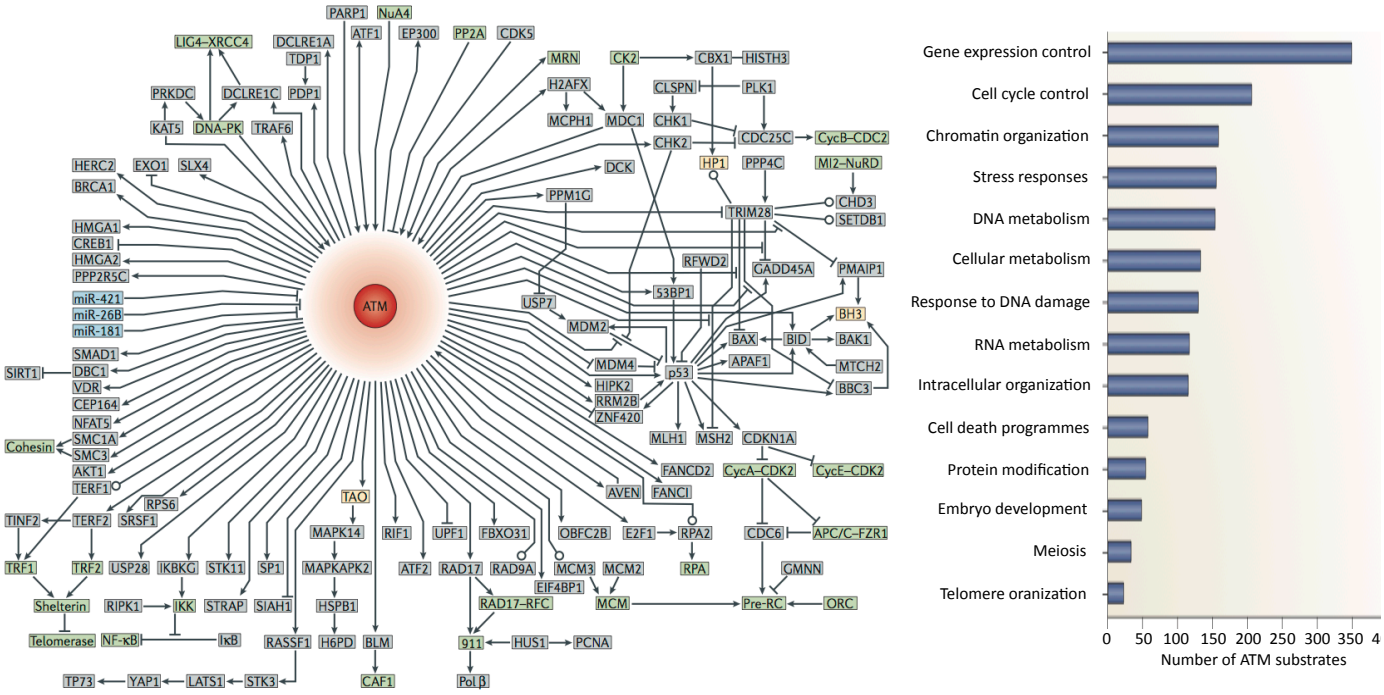
2.4 Beyond the genomic challenge: alternative mechanisms of ATM activation and its role outside the nuclear envelope.

2.4.1 Non-canonical substrates of ATM activation.

Despite the main function of ATM in DSB repair, the variety of cellular dys-functions observed in ATM-deficient cells suggested that this kinase could play important roles in the regulation of cytoplasmic processes as well.

In support of this hypothesis, different studies described the presence of fractions of ATM in the cytoplasm (Kim et al, 2010; Li et al, 2009; Lim et al, 1998; Watters et al, 1999). Around the same timeline, large proteomic screenings carried out by several groups unveiled hundreds of putative ATM substrates. Interestingly all these screens identified a plethora of cytoplasmic factors

(Bensimon et al, 2010; Kozlov et al, 2016; Matsuoka et al, 2007; Mu et al, 2007; Siddoway et al, 2014) (a summary map of the ATM targets is shown in figure2).



(Adapted from Shiloh and Ziv, 2013)

Figure 2. The ATM interaction network.
A summary of ATM functional interactions is depicted on the left panel. Grey: proteins, blue: microRNAs, green: protein complexes, yellow: protein families. Arrows correspond to activation, T-shaped edges to inhibition, and open circles are other regulations that are not yet understood. On the right panel, the bar plot shows the functional classification of 1077 proteins that were found as putative ATM targets in multiple proteomic screenings (Matsuoka et al., 2007, Mu et al., 2007, Bensimon et al., 2010).

These findings prompted the investigation of possible DNA-damage independent mechanisms of ATM activation. ATM was found activated under hypoxia and hypertermia in the absence of DNA damage; these activations were independent of MRE11 as well (Bencokova et al, 2009; Hammond et al, 2007; Hunt et al, 2007).

In 2007, Axel Behrens and colleagues identified a novel pathway of ATM activation that depends on ATMIN (ATM interactor) (Kanu & Behrens, 2007).

ATMIN physically interacts with ATM and compete for NBS1 binding (Zhang et al, 2012). ATMIN is required for ATM activation in different stress conditions that do not cause DNA damage, such as hypotonic stress or chloroquine treatment.

Low levels of ATM activation have been described in relation to the mitotic spindle checkpoint; the Aurora B kinase targets ATM and causes it activation by auto-phosphorylation in an MRE11-independent manner. ATM then activates BUB1, an essential kinetochore protein of the spindle checkpoint (Yang et al, 2012).

Finally, ATM works also as a redox sensor; increased ROS levels have been shown to activate ATM without the need of MRN complex. This mechanism of activation is diverse from the canonical one, because in this conditions ATM becomes active in a dimer conformation. As a consequence of oxidation, disulphide bonds are formed between cysteine residues C2991 and generate an active dimer of ATM (Guo et al, 2010; Rotman & Shiloh, 1997a; Rotman & Shiloh, 1997b). Indeed the point mutant C2991L prevents ATM activation by ROS but not by DNA damage.

2.4.2 Non-nuclear functions of ATM.

ATM activity itself has been shown to influence many processes outside the nuclear envelope. A major consequence of ATM loss is the increased oxidative stress that was observed both in human and mouse models of A-T (Ditch & Paull, 2012; Rotman & Shiloh, 1997b).

ATM modulates the redox homeostasis in different ways. In response to genotoxic stress ATM was found to activate the enzyme glucose-6-phosphate dehydrogenase stimulating the pentose phosphate cycle and leading to the production of NADPH, which neutralizes ROS and thus protects the cell against oxidative stress (Cosentino et al, 2011). Moreover, in response to ROS, ATM activates a cascade of phosphorylation events involving LKB1, AMPK and TSC2 that ultimately inhibits mTORC1 (Alexander et al, 2010).

Recently, ATM kinase was proposed to play a role at peroxisomes. These organelles are responsible for the production of ROS as a consequence of fatty acid β-oxidation. ATM was found to localize at peroxisomes through the interaction with PEX5, one of the peroxisomes import receptors. Here ATM is activated by peroxisomal ROS and phosphorylates PEX5 at S141, this phosphorylation causes PEX5 ubiquitylation and binding to p62, a factor that target peroxisomes for pexophagy (Tripathi et al, 2016; Zhang et al, 2015). Thus ATM regulates peroxisomes homeostasis and this can affect the level of ROS in the cells.

Another cytoplasmic function of ATM is at the mitochondria. The mitochondrial connection was hypothesized when increased number of mitochondria and mitochondrial dysfunction were observed in ATM-deficient cells (Ambrose et al, 2007; Eaton et al, 2007). Later, a role of ATM in the regulation of mitophagy was proposed in mouse thymocytes (Valentin-Vega et al, 2012). Moreover, ATM has been found to phosphorylate BID (BH3-interacting domain death agonist), a factor required for the mitochondrial apoptotic programme (Zinkel et al, 2013).

Another organelle that might be affected by ATM function is the endosome, where ATM was found to localize in mouse neurons (Kuljis et al, 1999).

In response to DNA damage, ATM also regulates metabolic pathways such as ceramide bio-synthesis in the endoplasmic reticulum (Liao et al, 1999). ATM also stimulates protein synthesis in response to insulin by phosphorylation of 4EBP1 and consequent activation of eIF4E (Yang & Kastan, 2000). Insulin also causes the activation of AKT by ATM (Halaby et al, 2008; Viniegra et al, 2005).

Finally, different studies showed that the absence of ATM causes defects in calcium and potassium currents in human fibroblasts and mouse neurons (Chiesa et al, 2000; Famulski et al, 2003; Rhodes et al, 1998).

A summary of ATM-modulated cytoplasmic pathways is depicted in figure 3.

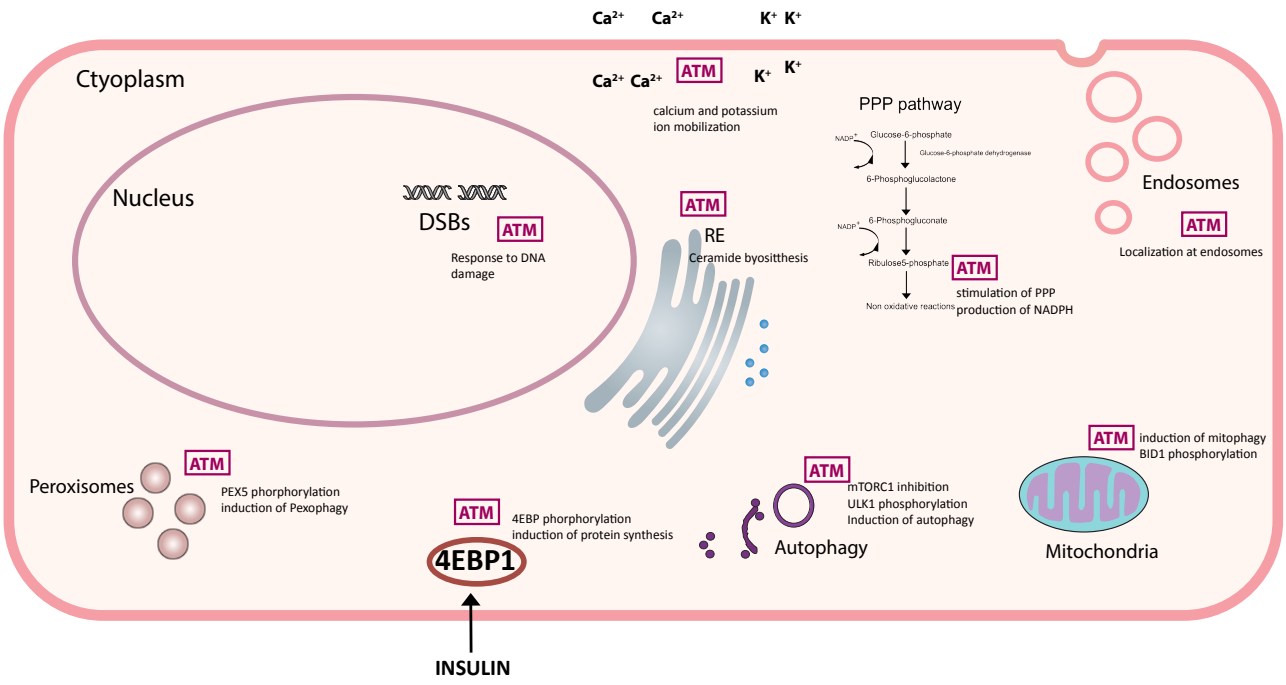


Figure 3. The cytoplasmic functions of ATM.
The image summarizes the documented cytoplasmic functions of ATM that have been discussed in this chapter.

2.5 ATM as a member of the PIKK family.

ATM is a large protein kinase of 370kDa composed of several functional domains. It belongs to the phosphatidylinositol 3-kinase- related kinase (PIKK) family of serine/threonine protein kinases, which include five additional members, namely, ATR, mTOR, hSMG-1, TRRAP and DNA-PK. This protein family was defined in the mid-1990s, and accounts for some of the most critical cell stress-sensors that safeguard the genetic information of cells and regulate metabolism in response to nutrients, oxygen and energy levels (Abraham, 2001; Abraham, 2004; Durocher & Jackson, 2001).

Interestingly all the PIKKs are giant proteins and share a very similar domain composition.

The N terminus is characterized by 40-54 HEAT repeats (Perry & Kleckner, 2003) and is considered to be a critical mediator of protein-protein interactions. The N terminus of ATM harbors the binding sites for NBS1 and ATMIN, factors required for ATM activation (Jazayeri et al, 2008; Kanu & Behrens, 2007; Lee & Paull, 2005; Zhang et al, 2012). Most of the auto-phosphorylation sites and other regulatory phosphorylation sites are also located at the N terminus (Kozlov et al, 2011; Tian et al, 2009; Yang et al, 2011). Moreover, this domain contains sites for chromatin interaction, nuclear localization signal, two sites for caspase 3 cleavage and a putative leucine zipper domain (Chen et al, 2003; Fernandes et al, 2005; Smith et al, 1999; Young et al, 2005).

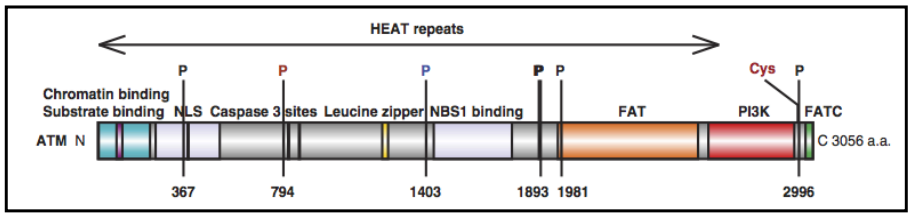
Following HEAT repeats, prior to catalytic domain, is the FAT domain (FRAP, ATM ad TRAPP) and spans approximately 500 amino acids (Bosotti et al, 2000).

The kinase domain identifies PIKKs because of the significant amino acid

sequence homology with the kinase domain of the PI-3 kinases, although PIKKs phosphorylate protein targets instead of lipids. With the exception of TRRAP, all six PIKKs have kinase activity. ATM, ATR, hSMG1-1 and DNA-PK phosphorylate preferentially on serine or threonine residues that are followed by a glutamine residue (SQ/TQ motifs). The kinase mTOR, instead, does not target SQ/TQ motifs with a strong preference; a specific consensus site for mTOR has not been identified yet.

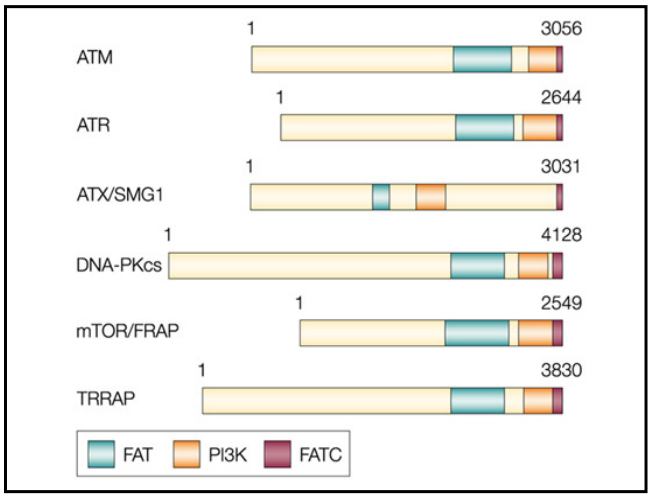
The fourth domain that characterizes PIKKs is positioned at the C terminus of the protein after the kinase domain and it is called the FACT domain (FAT at C-terminus). Schematic representations of ATM and the whole PIKK family are depicted in figure 4a and 4b.

a



(Adapted from Cremona and Behrens 2014)

b



(Adapted from Shiloh 2003)

Figure 4. Schematic representations of ATM and the PIKKs family.
a) The PIKKs common domains FAT, FATC and the kinase domain are represented on the linear amino acid sequence of ATM. ATM specific domains at the N terminus are indicated together with important phosphorylation sites (Cremona and Behrens, 2014). The serine residues 367, 1893, 1981 and 2996, are known auto-phosphorylation sites induced by IR. Colored lines outline important regions of the N terminus required for the interaction with NBS1, for caspase 3 cleavage and for the nuclear localization (NLS). The purple line marks the residues 91-97 that are required for the formation of nuclear ATM foci upon IR treatment. A putative leucine zipper domain is also shown in yellow.
b) The six members of the PIKK family are shown with the conserved motifs and protein size. Numbers indicate the total amino acid residues.

The large size of these proteins, (300 to 500 kDa), confers challenge for crystallization studies limiting our understanding of the three-dimensional structure and domain interactions. In 2013 Yang and colleagues, published the first high resolution structure of a truncated form of the PIKK mTOR bound to its subunit mLST8 (Yang et al, 2013), and more recently another group was able to solve the structure of the mTORC1 complex (mTOR bound to mLST8, raptor and FKBP) (Aylett et al, 2016).

The similar domain composition of PIKKs combined with low-resolution electron-microscopy models of the SMG-1, DNA-PK and ATM structures (Llorca et al, 2003; Melero et al, 2014; Sibanda et al, 2010) allowed the creation of a three-dimensional map of the domain organization starting from the crystal structure of mTOR. The model proposes that the FAT domain, made of helix-turn-helix repeats, wraps around the kinase domain and plays a role in its structural preservation (figure 5).

In ATM, the FAT domain is proposed to inhibit the kinase domain when ATM is in an inactive dimer conformation. The FAT domain of ATM harbors the site S1981 that is auto-phosphorylated upon ATM activation and this phosphorylation causes the dissociation of ATM dimers and the full activation of ATM (Bakkenist & Kastan, 2003).

The long N-terminal domain of PIKKs precedes the FAT domain and is composed of helical repeats forming an α-solenoid. This domain can assume different conformations and lengths among the PIKKs and in ATM it protrudes from the kinase domain a (Llorca et al, 2003). The α-solenoid is proposed to serve as a scaffold for protein-protein interactions in addition to regulation of the kinase activity of the protein.

Less is known about the function of the well-conserved FATC domain, it has been suggested that it might be involved in membrane localization of PIKKs, and isolated FATC peptides are hydrophobic and bind to membranes *in vitro* (De Cicco et al, 2015; Sommer et al, 2013).

A three-dimensional model of the structure of ATM is shown in figure 5 (Baretic & Williams, 2014).

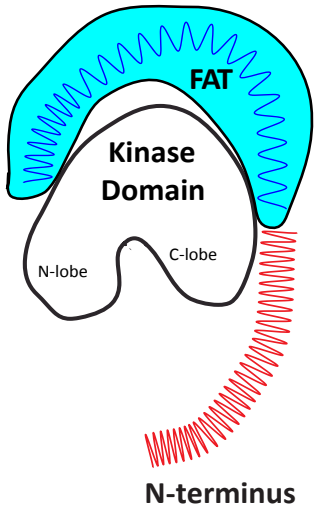


Figure 5. Model for the ATM three-dimensional protein structure.
The picture shows the predicted domain disposition of the FAT domain, the kinase domain and the N terminus. The FAT domain and the N-terminus are represented as spirals and the kinase domain is indicated. The image was modified from Baretic et al., 2014.

2.6 PIKKs and mechanical stress.

A recent discovery in our lab introduced a new connection between DDR and mechanical stress (Kumar et al, 2014).

In this study the authors showed that ATR activation can be triggered by mechanical stress at the nuclear envelope (Kumar et al, 2014). A fraction of ATR was found to localize at the nuclear envelope under physiological conditions and this fraction was significantly increased during prophase. ATR is normally distributed in the nucleoplasm where it responds to replication stress-induced RPA-coated ssDNA and activates the checkpoint to stabilize the replication forks and maintain genome integrity (Cimprich & Cortez, 2008; Zou & Elledge, 2003).

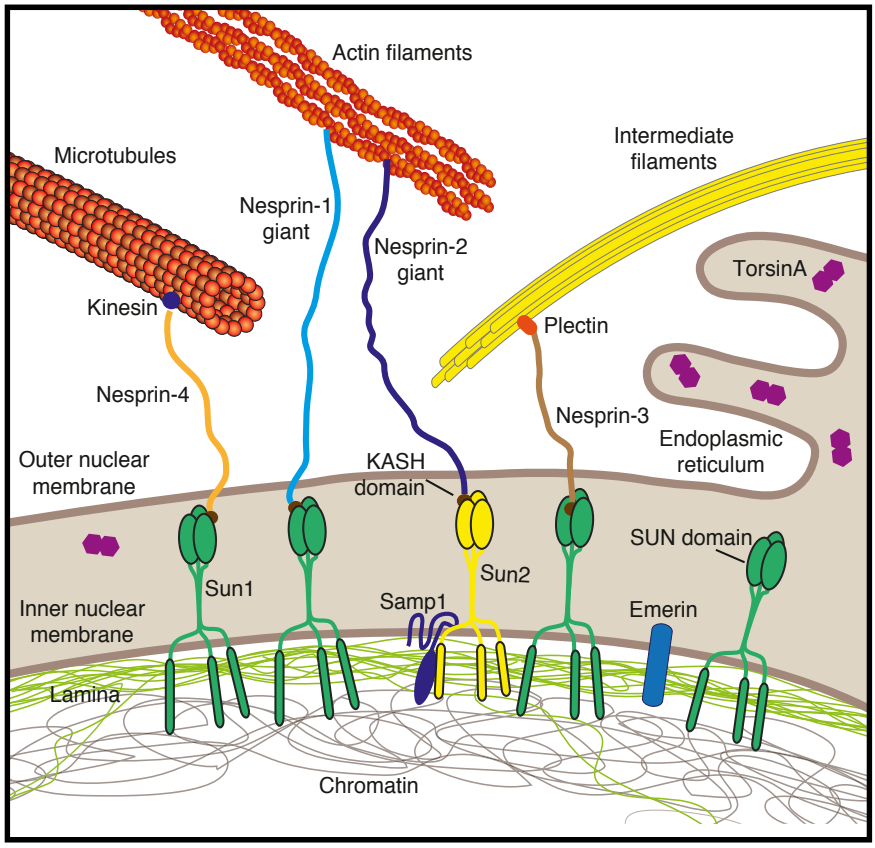
However, as previously described for ATM, additional substrates of ATR activation are coming to light and have been recently reviewed (Kidiyoor et al, 2016). Our group identified the nuclear envelope as one of these substrates (Baumann, 2014; Burgess & Misteli, 2015; Kumar et al, 2014).

The nuclear envelope (NE) represents the physical barrier between the cytoplasm and the nucleus. Anyway this description is rather simplified since the NE influences a variety of cellular processes.

The inner part of the nuclear envelope and its associated structural proteins (lamins, lamin-binding proteins, nuclear pore complexes) directly interact with the genomic DNA and participate in nuclear transport, transcription, replication, DNA repair, protein export, mRNA synthesis.

A complex of proteins called Linker of Nucleoskeleton and Cytoskeleton (LINC) provides the mechanical connection between the inner side of the NE and the cytoplasm, interacting with both the cytoskeleton and the nuclear lamina. Thus the

NE constitutes an ideal platform to sense the mechanical stress arising from the topological constraints of the DNA bound to the NE during processes of DNA replication, transcription, mRNA export, chromatin condensation, and from the continuous remodeling of the cytoskeleton in the cytoplasm (Figure 6).



(Adapted from Isermann and Lammerding, 2013)

Figure 6. The transmission of mechanical forces from the extracellular matrix to the nucleus.
The figure depicts the different cytoskeletal components involved in the transduction of mechanical stimuli from the plasma membrane towards the nucleus.
Actin, microtubules and intermediate filaments are bound to the LINC complex through the interaction with Nesprins, the forces are directly transferred to the nuclear lamina through the SUN proteins interacting with Nesprins (Isermann and Lammerding, 2013).

A role of the S-phase checkpoint at the nuclear envelope was hypothesized in a previous yeast study where Mec1 (the yeast ortholog of human ATR) was found to regulate the interaction between transcribed genes and nuclear pore complexes to facilitate fork progression during S phase (Bermejo et al, 2011). Following this hypothesis our lab showed that ATR acts as a sensor of nuclear envelope deformations caused by internal and external mechanical forces.

ATR localizes to NE where it phosphorylates its target CHK1 under physiological conditions during prophase when chromatin condensation imposes topological stress. Moreover a similar response is triggered when cells are exposed to hyperosmotic stress, a treatment known to cause nuclear deformations including ruffling of the nuclear envelope, nuclear shrinking and chromatin condensation.

Similarly, external cellular deformations, generated by compressive-load systems and patch clamp stimulation, are transmitted to the nuclear envelope through the cytoskeleton and activate ATR at the NE. All these ATR activations are independent of DNA damage.

Interestingly, similar conditions were found to activate two other members of PIKKs, ATM and mTOR. ATM is activated by hypotonic stress and chloroquine treatment, which causes chromatin condensation, in the absence of detectable DNA damage (ATMIN-dependent pathway).

mTORC2 is constituted of a complex that includes mTOR and RICTOR, and is involved in the regulation of cytoskeleton. In yeast, the mTORC2 complex is activated by plasma membrane stress generated by inhibition of sphingolipid metabolism or hypo-osmotic shock. This activation depends upon the interaction with Sml proteins (Berchtold et al, 2012). Evidence of mTORC2 activation under mechanical stress was shown in human keratinocytes. In this study, AKT

phosphorylation at S473 and T308 was reported in cells subjected to physical stretching. Although these phosphorylation events were attributed to PI3K in this study, AKT was also a known target of mTORC2 and it is possible to speculate that phosphorylation at S473 could also be mediated by mTORC2 (Kippenberger et al, 2005). Indeed, a recent study demonstrated the mTORC2 recruitment and activation at new assembly of focal adhesions in human Marrow-derived Mesenchymal Stem Cells subjected to mechanical strain. Here mTORC2 phosphorylates AKT and induces cytoskeletal reorganization. mTORC2 binds to vinculin at focal adhesions and this binding is required to induce AKT phosphorylation (Case et al, 2011; Sen et al, 2014). How these kinases sense mechanical stress is still unclear, this might depend upon the interaction with other proteins or might be a direct event.

The N terminal domain of PIKKs is interspersed of HEAT repeat domains predicted to adopt large superhelical conformations, similar domains are found in PR65, a subunit of the phosphatase PP2A that acts like an elastic connector (Grinthal et al, 2010; Perry & Kleckner, 2003). These data open the possibility that PIKKs could also be able to directly sense mechanical forces.

The fact that different members of the PIKK family share similar mechanisms of activation is intriguing. This might be related to the conserved domain structure of the proteins and open interesting questions regarding how their function can be essential or redundant in such contexts and how the absence of one kinase can affect the behavior of the others. Do these proteins play “promiscuous” roles in the absence of their family members or do they restrict their action to their own substrates? And how this can affect the cell homeostasis?

Together these findings open an entire new perspective connecting DNA repair, cytoskeleton and membranes suggesting that these factors can influence each other, possibly though mechanical transduction.

In agreement with this, different studies are now highlighting the interplay between cytoskeleton and DNA repair.

2.7 A novel connection between DDR and cytoskeleton.

2.7.1 DNA damage and DDR factors influence the cytoskeleton.

It has been shown that DNA damage triggered by ionizing radiation or bacterial genotoxins (Cytolethal distending toxins, CDT) causes activation of the small GTPase RhoA, an actin-regulating protein involved in cell survival, proliferation, adhesion, migration, gene expression and apoptosis. This activation causes the formation of actin stress fibers in adherent cells treated with CTD or ionizing radiation and promotes cell survival (Cortes-Bratti et al, 1999; Frisan et al, 2003; Gelfanova et al, 1999). Another study showed that RhoA can be localized to the nucleus through the interaction with Net1 and the nuclear fraction of RhoA is activated upon ionizing radiation (Dubash et al, 2011).

Induction of DSBs through CDT intoxication activates integrin-β1, a receptor located at the plasma membrane and involved in focal adhesions assembly and interaction with the extracellular matrix (EMC). Its activation upon DNA damage stimulates cell spreading and focal adhesion formation. All these processes are inhibited by inactivation of the DSB sensor ATM, although the mechanism that drives their regulation is not yet clear. ATM has also been associated to cell

migration through the regulation of the transcription repressor SNAIL, which is activated by ATM through phosphorylation of S100 and its activation represses the expression of cadherins, a family of protein involved in cell-cell adhesion. Thus SNAIL favors cell mobility and tumor invasion in breast cancer cells and its mutation at S100 seems to confer radio-sensitivity (Boohaker et al, 2013; Sun et al, 2012; Yin et al, 2016). Moreover ATM was recently found to promote migration by transcriptional regulation of interleukin-8 (IL-8) in a ROS-dependent manner with implications on tumor metastasis and progression (Chen et al, 2015). However, it is not clear if ATM could play a direct role in the regulation of cytoskeletal components.

Interestingly, DNA-PK also was proposed to impact the cell migration through direct phosphorylation of the intermediate filament protein vimentin at S459 (Kotula et al, 2013).

Several pieces of evidence associate activation of the transcription factor p53 with regulation of the cytoskeleton upon DNA damage as well. p53 induces the kinase LIMK2 involved in the regulation of actin dynamics through cofilin phosphorylation; its induction upon DNA damage is required to maintain the G2/M arrest (Croft et al, 2011; Hsu et al, 2010), p53 activates the expression of the cytoskeleton adaptor protein ankyrin-1 in the presence of DNA damage.

The depletion of ankyrin-1 in these conditions impairs migration and formation of actin protrusions (Hall et al, 2016).

The junction-mediating and regulatory protein JMY is known for its role in the regulation of the p53 response upon DNA damage. This factor accumulates in the nucleus and forms a complex with Mdm2 and p300 to promote p53 activation.

However, JMY is also involved in cell motility and invasion controlling the cadherin expression and actin nucleation (Coutts et al, 2010).

JMY directly promotes actin nucleation by binding to monomeric actin through its actin-binding domain WH2 and stimulating the Arp2/3 complex (actin-related protein 2/3), the major regulator of actin filament assembly (Coutts et al, 2009; Zuchero et al, 2009). Since JMY is localized to the nucleus upon DNA damage, it is worthwhile to ask whether its ability to nucleate actin is retained in such context.

Several reports confirm the presence of actin inside the nucleus and this has been linked to diverse processes (Pederson & Aebi, 2002). A recent study, published by Dyche Mullins showed that DNA damage induced by different genotoxic agents causes the formation of actin filaments inside the nucleus (Belin et al, 2015). These filaments seem to facilitate the repair of DSBs. The actin nucleation factors Formin 2 and Spire-1/2 are required for this process. Formin-2 is recruited to the nucleus upon DNA damage and its depletion impairs DSB repair (Belin et al, 2015).

Accumulating evidence suggests that replication stress can also affect cell morphology and cytoskeletal components. Chronic replication problems associated to DNA ligase I deficiencies impact cell morphology and migration by altering the expression of cadherins (Cremaschi et al, 2015; Soza et al, 2009). Another study showed that myosin 16 levels fluctuates during the cell cycle and are down regulated upon replication stress induction or replication inhibition (Cameron et al, 2013).

Myosins are actin-dependent motor proteins mainly localized in the cytoplasm but have also been found inside the nucleus.

2.7.2 Cytoskeleton influences the DNA damage response.

DNA damage and DDR proteins can affect the cytoskeleton in multiple ways; this suggests that the cytoskeleton should play a role in the DNA damage response, although the physiological meaning of such regulations is still matter of intense investigation. Here we describe pieces evidence that suggest how DNA repair can be affected by different cytoskeletal components: actin, microtubules and the LINC complex.

In budding yeast, TORC2-mediated actin filament remodeling has been recently associated with the survival of cells to low doses of DNA damage. TORC2 inhibition increases chromosome fragmentation in cells treated with zeocin or ionizing radiation and this phenotype was reproduced by treatment with latrunculin A and jasplakinolide, two drugs that interfere with actin cytoskeleton dynamics (Shimada et al, 2013). It was shown that treatment of mammalian cells with different types of drug targeting cytoskeleton, such as actinomycin D, cytochalasin D and jasplakinolide, can sensitize cells to DNA damage (Andrin et al, 2012; Takeuchi et al, 1998; Yamazaki et al, 2000).

p53 is one of the targets of such responses, since it was shown that p53 can bind to actin in a calcium-dependent manner (Metcalfe et al, 1999) and that actin de-polymerization impairs the nuclear import of p53 upon DNA damage (Wang et al, 2013).

Interestingly the Ku70-Ku80 heterodimer, an essential complex in NHEJ sub-pathway of DSB repair mediated by DNA-PK, was also found to bind polymerized actin *in vitro* and its ability to bind to DSB was affected by treatment with cytochalasin D resulting in defective repair (Andrin et al, 2012).

The inhibition of GTPases RhoA and Rac1, both involved in the regulation of cytoskeleton dynamics and cell motility, was found to impair DNA repair upon UV or ionizing radiations (Espinha et al, 2016; Osaki et al, 2016).

Many actin-binding proteins and actin nucleation factors are documented to shuttle between cytoplasm and the nucleus upon DNA damage. In budding yeast, the complex INO80 that works as a nucleosome remodeler contains the actin-related proteins Arp5 and Arp8. This complex is recruited to DSBs at the phosphorylated form of H2A and participates in chromatin remodeling favoring the processing of DSB into ssDNA. Deletion of INO80 confers sensitivity to DNA damaging agents (Morrison et al, 2004; van Attikum et al, 2004). Similar findings were confirmed in human cells where Arp5 was found to shuttle between cytoplasm and nucleus and its deletion impairs DBS repair (Kitayama et al, 2009).

The actin binding protein filamin A (FLNA), involved in the crosslinking of actin filaments and in their anchoring to membrane proteins, was found among the protein interactors of BRCA1 and BRCA2, two major factors of the homologous recombination machinery (Velkova et al, 2010; Yuan & Shen, 2001).

Depletion of FLNA results in defective homologous recombination repair and sensitizes cells to IR and cisplatin treatment (Yue et al, 2013; Yue et al, 2009). Moreover, cofilin-1, an actin de-polymerizing factor, has been implicated in DDR, although its role it is not very clear currently (Lee et al, 2005; Leu et al, 2013; Yan et al, 2012).

Together with actin, microtubules (MT) can also influence DDR. Poruchynsky and colleagues found that microtubule-targeting agents affect the transport of DNA repair proteins inside the cells. ATM, ATR, DNA-PK, Mre11, Rad50,

p95/NBS1, p53, 53BP1 and p63 were found to co-localize with tubulin and co-immunoprecipitated with the MT motor dynein. Treatment with MT-targeting agents sequesters these proteins in the cytoplasm resulting in increased toxicity of DNA damaging treatments (Poruchynsky et al, 2015).

Microtubules are implicated in 53BP1-dependent chromatin mobility at DSB sites, together with the LINC complex (Lottersberger et al, 2015).

The LINC complex resides at the nuclear envelope and is composed of different proteins: nesprins and SUN.

Nesprins interacts with the actin filaments in the cytoplasm, while the SUN proteins bind to nuclear lamina. Nesprin1 is down regulated at the nuclear envelope of several tumor cell lines; it interacts with proteins of the mismatch repair pathway and its depletion induces DNA damage, CHK1 and CHK2 phosphorylation and inhibition of the NHEJ pathway associated with Ku70 downregulation (Sur et al, 2014).

Collectively these findings point to a bi-directional regulation between DNA repair and cytoskeleton. Proteins of the DDR might play a role in cytoplasmic events influencing cell plasticity, migration and invasion while factors belonging to the cytoskeletal apparatus can affect nuclear events during DNA damage repair.

2.7.3 Role of cell mechanics in cell migration and tools to study the mechanical properties of cells.

One of the most dangerous features of cancer cells resides in their ability to migrate outside the tissue of origin and generate metastasis in the whole body.

Therefore diverse studies focused on the pathways involved in cell migration and

cancer cell migration to understand the molecular basis regulating this process. It is becoming clear how this transformation involves several alterations of the mechanical properties of cells and their interaction with the surrounding microenvironment. Tumor cells are continuously exposed to different tissue environments during the metastatic process and this requires the ability to sense and respond to different mechanical forces.

These mechanical challenges include modifications in cell and tissue structure, force-induced changes in the environment, and cell-directed remodeling of the extracellular matrix.

Recent advances in biomechanics and nanotechnology are allowing the study of mechanical influences acting on biological structures. Several biophysical tools have been used to describe the mechanical properties of different cell types: Atomic Force Microscopy (AFM) (E et al, 1998), micropipette aspiration (Ward et al, 1991) and optical stretchers (Guck et al, 2005).

Atomic Force Microscopy has been established as a versatile tool for imaging and measuring the elastic properties of living cells. In AFM, local deformation is induced on a cell surface through physical contact with the sharp tip at the free end of a cantilever. The applied force is then estimated and allows measurement of elastic and viscoelastic properties of cell membranes or subcellular components (Trache & Meininger, 2008).

AFM measurements were also applied to ex vivo cancer cells obtained from patients (Cross et al, 2007). Lekka and colleagues used AFM to measure the elasticity of normal and cancerous human bladder epithelial cells (Lekka et al, 1999). Another study focused on the mechanical properties of breast cancer cells

(Li et al, 2008). These studies reported that cancer cells are softer than normal cells, and this was attributed to the reorganization of the cytoskeleton. Alterations of cell mechanics might be relevant during migration processes leading to metastasis. *In vivo*, migrating cells undergo large deformations of cellular and nuclear structures to squeeze across small constrictions.

It is now possible to study the contribution of different cellular components to this process, combining live cell imaging technologies with micro-channel devices to mimic three-dimensional migration (Heuze et al, 2011). These studies recently showed the involvement of the endosomal sorting complexes required for transport-III (ESCRT-III) in the maintenance of nuclear membrane integrity during this type of migration (Denais et al, 2016; Raab et al, 2016). Moreover, actin polymerization around the nucleus was found to facilitate the fast-moving of cells through narrow gaps (Thiam et al, 2016).

If DDR proteins can influence such phenomena by interacting with cytoskeletal components, a better understanding of these regulatory pathways will unveil potential roles of DDR in metastasis. This field of research will possibly open new strategies to sensitize cancer cells and block their metastatic potential.

3. MATERIALS AND METHODS

3.1 Plasmids and Reagents

We received the HeLa control and ATM KO from Maria Vinciguerra (Vincenzo Costanzo group). The plasmid used for the generation of the KO was the lentiCRISPR 49535, the cas9 guide was cloned into the BbsI site and designed with the following primer pair:

5'-CACCGCGAATTCGAGTGTGTGAATT

3'-AAACAATTCACACACTCGAATTCGC.

Hela cas9 control cells were infected with the same plasmid lacking the cas9 guide. The plasmids pLKO.1-puro (Mission® Sigma-Aldrich) and shATM #951 were used for the generation of Hela and U2OS stable knockdown cells and were received from Martin Kosar (Marco Foiani's lab). HeLa cells with stable H2B-mCherry expression were from IFOM (Kumar et al, 2014). U2OS cells stably expressing 53BP1-GFP cells were a kind gift of Jiri Bartek's lab (Lukas et al, 2011).

Silicon molds of micro-channels were done in Matthieu Piel's lab.

The plasmids used to transfect U2OS cells for the FRET analysis of ATM activation are the cytoplasmic and H2B-targeted ATM reporter and were a kind gift of Tony Hunter (Johnson et al, 2007). The U2OS stable expressing the FUCCI reporter were from Libor Macůrek (Macurek et al, 2013).

To inhibit ATM, cells were treated with ATMi KU-60019 (ab144817) and Caffeine (Sigma-Aldrich).

3.2 Cell culture

HeLa and U2OS cells were maintained in minimum essential medium with GlutaMAX (MEM; Life Technologies 41090-093) supplemented with 10% (vol/vol) fetal bovine serum (FBS) South America (Biowest), 0.1mM NEAA (non essential amino acids, Microtech), Sodium pyruvate 1mM (Microtech) and penicillin-streptomycin (Microtech) in a humidified atmosphere (5% CO_2 , 37°C). Human primary fibroblasts derived from control patient and A-T patient (CORIELL AG04405) were maintained in MEM supplemented with 15% FBS North America (Sigma-Aldrich) and 0.1mM NEAA. HEK 293T cells were cultured in Dulbecco's Modified Eagle's Medium (DMEM, Lonza BE12-614F) supplemented with 10% FBS and 1% L-Glutamine (Microtech X0550).

When cells were subjected to lentiviral infection with shRNA constructs, puromycin was added at 1μg/ml as a selection. ATM inhibition was achieved with caffeine 1mM or ATMi KU-60019 3μM. For the trypsinization, cells were washed once with PBS1X sterile, trypsin-EDTA (Microtech) was added to the plate (1ml for 10cm plates) and the cells were incubated at 37˚C until a complete detachment was obtained (maximum 5 minutes). Cells were well re-suspended in complete medium and split.

3.3 Lipofectamine transfection

The following protocol was used for the transient transfection of DNA plasmids in HeLa and U2OS cells.

Protocol for one cell culture plate of 10cm:

- Plate cells so that they will rich 60-80% confluency the day of transfection
- remove the media
- wash once with sterile PBS 1X
- add 4ml of Opti-MEM media to the cells
- prepare two 1.5ml eppendorf tubes with 500µl of Opti-MEM
- add 6µl of Lipo2000 in one vial and 2µg of plasmid in the second vial
- wait 5 minutes at RT
- add the DNA solution drop by drop to the lipo2000 vial, mix well
- wait 25 minutes at RT
- add drop by drop the 1ml solution containing lipo2000 and plasmid DNA to the cell
- incubate cells at 37˚C
- after 4 hours of incubation remove the Opti-MEM medium and add normal cell culture medium to the cells
- 24 hours after the transfection check the efficiency of the transfection by immunofluorescence
- 24-72 hours after transfection cells were used for the experiments

Lipo2000: lipofectamine 2000 Life Technologies 11668-019

Opti-MEM: OPTIMEM-I w/Glutamax Life Technologies 51985-042

3.4 Lentiviral transduction

This protocol was used to obtain long-term knockdown of ATM in HeLa and U2OS cells through the stable integration of DNA constructs encoding shRNA targeting the ATM gene.

All the procedures were performed in Virus rooms of safety level II.

Protocol to infect one cell culture plate of 10cm:

Day1 (lentiviral packaging)

- Plate HEK293T cells in a 10cm plate at 5x 10^6 cells/plate

HEK239T calcium phosphate transfection:

ENV (VSV-G) 2.8µg
pMDL (gag&pol) 5µg
REV 2.5µg
Lentiviral vector 10µg
CaCl2 2M 62.4µg
0.1x TE (pH 8) sterile ut to 500µl

- Mix and add bubbling into 500µL of 2xHBS. Incubate up to 5 minutes at RT.
- Add drop wise to the medium (1mL/plate) and leave overnight at 37°C.

Day2 (virus concentration)

- Replace 293T transfection medium with 5.5mL of fresh medium.
- Plate target cells (HeLa or U2OS) so that they will be 30% confluent the day of infection.

Day3 (infection of target cells)

- Filter the viral supernatant with 0.45μm filters and add polybrene (8μg/mL).
- Infect target cells with 5mL (10cm plate) of viral supernatant.
- Incubate cells for 24 hours at 37°C and then replace the viral supernatant with normal medium.
- Wait until day 5 before adding the selection drug.

Day5

- Cells recovery for puromycin selection (puromycin 1μg/ml)

Successfully infected cells were selected with puromycin for 2 days, the efficiency of ATM knockdown was assayed by western blot. For the whole duration of the experiments the cells were cultured under puromycin selection.

3.5 Cell lysate preparation for western blot

Protocol to prepare whole cell extracts from a 10cm culture plate of human adherent cells:

- Plate cells in cell culture plates until 80% confluency
- Remove the culture medium
- Wash once with PBS 1x sterile
- Add 400μl of lysis buffer to each plate
- Proceed with cell scraping to remove the cells from the plate and mix them

in the lysis buffer

- Collect the solution of cell and lysis buffer in 1.5ml eppendorf tube
- Store the tubes on ice for 30 minutes-1 hour
- Centrifuge at maximum speed for 30 minutes at 4°C
- Transfer the supernatant in a new eppendorf tube
- Add Laemmli buffer 1X
- Boil the samples at 95°C for 10 minutes
- Store the samples at -20°C

Cell lysis buffer composition:

Tris-HCl pH 8.0 50mM
$MgCl_2$ 1mM
NaCl 200mM
$CaCl_2$ 1mM
Glycerol 10%
NP-40 1%
protease inhibitors 1:100 (complete inhibitors, Roche)
phosphatase inhibitors 1:200 (phosphatase inhibitor cocktail 2, Sigma)

Laemmli 1X buffer composition:

Tris-HCl pH 6.8 50mM
SDS 2%
Glycerol 10%
β–mercaptoethanol 0.1%
Bromophenol blue 0.0005%

3.6 Western blotting

Proteins were separated by SDS-page electrophoresis using polyacrylamide precast gels (Bio-Rad).

The % of acrylamide was chosen according to the protein size.

The protein migration was performed in a SDS-PAGE running buffer. The separated proteins were transferred on a nitrocellulose membrane of 0.2 μm (protein with a molecular weight< 100kDa) or 0.45 μm pore sizes (proteins of higher molecular weight).

For gradient precast gels a membrane of 0.45μm was chosen.

The transfer was carried for 1 hour at 100V in cold room using wet/tank blotting systems (Bio-Rad).

The transfer buffer (Glycin 1%, Tris-HCl 0.02 M) was prepared with methanol 10% for large proteins or 20% for smaller proteins.

After the transfer the nitrocellulose membrane was coloured with Ponceau S staining solution (Ponceau S 1gr, acetic acid 50 ml, up to 1000 ml ddH_2O) to allow the visualization of the total protein extracts and to check the quality of the transfer.

The Ponceau staining was removed washing the membrane with washing buffer PBST (0.2% Tween 20 PBS).

Blocking was performed overnight (or 1 hour at least) with 5% milk in PBST. After the blocking, the primary antibody diluted in 5% milk PBST was added for 3 hours at RT, then washed with PBST for three times (10 minutes each) to remove the excess of antibody. The horseradish peroxidase-conjugated secondary antibody diluted in 5% milk PBST was added for 1 hour followed by 3X PBST

washings of 10 minutes.

Finally, proteins were visualized using SuperSignal West Dura Extended Duration Substrate (Thermo Scientific).

SuperSignal West Femto Chemiluminescent Substrate (Thermo Scientific) was used in case of weak signals.

The signal was developed using ChemiDoc (Bio-Rad, Molecular Imager ChemiDoc XRS+).

Imagelab volume tool was used for the quantification of the signal.

Primary antibodies used in this work.

- Anti-ATM(D2ES) rabbit monoclonal 2873S Cell Signaling 1:1000
- Anti-lamin A/C mouse monoclonal 636 sc-7292 Santa Cruz 1:1000
- Anti-Lamin B1 rabbit polyclonal ab16048 abcam 0.1μg/ml
- Anti-ATM mouse IgG clone 9E6 used for protein immunoprecipitation (a kind gift from Domenico Delia)
- Anti-pS1981 ATM mouse monoclonal antibody 25484 Rockland 1:1000

Secondary antibodies used in this work.

-Anti-mouse, Goat polyclonal (Bio-rad #170-6516) IgG-HRP (H+L), 1:10000

-Anti-rabbit Goat polyclonal (Bio-rad #170-6515) IgG-HRP (H+L), 1:10000

3.7 BCA protein quantification

Whole cell protein extracts were quantified using the Pierce™ BCA Protein Assay Kit (Thermo Scientific). The procedure is described on the online guide for the users.

3.8 Protein immunoprecipitation (IP)

This protocol was used to immunoprecipitate ATM to perform a mass spectrometry analysis of the physical interactors of ATM.

Cell culture

Culture HeLa cells to 80-90% confluency and prepare a number of plates according to the amount of total protein lysate you need, considering that one plate of HeLa will produce approximately 1mg/ml whole protein lysate.

For the IP of mass spectrometry analysis 10mg of whole protein lysates were used for each sample.

The day of the experiment the cell lysis was performed as described in the lysate preparation section.

To preserve the protein interactions during the immunoprecipitation steps, the composition of the lysis buffer was adjusted as follows.

Lysis buffer composition (50ml)

	Reagent	Final Concentration	Stock	Volume to make 50ml buffer
1	TRIS-HCl pH8.0	50mM	1M	2.5ml
2	$MgCl_2$	1mM	1M	50uL
3	NaCl	150mM	5M	1.5mL
4	$CaCl_2$	1mM	1M	50uL
5	Glycerol	2%	50%	2mL
6	NP-40	0.2%	10%	1mL

Added freshly according to the experiment:

1. Protease Inhibitor Roche Tablets (1/10 mL).
2. Phosphatase inhibitors – (1:200) Sigma cocktail 2
3. Benzonase – Only required for the fraction of the lysis buffer which is used for cell lysis (50 U/mL).

Pre-clearing of lysates

Since the immunoprecipitation step is performed using protein A or protein G dynabeads, a pre-clearing of the lysates is recommended to remove proteins that aspecifically bind to protein A or protein G. Protein G dynabeads were used in this work, thus the clearing was done incubating the lysates with protein G agarose beads 1 hour in rotation in cold room.

Next the lysates were spinned for 10 minutes at maximum speed at 4˚C. The supernatant was transferred in a new eppendorf tube to proceed with the immunoprecipitation, an aliquot was kept for the protein quantification.

Lysates were quantified with the Pierce™ BCA Protein Assay Kit (Thermo Scientific) and the protein concentration was adjusted to 1mg/ml. 50µl of lysates were stored at -80˚C (Input).

Immunoprecipitation

10mg of protein lysates were incubated with 60µg of antibody (Anti-ATM mouse IgG clone 9E6) and 250µl of protein G dynabeads (Dynabeads™ Protein G Thermo Fisher Scientific) for 2 hours in rotation at 4°C.

During this step the primary antibody will bound to the target protein (ATM) and at the same time the protein G dynabeads will bind to the Fc of the mouse IgG. This allows the isolation of ATM and its interactors from the rest of the proteins present in the lysate.

Following the incubation, the complexes of dynabeads-antibody-proteins were isolated using a magnet, 50µl of supernatant were stored at -80°C (flow-through).

Beads were washed 4 times with lysis buffer, each washing was performed for 5 minutes in rotation in cold room and each time the buffer was removed isolating the beads with the magnet.

When the washing was completed, the supernatant was removed completely and 50µl of Laemmli buffer 2X were added to the beads. Laemmli buffer was added to the input and flow-through at 1X final concentration.

Finally samples were boiled 15 minutes at 95°C and stored at -20°C. Samples were separated by SDS-page electrophoresis on a 4-12% gradient precast gel (Invitrogen) for mass spectrometry analysis.

3.9 Coomassie Blue protein gel staining

The 4-12% acrylamide gels for the mass spec analysis were stained with Coomassie Blue (acetic acid 10%, ethanol 30%, Coomassie brilliant Blue R-250 0.2%) for 10 minutes at RT. De-staining was performed for 3 hours washing with de-staining solution (acetic acid 10%, ethanol 30%) until clear bands appear in the

gel. The Coomassie dye binds to proteins through ionic interactions between its sulfonic acid groups and the positive protein amine groups as well as through Van der Waals attractions, this binding allow to visualize the protein bands in the gel as blue color. The sensitivity of Coomassie R-250 reach 0.1mg/band.

3.10 Mass spectrometry

The mass spectrometry analysis of ATM interactome was performed by Vittoria Matafora (Angela Bachi group) in collaboration.

In order to study ATM putative interactors, we analyzed a label free ATM immunoprecipitation by quantitative proteomic approach. We selected the proteins more enriched in the IP respect to the control (ATM KO). IP eluates were separated by 4–12% SDS–PAGE (Invitrogen Bolt™ 4-12% Bis-Tris-Plus), stained with Coomassie Brilliant Blue (Bio-Rad) and excised in three slices for LC-MS/MS analysis. Mass spectrometry analysis was performed by LC-MS/MS using a quadrupole Orbitrap Q-exactive HF mass spectrometer (Thermo Scientific). Each slice was reduced, alkylated and Tryptic digested as described elsewhere (Shevchenko et al, 1996). Tryptic digestions were first cleaned using Stage Tips as described previously (Rappsilber et al, 2007) and then injected into a capillary chromatographic system on a linear gradient from 95% solvent A (2% ACN, 0.1% formic acid) to 55% solvent B (80% acetonitrile, 0.1% formic acid) over 45 min at a constant flow rate of 0.30 μl/min on UHPLC Easy-nLC 1000 (Thermo Scientific) where the LC system was connected to a 23-cm fused-silica emitter of 75 μm inner diameter (New Objective, Inc. Woburn, MA, USA), packed in-house with ReproSil-Pur C18-AQ 1.9 μm beads (Dr Maisch Gmbh, Ammerbuch, Germany) using a high-pressure bomb loader (Proxeon, Odense,

Denmark). (EasyLC, Proxeon Biosystems, Odense, Denmark). The mass spectrometer was operated in DDA mode with dynamic exclusion enabled (exclusion duration = 20 seconds), MS1 resolution = 60,000, MS1 automatic gain control target = 3 x 10^6, MS1 maximum fill time = 20 ms, MS2 resolution = 15,000, MS2 automatic gain control target = 1 x 10^5, MS2 maximum fill time = 80 ms, and MS2 normalized collision energy = 28. For each cycle, one full MS1 scan range = 200-2000 m/z, was followed by 15 MS2 scans using an isolation window size of 1.2 m/z. Protein identification and quantification were achieved using the MaxQuant software version 1.5.2.8. Cysteine carbamidomethylation was searched as a fixed modification, whereas N-acetyl protein and oxidized methionine were searched as variable modifications. Protein quantification was based on extracted ion chromatograms of contained peptides. Peptides and proteins were accepted with a false-discovery rate of 0.01, two minimum peptides identified per protein of which one unique. The experiments were done performing two technical replicate for each biological one.

3.11 Electron microscopy (EM) sample preparation

Grids, osmium tetraoxide, paraformaldehyde and glutaraldehyde were purchased from Electron Microscopy Sciences (EMS, USA). Sodium cacodylate and Epoxy resin kit were purchased from Fluka (SIGMA, USA). Potassium ferrocyanide,

ethanol and acetone were purchased from Carlo Erba (Italy), and Mat Tek dishes (P35G-1.5-14-C-GRID) from MatTek Corporation (USA).

The cells grown on MatTek dishes were fixed with a mixture of 4% paraformaldehyde and 2,5% glutaraldehyde in 0.2 M sodium cacodylate pH 7.2 for 2 h at RT. Afterwards, the cells were washed 6 times in 0.2 sodium cacodylate pH 7.2 at RT. Osmification followed: the cells were incubated for 1 h at RT with a 1:1 mixture of 2% osmium tetraoxide in distilled water and 3% potassium ferrocyanide in 0.2 M sodium cacodylate (pH 6.9) and then rinsed 6 times with the cacodylate buffer, for 5 min treated with 0.3% Thiocarbohydrazide in 0.2 M cacodylate buffer (pH 6.9) for 10 min, washed 3 times with 0.2 M cacodylate buffer (pH 6,9), treated with 1% OsO4 in 0.2 M cacodylate buffer (pH 6,9) for 30 min. Then, samples were rinsed with 0.1 M sodium cacodylate (pH 6.9) buffer until all traces of the yellow osmium fixative have been removed, washed in de-ionized water, treated with 1% uranyl acetate in water for 1 h, washed in water again.

The samples were then dehydrated: 3x10 min in 50% ethanol; 3x 10 min in 70% ethanol; 3x 10 min in 90% ethanol; 3x 10 min in 100% ethanol. The samples were subsequently incubated for 2 h in 1:1 mixture of 100% ethanol and Epoxy resin (Epon) at RT, the mixture was then removed with a pipette and finally samples were embedded for 4 h in Epoxy resin at RT. The resin was polymerized for at least 72 h at 60 °C in an oven.

The samples embedded into resin were carefully picked up from glass and sectioned with diamond knife (Diatome, Switzerland) using Leica ultramicrotome. Sections were analysed with a Tecnai 20 High Voltage EM (FEI, The Netherlands) operating at 200 kV.

The EM analysis and samples preparation were performed by the IFOM EM facility (Galina Beznusenko and Alexandre Mironov) (Beznoussenko et al, 2007; Kweon et al, 2004).

3.12 Preparation of micro-channel devices used for 3D migration analysis

To study the migration properties of cells in a 3D confinement, we took advantage of a cell migration assay based on micro-channels.

The channels are made of silicone rubber (here polydimethylsiloxane, PDMS) stuck to glass to allow the imaging of cells migrating inside the channels.

The structure of the channels is designed with specialized softwares, a photomask is produced and used to fabricate a silicon wafer by photolithography. An example of silicon wafer is shown in figure 7.

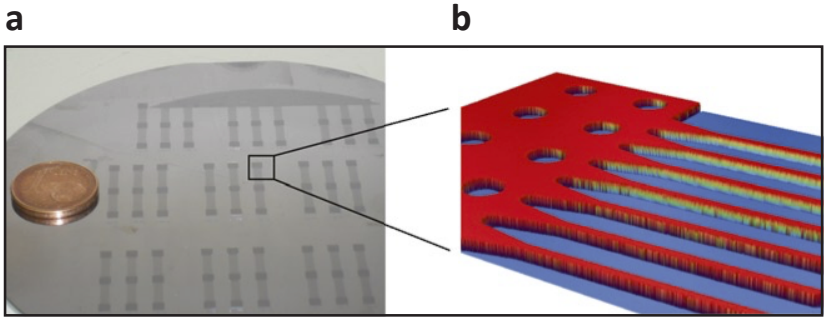


Figure 7. Example of a silicon wafer used to produce PDMS mold of micro-channels.
a) Example of a silicon wafer where channels were fabricated by photolitography.
b) Image showing the structure of the channels printed on the wafer.
The figure was adapted from (Heuze et al, 2011).

We received silicon wafers in collaboration with Matthieu Piel's lab. All the procedures to prepare the wafers are described in details in (Raab et al, 2016).

The channels were then produced in our lab.

PDMS mold fabrication

A mix of uncured silicon rubber and curing agent at a ratio of 10:1 was prepared (RTV-615, Momentive), mixed well to reduce air bubbles and poured in the silicon wafer to prepare PDMS molds of the channels.

The mold with PDMS layer (thickness of approximately 3mm) was put in a vacuum bell for at least 1 hour to remove all the air bubbles. The PDMS molds were left in the wafer for at least one day to allow a complete polymerization, then they were removed from the mold cutting with a surgical blade. To prepare the PDMS channels we followed the procedure described in Raab et al., 2016 (chip assembly). Punchers were used to drill the PDMS in the regions designed for seeding chambers, the holes thus generate areas where cells are seeded inside the channels and can migrate.

PDMS bonding to slideglass

In order to bond the PDMS layers on the slide-glasses a treatment with plasma cleaner was performed to activate the surfaces of the PDMS and glass.

For the migration experiments the PDMS channels were mounted on 2 chambers Lab-TeK II 155379 glasses in order to allow the simultaneous analysis of control cells and ATMi-treated cells (or mutant cells) at the same time.

Thus, chamber glasses and PDMS layers were put inside the plasma cleaner (PDG-32G-2, Harrick Plasma), the PDMS was positioned with the channel side on top. The instrument was allowed to reach vacuum for 1 minute and then plasma cleaning was performed for 35 seconds setting the instrument to “high”. The plasma cleaning sterilizes and activates the surfaces, in this way PDMS and glass are stuck together to create a sterile chamber made of channels.

Once the chambers are made, the PDMS-glass bonding is strengthened putting them at 65°C for one hour. One more round of plasma cleaning is needed to sterilize the chambers, followed by 5 minutes in vacuum to lower the air pressure inside the PDMS channels and facilitate the entrance of the culture medium. The chambers are immediately filled with fibronectin 20μg/ml in sterile PBS 1x and incubated overnight (ON), the next day fibronectin is removed by aspiration and the channels are washed three times with sterile PBS 1x. After washing, the culture medium is added inside the channels and incubated ON. This step is required before cell seeding to generate a good culture condition inside the channel and facilitate the migration of the cells. When a treatment was required, as ATMi treatment, the drug was already added to the medium at this step to equilibrate the PDMS with the medium. The figure 8 illustrates an example of PDMS channels bonded to a chamber slide-glass and the structure of the channels.

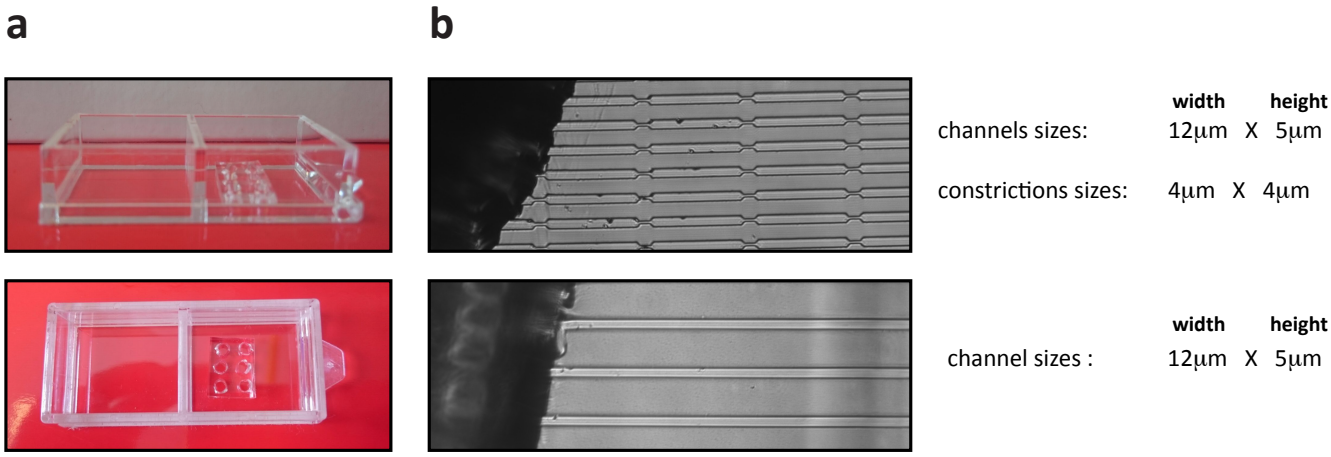


Figure 8. Example of PDMS mold bonded to chamber glass and structure of channels.
a) Representative example of a PDMS mold bonded to a two chambers slide-glass after plasma cleaning. The holes in the PDMS are the seeding chambers. The migrating cells are imaged from the bottom.
b) The pictures captured with a bright-field (BF) microscope show the structure of the PDMS channels once the mold is bonded to the glass.
The first image shows the channels with constrictions, the second image shows the channels without constrictions. Both types of channel were used in this work for HeLa and U2OS migration assay. The black area on the left side is the seeding chamber.

Cells seeding

Cells were seeded 12 hours (HeLa) or 4 hours (U2OS) before starting imaging acquisition. One 10cm plate of 80% confluent cells was tripsinized, re-suspended in 10ml of cell culture medium.

Cells were counted manually with a Burker chamber and then centrifuged at 1200 rpm for 5 minutes.

The supernatant was discarded and the pellet re-suspended at a concentration of 10^6 cells/ml (ATMi was added at this step when needed). Cells were loaded gently inside the seeding chambers using a P 20 pipette. Cells were incubated at 37°C for 2 hours before filling the chamber with medium in order to promote cell adhesion inside the channels.

3.13 Immunofluorescence (IF)

Imaging of fixed samples

For the IF, cells were plated on coverslips, the day of the experiment cells were washed with PBS 1x for 5 minutes and then fixed with 4% formaldehyde (15 minutes at RT).

After fixation cells were washed three times with PBS1X (10 minutes/wash), and permeabilized with 0.5% TritonX-100 PBS (5 minutes at RT). The blocking was done after permeabilization incubating the cells with 3% BSA 0.1% TX-100 PBS for one hour.

Primary antibody staining was done with mouse anti-lamin A/C 636 sc-7292 Santa Cruz (1:500) in blocking buffer (1 hour at RT), followed by three washes in PBS (10 minutes each). Species-specific secondary antibodies were added to samples and incubated (1 hour, RT), followed by three washes with PBS1X. Samples were mounted on coverslips with mounting medium containing DAPI (VectaShield). Cells were then visualized and captured using a UltraVIEW VoX spinning-disk confocal system (PerkinElmer) equipped with an EclipseTi inverted microscope (Nikon) provided with a Nikon Perfect Focus System and a Hamamatsu CCD camera (C9100-50) and driven by Volocity software (Improvision; Perkin Elmer). All images were acquired through a 60X oil-immersion objective (Nikon Plan Apo VC, NA 1.4).

Up to 200 fields of view were automatically acquired using the multi point acquisition tool of the Volocity software that drives the spinning disk microscope.

9 optical sections were acquired for each channel.

Z stack maximum projections of the images were used to represent the staining

with different antibodies, and images were processed using ImageJ.

Antibodies used for immunofluorescences:

- Anti-lamin A/C mouse monoclonal 636 sc-7292 Santa Cruz 1:500
- Alexa488 Donkey anti-mouse Life Technologies (A21202)

Live cell imaging

The live cell imaging acquisitions of cells migrating inside micro-channels were performed on an UltraVIEW VoX spinning-disk confocal system (PerkinElmer) equipped with an EclipseTi inverted microscope (Nikon) provided with a Nikon Perfect Focus System and a Hamamatsu CCD camera (C9100-50) and driven by Volocity software (Improvision; Perkin Elmer). All images were acquired through a NIKON Plan Apo 20x (NA 0.75) and cells were maintained in an environmental chamber at 37°C in an atmosphere of 5% CO_2.

Images were collected every 15 minutes for 18 hours, 13 optical sections were acquired for the fluorescence channel and one reference section was taken for the bright field image of the micro-channels. Z stack maximum projections of the fluorescence images were used to analyze the cells during migration and merged with the bright field image of the channels.

3.14 Fluorescence resonance energy transfer (FRET) analysis

This technique was used to measure the activity of ATM during live cell imaging of cells migrating inside micro-channels.

The constructs expressing the cytoplasmic and H2B-targeted ATM reporter were a gift of Tony Hunter and are described in Johnson et al., 2007.

U2OS cells were transfected with the constructs 48 hours before the imaging acquisition. The efficiency of transfection was very high and transfected cells were able to grow normally.

The imaging was carried out using a DeltaVision Elite imaging system (Applied Precision) driven by softWoRx software and equipped with a CoolSNAP HQ2 CCD camera (Photometrics) and an environmental chamber (Applied Precision) maintained at 37°C in an atmosphere of 5% CO_2. Images were acquired using an Olympus 60x/1.42 Plan Apo N oil immersion objective.

4 z stacks were acquired for each field of view and cells were imaged every 15 minutes for 18 hours. Three images were collected in sequence at each time point: CFP (ex: 438/24nm, em: 470/24nm), FRET (ex: 438/24nm, em: 559/38nm) and YFP (ex: 513/17nm, em: 528/38nm). Using an in-house macro in ImageJ, images were background corrected, realigned, converted in 32 bits, smoothed and the YFP channel was thresholded and used as a binary mask as described in (Kardash et al, 2011). The average FRET/CFP ratios calculated for regions of interest were measured at time 0 and at the end of the acquisition in order to compare the FRET efficiency of the reporter in cells migrating inside channels. This analysis was done to measure any aspecific change in FRET associated to the imaging/sample

conditions and was defined as background ΔFRET ratio.

The same analysis was performed in cells approaching a constriction to measure the ΔFRET ratio before and after the constriction. This value was compared to the background signal.

3.15 Atomic force microscopy (AFM)

The AFM experiments were done in collaboration with Qingsen Li (Marco Foiani's lab) (Li et al, 2008). We took advantage of a Nanowizard 3 (JPK instruments, Germany).

For AFM indentation, a modified silicon nitride AFM cantilever (NovaScan, USA) having a spring constant of 0.03N/m with a 5μm diameter polystyrene bead adhered to the tip was used to indent the cells. A spherical bead indenter was used here instead of a sharp tip to get better assessment of cell elasticity by averaging over a larger cell surface area with a well-defined contact geometry.

The cells were grown on round glass coverslips of 24mm diameter that were mounted on the AFM stage and the cells were kept in their culture medium using a standard fluid cell (JPK instruments, Germany). The sample was always maintained at physiological temperature (37 °C) during indentation using a heater (JPK instruments, Germany). Indentation was carried out at the center of cell using a loading rate of 1.5 μm/s. The ramp size used in this study was 3 μm and an indentation force of 2 nN was applied during the tests in order to ensure that a small deformation was exerted on the cell and minimize any substrate contributions.

The Young's modulus was subsequently determined using Hertz's contact model

$$F = \frac{4}{3}\frac{E}{(1-\nu^2)}\sqrt{R\delta^3}$$

where F is the indentation force, E is the Young's modulus to be determined, ν is the Poisson's ratio, R is the radius of the spherical bead, and δ is indentation depth. The cell was assumed incompressible and a Poisson's ratio of 0.5 was used.

3.16 Nuclear isolation for AFM analysis

This protocol was used to isolate HeLa nuclei for AFM analysis.

- Confluent HeLa cells grown in six-well chambers were rinsed

once with PBS.

-Cells were treated for 5 min with 1 ml of a 0.01% Igepal CA-630 (a non-ionic detergent, Sigma), 1% citric acid solution in water. Nuclei were expelled, while the cytoplasm remained adherent.

-The medium was collected, mixed with 5 ml PBS, and centrifuged at 300g for 5 minutes.

-The nuclei pellet was resuspended in PBS, the suspended nuclei solution was dropped onto coverslip for AFM experiment.

3.17 Analysis of single cell migration by manual tracking

To understand the role of ATM in 2D locomotion we performed single cell migration assay with U2OS cells.

ATM was depleted by short-hairpin RNA and cells were grown in medium under puromycin to select infected cells.

ATM protein levels were assayed by WB.

Cells were maintained in cell culture Petri dishes until the day of the experiment. Immediately before imaging acquisition cells were trypsinized and re-suspended on fibronectin-coated 35mm round glass bottom dishes. Cells were diluted to ensure that each cell could move freely on the surface throughout the imaging acquisition.

25 fields of view were acquired for each culture dish and 4 dishes were analyzed for each experiment (two for shControl and two for shATM cells).

Cells were captured with a bright-field NIKON Eclipse TE2000-E microscope equipped with a Prior Stage and CascadeII-512 camera (Photometrics) Objective Plan Fluor 20x/0.5 and the incubator OKOlab. Images were acquired every 2 minutes for 16hours cells were maintained at 37°C in an atmosphere of 5% CO_2.

The cell tracking was performed manually using the MtrackJ tool of ImageJ and around 100 cells were analyzed for each condition.

4. RESULTS

The aim of this study is to investigate the potential role of ATM in the regulation of nuclear and cellular plasticity.

As described in the introduction, increasing observations are pointing to a function of the DDR proteins, including ATM and ATR, in cytoplasmic pathways.

Among the cytoplasmic pathways, the regulation of cytoskeletal proteins is emerging as an intricate network interacting with the DDR.

Our group recently showed that ATR mediates a response to mechanical stress by relocating at the nuclear envelope suggesting that functions of ATR could be involved in the control of cell plasticity in response to structural deformations (Kidiyoor et al, 2016; Kumar et al, 2014).

Here we explore the relation between ATM and cell mechanics using a variety of techniques to study the mechanical properties of the cells, their plasticity and their ability to migrate across constrictions. We take advantage of atomic force microscopy, micro-channel devices for 3D migration, electron microscopy of cellular ultrastructure and immunofluorescence to investigate the consequences of ATM dysfunction at the mechanical level. Finally, we performed mass spectrometry analysis to identify cytoskeletal and structural proteins interacting with ATM.

4.1 ATM influences cell plasticity measured by Atomic Force Microscopy (AFM).

Atomic force microscopy (AFM) has been widely used to analyze the elastic properties of cells (Cross et al, 2007; E et al, 1998; Li et al, 2008; Trache & Meininger, 2008).

This system is based on the interaction of the tip of a cantilever with the cell surface. When the tip encounters the cell surface, the contact generates a force causing the deflection of the cantilever that can be optically measured by a photosensitive detector and converted into an interaction force (Figure 9A).

The power of AFM relies on the possibility to capture the mechanical properties of living cells growing in culture medium under controlled temperature.

The process to measure cell stiffness requires three steps: (i) the approach, when the AFM tip is positioned close to the cellular surface, (ii) the compression step, when the tip is indented into the cell surface, and finally (iii) the decompression step, the tip is retracted to allow extension of the sample surface. (Yallapu et al, 2015). The result of these measurements is a force-indentation curve (Figure 9A) that is converted into the Young's modulus of the cell surface.

Young's modulus is also known as elastic modulus, and defines the mechanical properties of a linear elastic material (in this case an adherent cell). If the cell is stiffer, a higher force will be required to indent the cell; the Young's modulus of the cells will be higher. Thus, this value is a measure of the stiffness of a material.

The deformability of cells, measured by AFM, is associated with several cell functions. Increased cell stiffness is associated with differentiation, aging and disease states (Haase & Pelling, 2015).

The cellular stiffness seems to correlate with the structure of actin cytoskeleton; indeed actin depolymerization, induced by different drugs, was shown to cause a strong reduction of cell stiffness while this was not observed with microtubule targeting agents (Ketene et al, 2012; Rotsch & Radmacher, 2000). Thus, changes of cell stiffness, detected by AFM measurement, may indicate alterations of the cytoskeletal organization.

Recent studies in our lab showed that ATR depletion increases the softness of cells and nuclei, suggesting that ATR influences nuclear plasticity causing nuclear envelope invaginations and chromatin condensation (Kidiyoor et al., unpublished). Thus, we asked whether ATM could play a similar function.

To address the impact of ATM on the mechanical properties of cells, we measured the stiffness of HeLa cells treated with ATMi KU-60019 for 2 hours or overnight. HeLa cells were grown at 80% confluence on 24mm round coverslips, treated with ATMi for the indicated times, and finally analyzed with AFM. Cell indentation was performed at the center of the cells as described in material and methods. We found that overnight treatment with ATMi resulted in a significant increase of cell stiffness (Figure 9B).

To exclude that this phenotype was associated with a non-specific effect of ATMi treatment, we performed the same experiment in ATM KO HeLa cells generated with cas9. The ATM KO clone showed almost a complete depletion of ATM protein levels (WB in figure 9C). Similarly as observed after 18 hours of ATMi treatment, HeLa ATM KO cells showed a significant increase of cell stiffness (Figure 9C).

These results suggest that ATM might play a role in the regulation of cell mechanics in proliferating cells in the absence of DNA damage or other exogenous sources of ATM activation. Moreover, the consequences of ATM depletion are opposite to the ones observed for ATR, indicating that these kinases play diverse roles in mechanotransduction.

Because similar phenotypes were observed with ATMi treatment or genetic depletion of ATM, its role in this process likely requires the kinase activity of the protein. AFM indentation was carried out on the central part of the whole cell, above the nucleus, which is known to be the stiffer organelle of the cell (Dahl et al, 2008), therefore at this stage it was impossible to address whether ATM was affecting the nuclear or cytoplasmic plasticity.

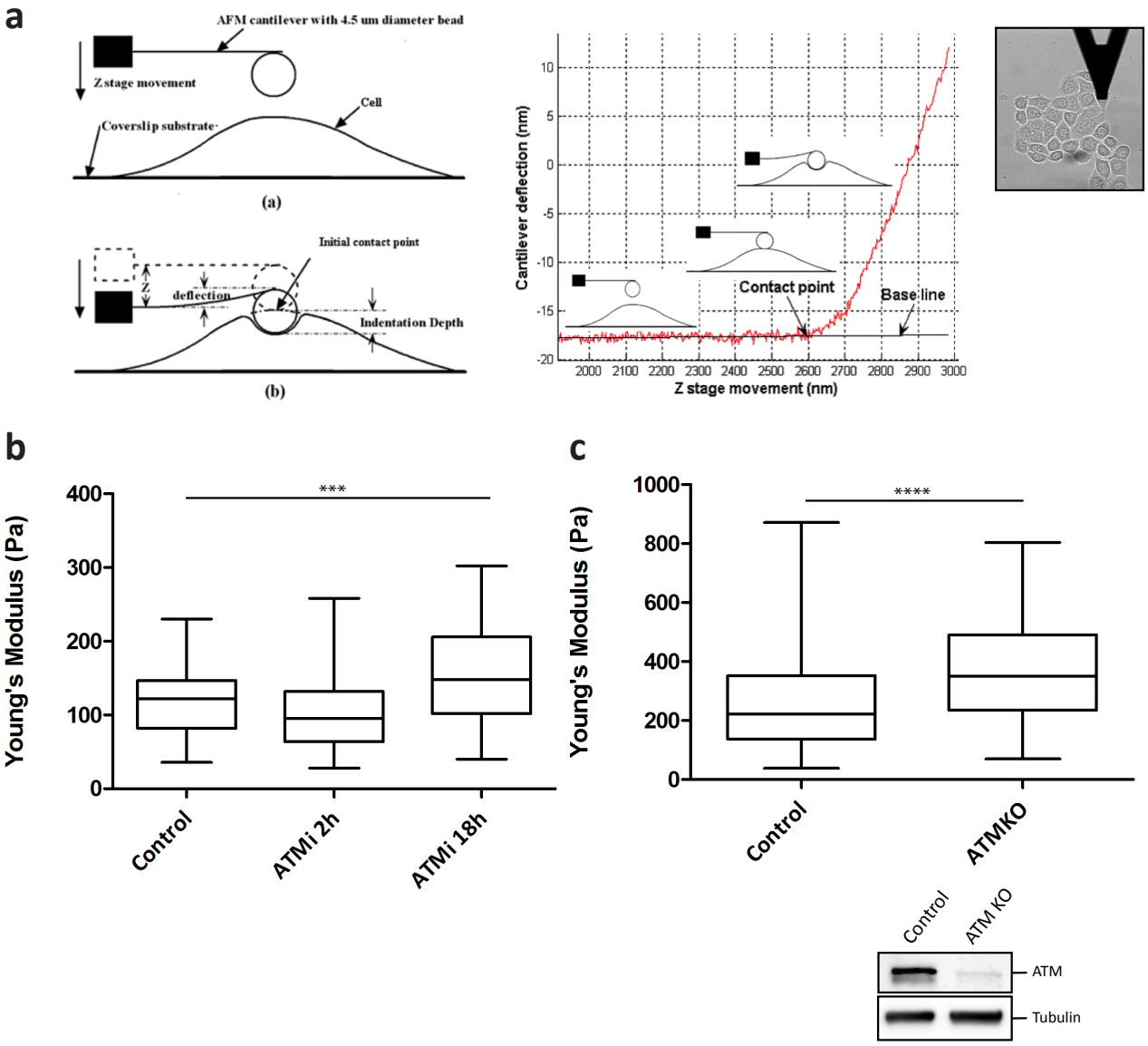


Figure 9. Atomic force microscopy (AFM) analysis of cell stiffness in ATM defective cells.
a) Schematic representation of the indentation of a cell using a 4.5 μm diameter spherical probe (left panel). The illustration shows that the indentation depth is given by the difference between the z stage position and the cantilever deflection. On the right panel is an example of the plot of relative cantilever deflection versus indentation depth curve obtained from the approaching curve of the AFM indentation experiment (figures adapted from (Li et al, 2008)).
At the top right corner an image showing the AFM tip in contact with HeLa cells during the measurements is illustrated.
b) Overnight treatment of HeLa cells with ATMi results in increased cell stiffness. HeLa cells at 60-80% confluence were analyzed as shown in a) in the presence or absence of ATMi KU-60019 3μM for the indicated times (***= P value<0.001).
c) AFM measurements of HeLa ATM KO cells generated with Cas9. ATM KO cells are stiffer compared to control cells, similarly to the results obtained with long ATMi treatment (****= P value<0.0001 Two-tailed t test). The levels of ATM protein were assayed by WB as shown on the bottom panel.

As we detected increased cell stiffness upon inhibition or genetic depletion of ATM in HeLa cells, we further investigated whether this phenotype was reproducible in primary fibroblasts derived from patients suffering of Ataxia-telangiectasia. Human primary fibroblasts derived from a healthy individual (CORIELL IMR90) and A-T patient (CORIELL AG04405) were grown on 24mm round coverslips at 80% confluence and subjected to AFM measurements as previously described (Figure 9A). We found that A-T fibroblasts were significantly stiffer compared to healthy individual fibroblasts (Figure 10) in agreement with the previous data (Figure 10B, C). Although this result is interesting as it suggests that defects in cell mechanics might be conserved in human A-T patients, this analysis requires a higher number of samples in order to be conclusive, due to the difficulties in finding appropriate controls for patient cell lines.

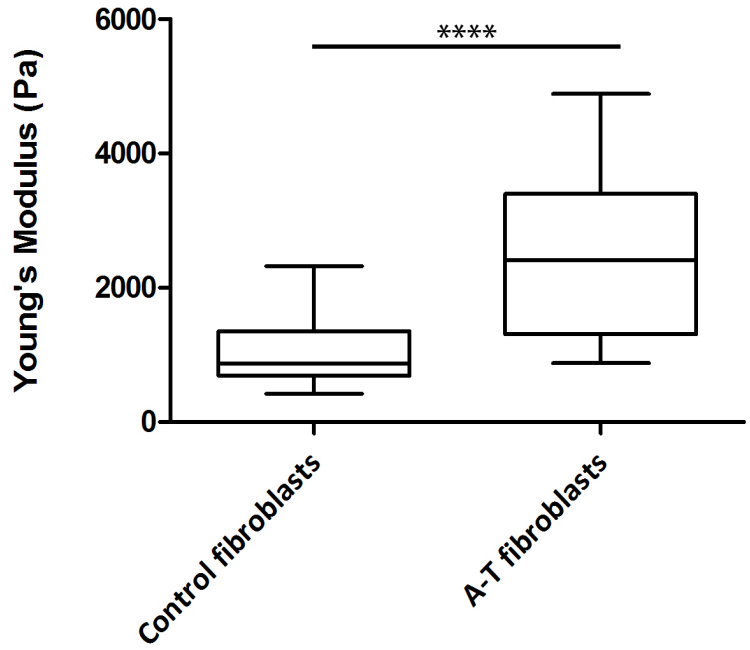


Figure 10. AFM measurements of primary fibroblasts derived from healthy individual and A-T patient.
Fibroblasts derived from A-T patients are stiffer compared to the control (****= P value<0.0001 Two-tailed t test).

4.2 ATM depletion alters the nuclear shape.

Because the cell nucleus is the stiffer organelle of the cell (Dahl et al, 2008), we hypothesized that the major contribution to our AFM indentation analysis could arise from altered nuclear shape and mechanics in the absence of functional ATM. The nucleus of most cells is round or oval, with nuclear shape alterations being found in specialized cell types or in association with various disease states.

Neutrophils are one of the cell types exhibiting deformed nuclei under physiological conditions, and this feature is associated with their ability to migrate towards the site of infections (Rowat et al, 2013).

Aberrant nuclear morphology is typically found in diseases in which lamina proteins are mutated, called laminopathies (Capell & Collins, 2006).

The nuclear lamina is strongly implicated in maintaining the spherical shape of the nucleus. Defects in nuclear lamina are found in premature aging syndromes and also in normal human aging causing deformation of the nuclear envelope (Brandt et al, 2008; Eriksson et al, 2003). Nuclear shape alterations are also common in cancer cells (Zink et al, 2004).

Together with lamins, the endoplasmic reticulum and lipid sytnthesis can also influence the structure of the nuclear membranes (Golden et al, 2009; Matynia et al, 2002; Siniossoglou et al, 1998).

We analyzed the nuclear shape of HeLa cells after depletion of ATM with short-hairpin RNA. HeLa cells were infected with lentivirus as described in materials and methods, selected with puromycin and tested by WB for ATM protein levels.

The generated cell lines, shControl and shATM HeLa, were grown in normal medium under puromycin selection and plated on coverslips at approximately

60% confluence. The cells were fixed for immunofluorescence analysis and the nuclei were stained with DAPI staining and Alexa488-conjugated anti-lamin A/C antibody.

DAPI staining marks the DNA inside the nucleus, while lamin A/C stains the whole nucleus and accumulates at the nuclear periphery, allowing the visualization of nuclear membrane invaginations. For each sample, 200 fields of view were automatically acquired using a multi point acquisition tool. The details of the imaging acquisition are described in materials and methods. 300 cells/sample were analyzed and the number of cells with altered nuclear shape was manually counted. We found that shATM HeLa cells had an increased number of nuclei with aberrant morphology due to nuclear envelope invaginations and membrane blebbing (Figure 11A, B). To overcome any possible biased interpretation caused by manual counting, we repeated the analysis using an ImageJ semi-automated macro. 150 cells/sample were analyzed measuring the perimeter and the circularity of the nucleus.

The nuclear circularity is a parameter measured by the macro; a value equal to 1 indicates that the analyzed structure (in this case the nucleus) is a perfect circle. The perimeter, instead, is a measure of the length of the boundary of the nucleus. If the nuclear shape is altered without changing the total area of the nucleus, the perimeter remains unchanged, suggesting the presence of nuclear membrane invaginations.

These measurements confirmed the previous manual analysis; indeed the circularity of shATM HeLa cells was significantly decreased compared to the shControl HeLa without altering the nuclear perimeter (Figure 11C). Similar results were obtained with shControl and shATM U2OS cells (data not shown).

Together, these data suggest that ATM depletion alters the shape of the nucleus causing an increase of membrane invaginations similarly as observed in laminopathies and other pathological situations.

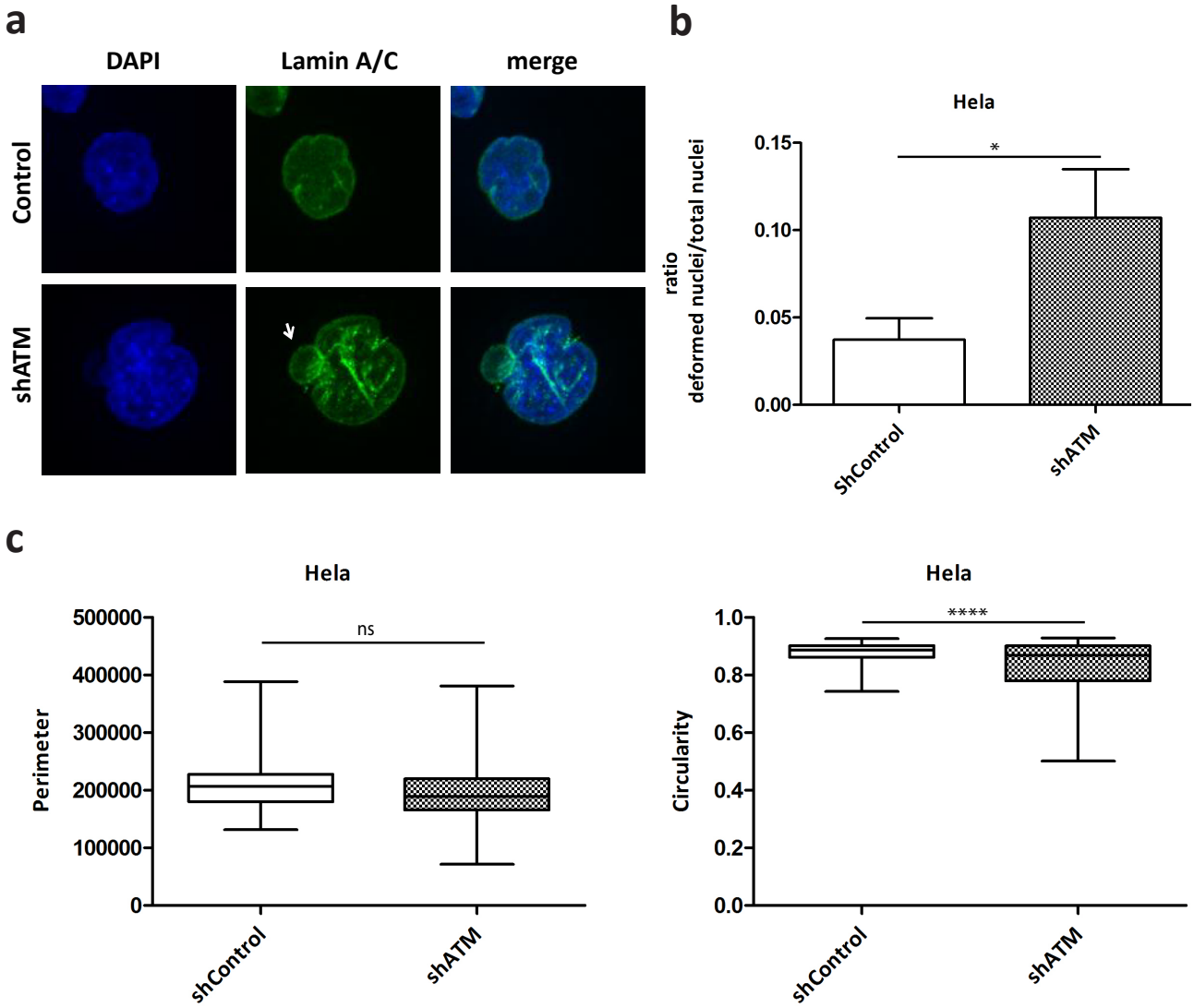


Figure 11. Analysis of nuclear shape in shATM HeLa cells.
a) Z stacks maximum projections of HeLa nuclei stained with DAPI and anti lamin A/C antibody. Immunofluorescence was used to analyze the nuclear shape of shATM cells, the white arrow marks a deformed nucleus in shATM cells. 200 images were acquired randomly for each slide-glass.
b) Manual quantification of 300 cells/condition showing the increased number of nuclei with membrane invaginations in shATM sample.
c) Summary of nuclear morphology analysis using ImageJ semi-automated macro. The results show that depletion of ATM mildly affects the nuclear perimeter of cells, while nuclear circularity is decreased. 150 cells have been analyzed for each condition using the macro.
*= P value<0.05 Two-tailed t test
****= P value<0.0001 Two-tailed t test

4.3 ATM depletion does not affect the expression of lamins in our experimental conditions.

Misshapen nuclei in ATM defective cells were previously described in the study of Pascale Bertrand (Barascu et al, 2012). Lack of ATM caused overexpression of lamin B1 in lymphoblasts or primary fibroblasts derived form A-T patients resulting in alteration of the nuclear shape. Increased lamin B1 levels correlated with the accumulation of ROS and activation of p38 MAPK in A-T cell lines (Barascu et al, 2012). Lamin B1 is one of the major components of the nuclear lamina, together with lamin A/C and lamin B2. Lamins are type V intermediate filaments that interact with the inner nuclear membrane and are responsible for the mechanical stability of the nucleus. Alterations of lamin levels are known to affect the nuclear stiffness. For example loss of A-type lamins reduces nuclear stiffness. Conversely, accumulation of lamin A and its mutant form, in Hutchinson Gilford progeria syndrome cells, results in stiffer nuclei. Lamin B1 overexpression in autosomal dominant leukodystrophy (ADLD) fibroblasts was found to increase the number of misshapen nuclei and the nuclear stiffness measured by AFM indentation on isolated nuclei (Ferrera et al, 2014). In the same study, exogenous expression of lamin B1 caused an increase in nuclear stiffness in HEK293 and N2a neuronal cells (Ferrera et al, 2014).

Because ATM deficiency was associated with increased lamin B1 levels (Barascu et al, 2012), and lamin B1 overexpression caused stiffer nuclei (Ferrera et al, 2014), we investigated whether the increased stiffness and nuclear shape defects observed in ATM depleted cells (Figure 9B,9C, 10) were due to abnormal expression of lamins. We assayed by WB the protein levels of lamin A/C and lamin B1 in HeLa cells treated with ATMi KU-60019 3μM overnight. We could not detect significant differences in lamin expression compared to the control (Figure 12). Similar results were obtained after depletion of ATM with short hairpin RNA in HeLa and U2OS cells (Figure 12). Moreover, ATM KO HeLa and A-T primary fibroblasts that showed increased stiffness in the AFM indentation experiments, had comparable levels of lamin B1 and lamin A/C with control cells (Figure 12). Lamin B1 levels were extremely low in human primary fibroblasts and could not be measured. Although these data seem discordant with the previously-cited publication (Barascu et al, 2012), in their study the majority of experiments were carried out using lymphoblast cell lines from healthy individual and A-T patients, thus the discrepancy could be related to the model cell line.

In conclusion, our results suggest that, in our experimental conditions, the increased cell stiffness observed in HeLa treated with ATMi, HeLa ATMKO, and A-T fibroblasts, is not associated with overexpression of lamin B1 neither to deregulation of Lamin A/C. We cannot exclude that ATM depletion could still influence the organization of lamins, without affecting their expression, leading to altered nuclear shape and stiffness.

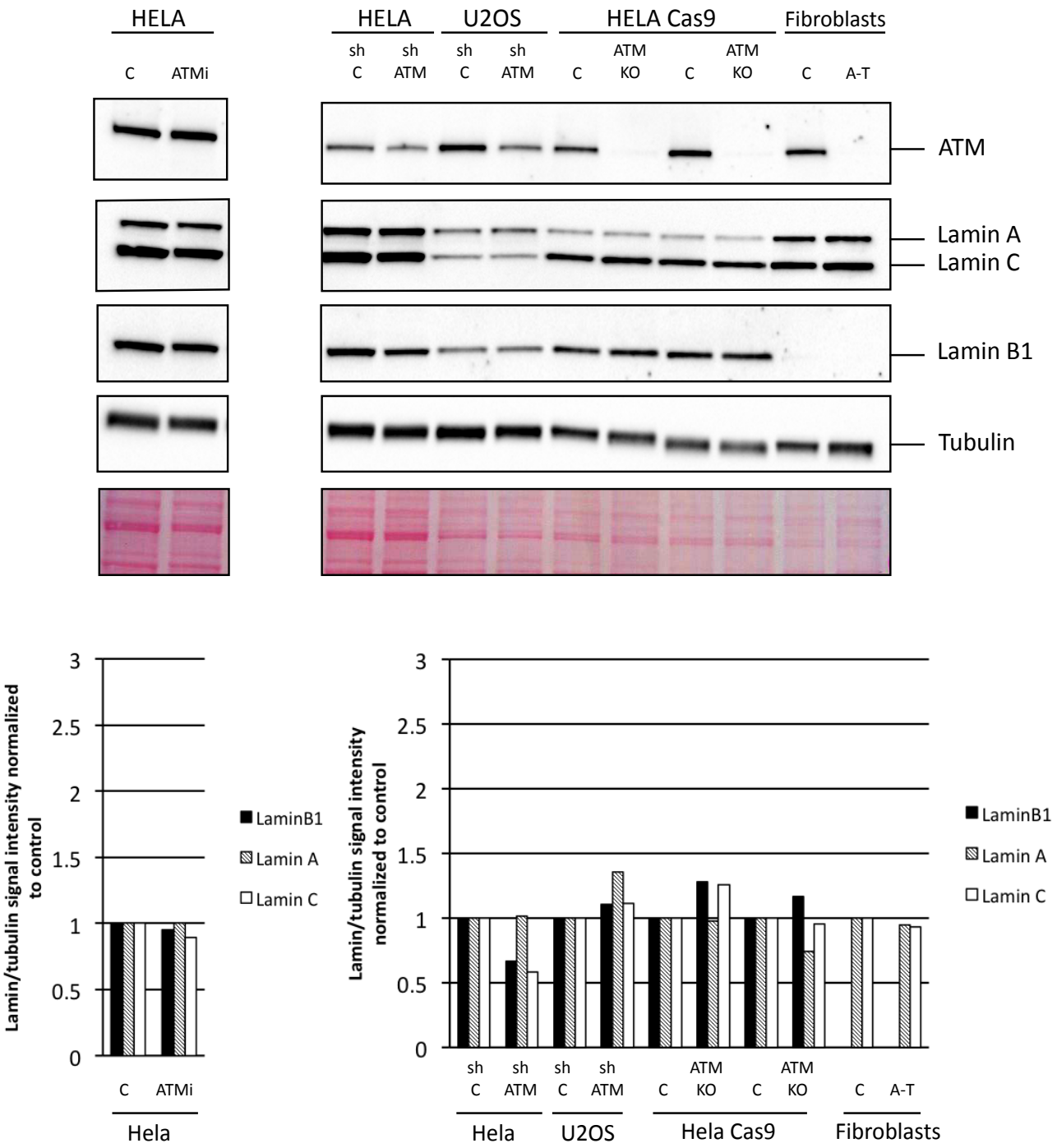


Figure 12. ATM inhibition or depletion does not significantly affect lamin B1 and lamin A/C protein levels in our conditions.

The endogenous protein levels of LaminB1 and Lamin A/C were measured by WB. Whole cell extracts were prepared from different cell lines in which ATM was inhibited, depleted by short hairpin RNA, knocked out with cas9, and in primary fibroblasts of A-T patients. We did not observe significant and reproducible alterations of lamin protein levels in these cells compared to the control. ATMi: KU-60019 3µM overnight.

Bottom panel: quantification of the signals performed using Imagelab volume tools.

Lamin protein levels were normalized to tubulin expression level for each sample and finally normalized to the control. For the primary fibroblasts, laminB1 quantification was not performed due to the extremely weak signals.

4.4 ATM influences cell stiffness independently of nuclear plasticity.

To address whether the impact of ATM on cell mechanics was related to alterations of nuclear plasticity, we performed an AFM indentation analysis on isolated nuclei. The process of nuclei isolation separates the cell nucleus from the rest of the cytoplasm and thus disconnects the interactions between cytoskeleton and nuclear membrane. Previous analysis, using AFM on isolated nuclei, showed that nuclear stiffness is affected by the surrounding cytoskeleton. Nuclei measured in intact cells appeared stiffer compared to isolated nuclei, suggesting significant contributions from adhesive forces, the underlying cytoskeleton and cytosolic factors (Ferrera et al, 2014; Liu et al, 2014). Measuring the mechanical properties of isolated nuclei is a way to address the contribution of chromatin and nucleoskeleton to nuclear deformability. Therefore, we measured the stiffness of HeLa isolated nuclei in control and ATMi-treated cells. Differently from the whole-cell AFM indentation experiments, ATMi-treated nuclei were not stiffer compared to the control; instead they were slightly softer (Figure 13A). The same experiment was performed in HeLa control and ATM KO isolated nuclei and showed no difference in the nuclear plasticity (Figure 13B).

These results indicate that defects of ATM activity do not alter mechanical forces inside the nucleus arising from chromatin condensation or lamin structure. One possibility is that ATM rather affects cytoplasmic factors, such as the cytoskeleton, that confer increased stiffness.

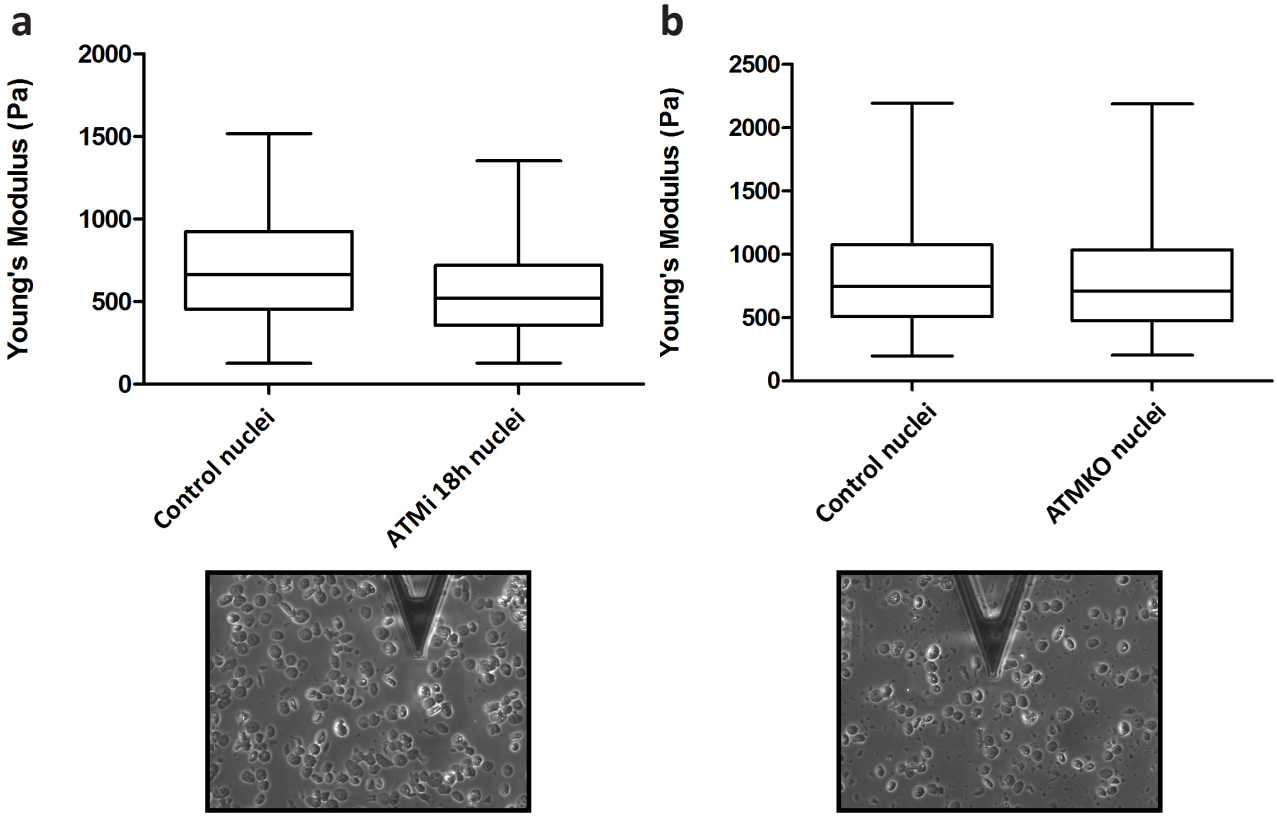


Figure 13. The increased stiffness observed in ATMi-treated cells and ATM KO cells is not due to the nucleus.
a) AFM measurements of isolated nuclei of HeLa cells in the presence or absence of ATMi KU-60019 3μM. ATM inhibition mildly decreases nuclei stiffness, an opposite effect compared to the one observed in whole cell measurements.
b) The nuclei of ATM KO HeLa cells have the same elastic modulus of control cells.
Bottom panel: pictures taken during the experiment showing the AFM tip and isolated nuclei.

4.5 Analysis of the ultrastructure of ATM defective cells by electron microscopy.

Our results suggested that ATM deficiency causes alterations of cell plasticity possibly associated with structural deformation in the cytosol.

To investigate the effect of ATM depletion on cell structure, we performed electron microscopy (EM) analysis of different cell lines where ATM was depleted.

We knocked down ATM by short-hairpin RNA in HeLa and U2OS cells, as described in materials and methods, we confirmed the depletion of ATM by western blot. The cells were grown on Mat Tek dishes (P35G-1.5-14-C-GRID) at 80% confluence and the samples were processed for electron microscopy.

The ultrastructure analysis of shATM HeLa cells confirmed the presence of nuclear envelope invaginations of type II as observed by immunofluorescence (Figure 11A, Figure 14a). Type II invaginations involve both the inner and outer sides of the nuclear envelope and differ from the type I invaginations in which only the inner membrane is protruding inside the nucleus.

The EM also revealed the presence of nuclear membrane blebbing (data not shown) confirming our results that ATM deficiency influences nuclear shape.

In agreement with the AFM indentation experiments, suggesting a prominent role of ATM in the mechanical regulation of cytoplasmic component, most of the structural alterations observed in ATM-deficient cells were confined to the cytosol.

Interestingly, accumulation of lipid droplets was clearly evident in shATM HeLa cells compared to the control (Figure 14a).

Lipid droplets were found at higher numbers and their distribution in the cytoplasm was altered, often showing contact with mitochondrial membranes (Figure 14a, panel 1).

Another phenotype associated with ATM depletion was the accumulation of autophagosomal structures in the cytosol (Figure 14a, panel 2).

Finally, in agreement with previous publications (Ambrose et al, 2007; Valentin-Vega et al, 2012), we found alterations in mitochondrial structures. The mitochondria of HeLa shATM had elongated shapes and often presented deformed mitochondrial cristae (Figure 14a, panel 3).

These abnormalities were not specifically restricted to HeLa cells, since the knockdown of ATM in U2OS cells reproduced identical phenotypes (Figure 14b).

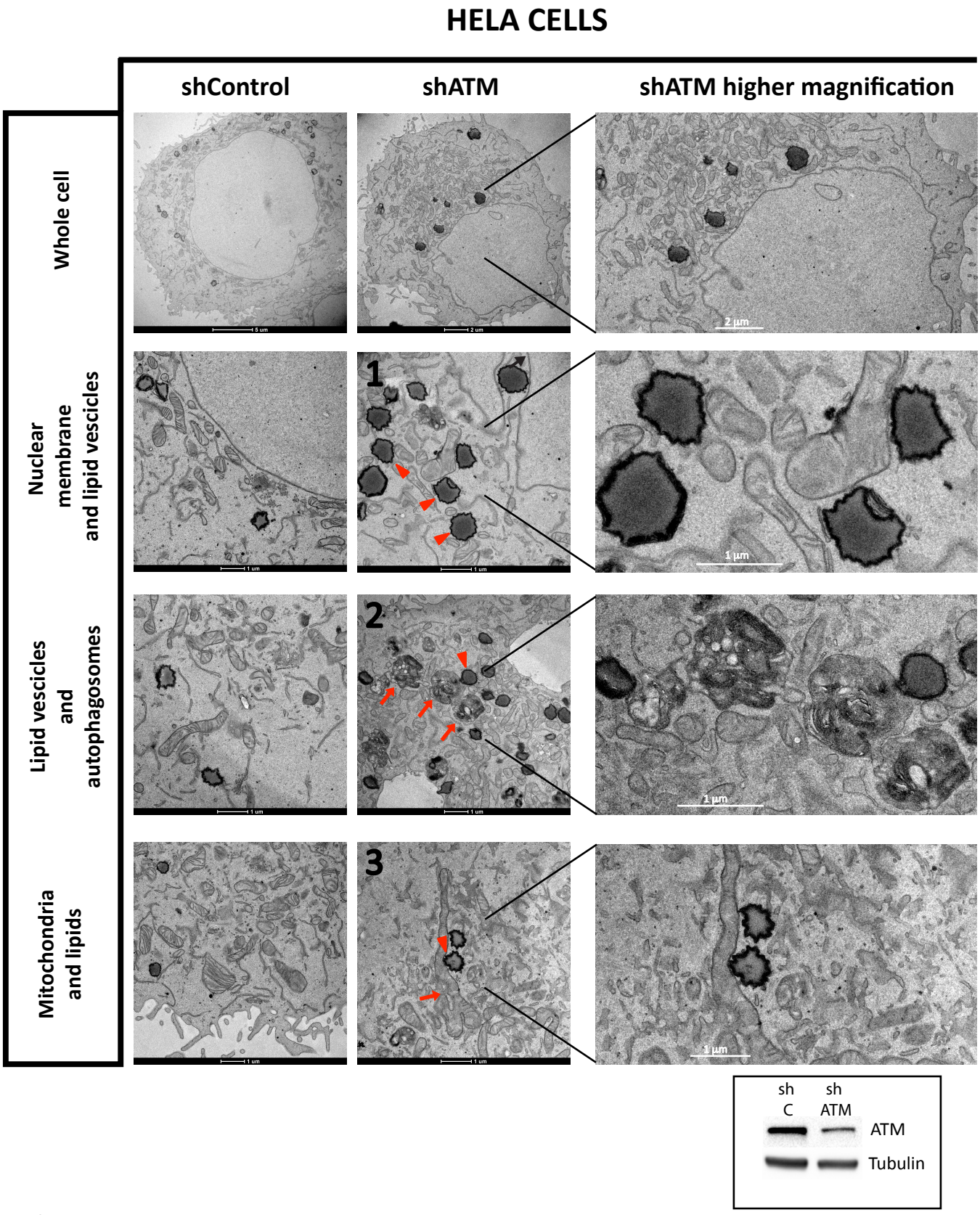

HELA CELLS
shControl
shATM
shATM higher magnification
Whole cell
Nuclear membrane and lipid vescicles
Lipid vescicles and autophagosomes
Mitochondria and lipids
1
2
3
2 µm
1 µm
1 µm
1 µm
sh C
sh ATM
ATM
Tubulin

Figure 14a. EM analysis of the morphology of HeLa shATM cells.
a) EM analysis of cellular ultrastructure of HeLa shATM cells. Control cells have a normal morphology of the nucleus and nuclear membrane, mitochondria and other cytoplasmic organelles are normally distributed in the cytoplasm and do not show abnormalities. Similar observations were found in U2OS shATM (data shown in supplementary results).
HeLa shATM cells present alterations of the nuclear shape with type II invaginations of the nuclear membrane and micronuclei formation (1, arrows). Moreover these cells display many alterations in the cytosol: accumulation of lipid droplets (1,2 arrowheads), increase of autophagosomal structures (2, arrows), elongated mitochondria and contacts between lipids and mitochondria (3, arrows and arrowheads).
ATM protein levels were assayed by WB as shown on the bottom panel.

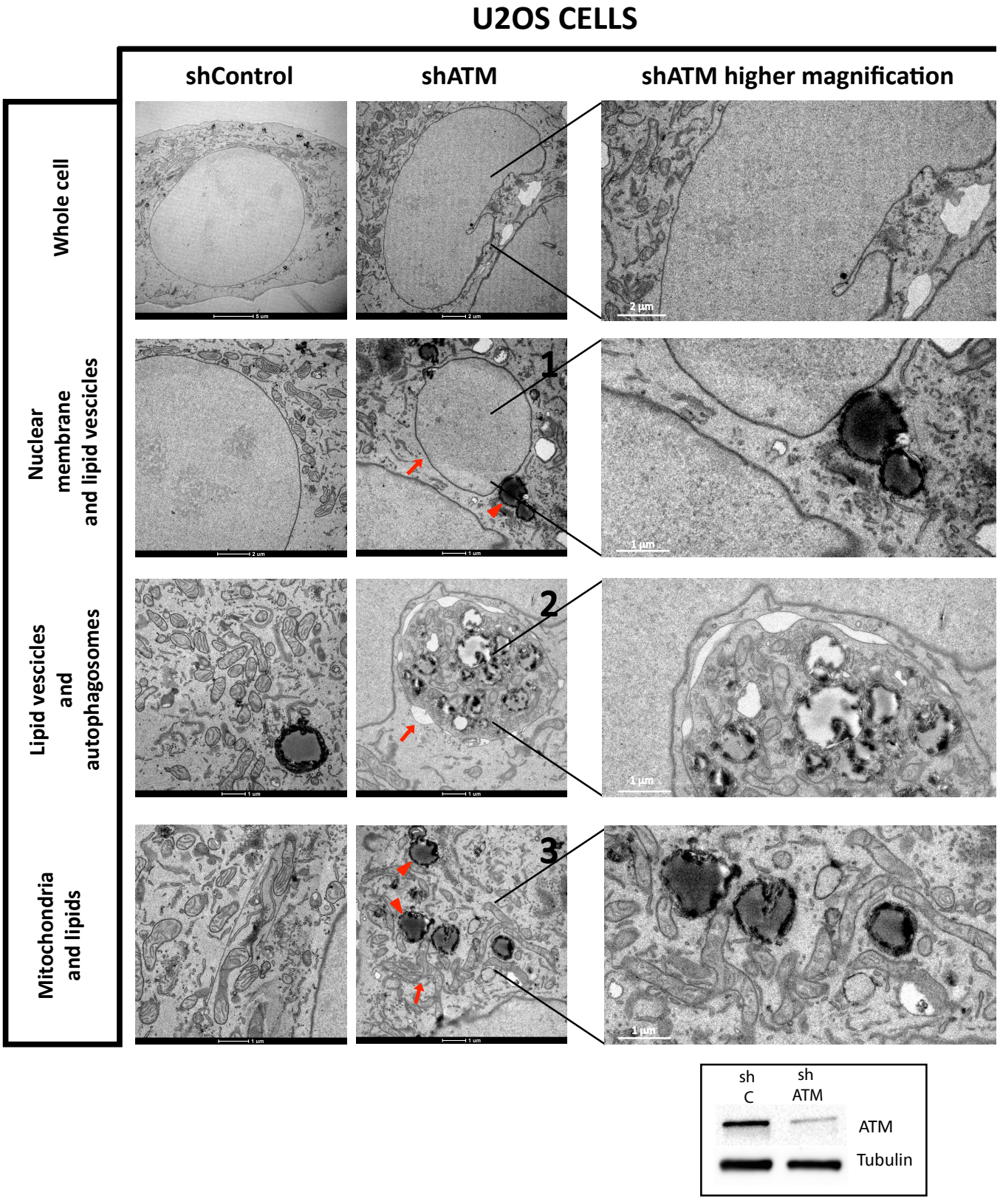

U2OS CELLS
shControl
shATM
shATM higher magnification
Whole cell
Nuclear membrane and lipid vescicles
Lipid vescicles and autophagosomes
Mitochondria and lipids
1
2
3
2 µm
1 µm
sh C
sh ATM
ATM
Tubulin

Figure 14b. EM analysis of the morphology of U2OS shATM cells.
a)EM analysis of cellular ultrastructure of U2OS shATM cells. Control cells have a normal morphology of the nucleus and nuclear membrane, mitochondria and other cytoplasmic organelles are normally distributed in the cytoplasm and do not show abnormalities. Similar observations were found in U2OS shATM (data shown in supplementary results).
ShATM cells present alteration of the nuclear shape with type II invaginations of the nuclear membrane and micronuclei formation (1, arrows). Moreover these cells display many alterations in the cytosol: accumulation of lipid droplets (1,2 arrowheads), increase of autophagosomal structures (2, arrows), elongated mitochondria and contacts between lipids and mitohondria (3, arrows and arrowheads).
ATM protein levels in the knockdown were assayed by WB as shown in the bottom panel.

Since we performed the EM analysis in immortalized cancer cells expressing artificially-reduced ATM levels by shRNA, it is possible that these alterations could be caused by the procedure of lentiviral infection or could be related to a specific function of ATM in immortalized cancer cells.

Thus, the EM analysis was also carried on human primary fibroblasts derived from a patient suffering from Ataxia-telangiectasia disease (CORIELL AG04405).

Interestingly, all the structural aberrations described in shATM HeLa and U2OS cells were recapitulated in A-T fibroblasts in a similar fashion (Figure 15). These results indicate that ATM dysfunction influences the structure of nuclear envelope, mitochondria, lipid droplets and autophagosomes also in patient cell lines.

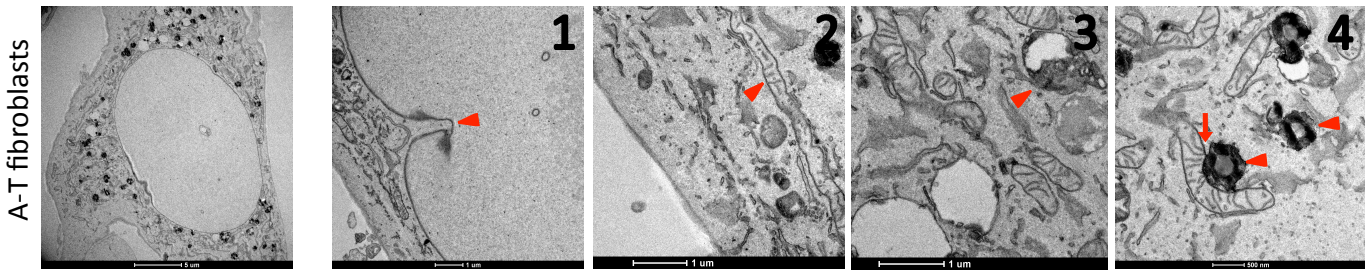


Figure 15. The EM cellular ultrastructure of A-T fibroblasts.
EM samples obtained from A-T primary fibroblasts show similar features as observed for shATM HeLa cells (FIgure 6). Nuclear envelope invaginations of type II (1, arrowhead), elongated mitochondria with alterations of mitochondrial cristae (2, arrowhead), accumulation of autophagosomes (3, arrowheads), accumulation of lipid droplets and contacts between mitochondria and lipids (4, arrow and arrowheads).

Our observations connecting ATM and cell plasticity, measured by AFM analysis, suggested that ATM could play a role in the regulation of cytoskeletal components.

In agreement with this hypothesis we found accumulation of actin stress fibers in shATM HeLa cells and altered organization of actin filaments in proximity to the plasma membrane of A-T fibroblasts (Figure 16).

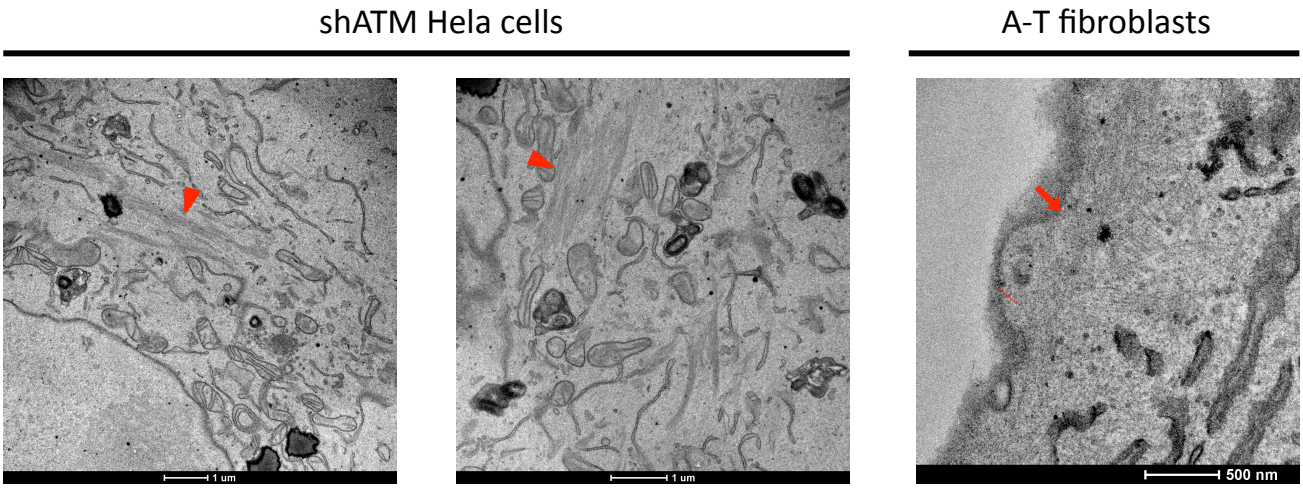


Figure 16. Accumulation of actin stress fibers in HeLa shATM and A-T fibroblasts.
The images show accumulation of actin stress fibers (arrowhead) and altered organization of actin filaments (arrow) in the cytoplasm of HeLa shATM and A-T primary fibroblasts respectively.

4.6 ATM inhibition impairs the movement and survival of cells during interstitial migration.

It has been shown that cellular stiffness has significant effects on cell migration (Lange & Fabry, 2013). Cell motility in vivo usually occurs across three-dimensional (3D) tissue environments and is a fundamental phenomenon that is essential for embryonic development and throughout life (Lange & Fabry, 2013). Cell migration participates in numerous physiological and pathological processes including wound healing, immune cell trafficking and tumor metastasis.

Three-dimensional migration differs from 2D migration because it requires deformation of the cell body and the nucleus to allow cellular passage through the available spaces (Liu et al, 2016). To resolve this problem, cells can adopt two strategies, they can modify the extracellular matrix through proteolytic degradation or they adapt their shape and stiffness to penetrate small pores. The second strategy imposes strong deformations of the cell nucleus, which can become a rate-limiting factor for the migration across constrictions (Davidson et al, 2014).

Diverse studies showed that both nuclear and cytoskeletal components are required for nuclear squeezing and successful migration (Liu et al, 2016).

ATM defective cells showed altered cell plasticity arising from structural alterations in the cytosol. A physiological relevance of this phenotype could be the impairment of cell migration, thus we studied the effect of ATM depletion on 3D migration.

We took advantage of a micro-channel device that allows the imaging of cells during three-dimensional migration. The channels, made of Polydimethylsiloxane (PDMS) stuck to glass, are produced using silicon molds (Figure 17A).

Two different channel designs were used in order to study cell migration in the presence or absence of constrictions (Figure 17B). We performed our experiment with HeLa and U2OS cells and we found that the optimal constriction size for these cells was 4μm. The channels were mounted on chamber slide glasses and cells were seeded as described in Figure 17C.

As a pilot experiment, we analyzed HeLa H2B-mCherry cells migrating inside the channels in presence or absence of caffeine 1mM (Figure 18A). Caffeine is known to inhibit ATM at this concentration (Sarkaria et al, 1999). We observed that the number of cells entering inside the channels was strongly reduced in presence of caffeine (Figure 18B). Moreover, caffeine-treated cells showed increased cell death following nuclear deformation during the squeezing (Figure 18C). The number of migrating cells was normalized to the number of analyzed channels for each condition, while the number of dead cells was normalized to the number of cells migrating into the channels. Dead cells were identified because their nuclei showed deformation and chromatin condensation and the cells ceased to move.

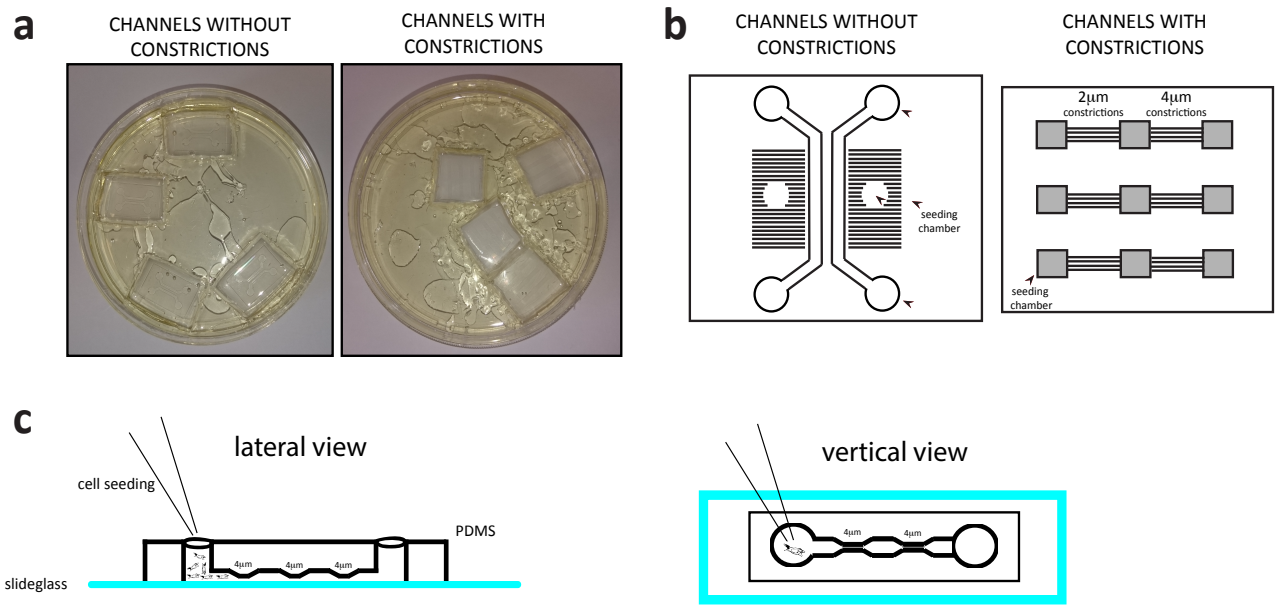


Figure 17. Description of microchannel devices used for 3D migration analysis and cell seeding process.

a) Pictures of the mold used to produce PDMS channels with and without constrictions (Matthieu Piel's lab). b) Schematic representations of the channel designs obtained for each mold. Black lines representing channels and seeding chambers are depicted by arrows. Where not indicated, the width of the channels is 12µm and the height is 5µm. c) Cell seeding process. Cells are seeded in the 3D culturing space enclosed by PDMS and slideglass through the seeding chambers. The loading happens between 12 hours (for HeLa cells) and 4 hours (U2OS) before imaging. Before cell seeding, the culturing space is coated with fibronectin O/N and then filled with medium O/N (any treatment or drugs used are already added at this step). Lateral and vertical views of a representative single channel with 4µm constrictions are shown.

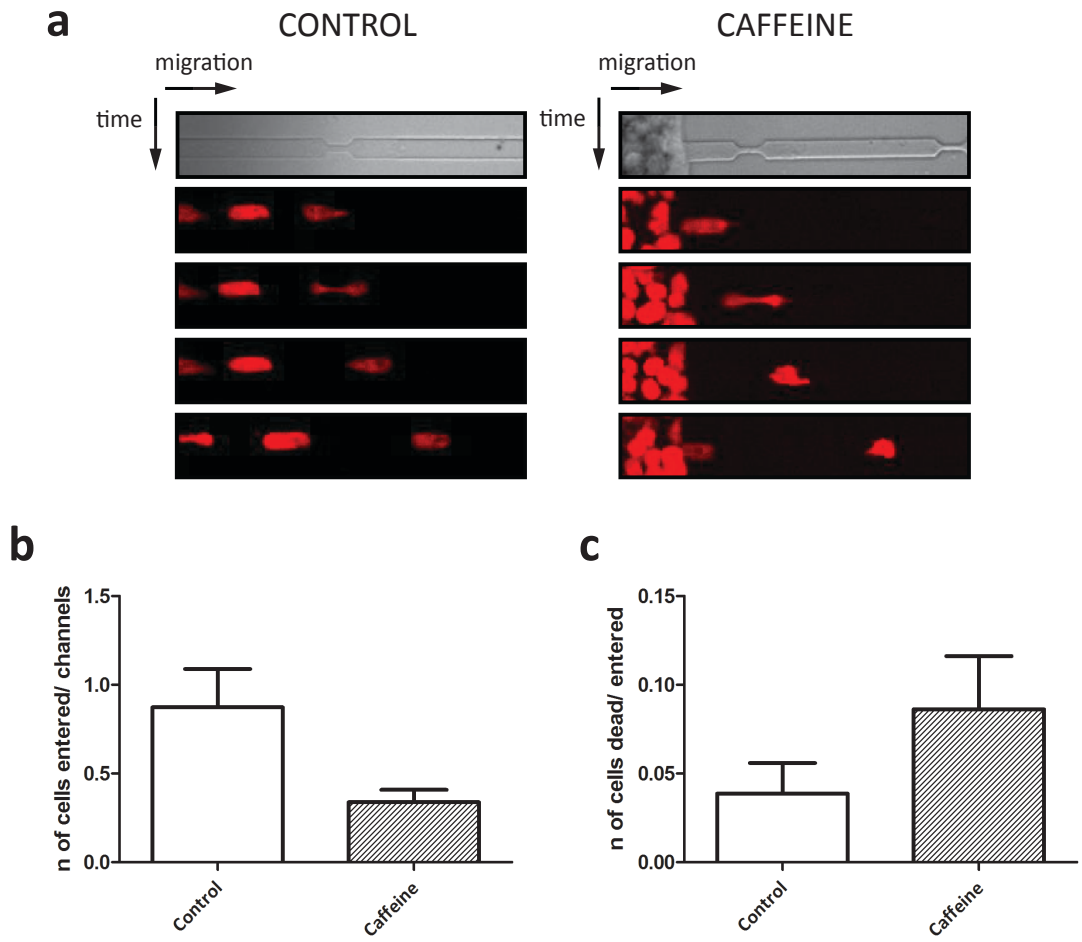


Figure 18. Caffeine treatment impairs movement and survival of HeLa cells during interstitial migration.

a) A representative example of HeLa H2B-mCherry migrating inside the channel device. Projections of four different time points showing one cell migrating across the constriction in control and caffeine-treated cells. Migration of the nuclei was recorded for 18 hours in live cell imaging. Control cells are able to perform 3D migration across 4mm constrictions while cells treated with caffeine 1mM show chromatin condensation and cell death. b) Caffeine treatment reduces the number of cells entering inside the channels (error bars= SEM). c) Caffeine-treated cells have higher frequency of cell death inside the channels (error bars= SEM).

Because caffeine treatment could affect the function of other PIKK kinases such as ATR or DNA-PK, we tested the effect of the ATM specific inhibitor KU-60019 on migration and survival of cells.

For this experiment we used straight channels (no constriction) as a control to exclude any possible effects on cell survival related to the ATMi treatment itself or to imaging conditions.

HeLa H2B-mCherry cells were loaded into channels in the presence or absence of 3μM ATMi KU-60019 (Figure 19A). ATMi caused a significant reduction of the total number of cells migrating through the channels, and this phenotype was observed also in straight channels (Figure 19A). However ATMi strongly increased the cell death only in the presence of constrictions (Figure 19A). These data indicate that selective inhibition of ATM affects the movement of cells regardless of the presence of constrictions, while ATM activity is required to survive interstitial migration.

Similar observations were confirmed with U2OS 53BP1-GFP cells (Figure 19B). U2OS cells migrate faster compared to HeLa; this allowed us to seed cells just 4 hours before imaging acquisition reducing the timing in the presence of ATMi. We confirmed that inhibition of ATM impaired cell survival associated to the constrictions (Figure 19B). We did not observe reduction of cell movement in this experiment, likely because of the shorter treatment with the inhibitor and the fast speed movement of U2OS cells.

Finally, to exclude potential non-specific effects caused by the use of an inhibitor molecule, we analyzed control and ATM KO HeLa cells (Figure 19C). In agreement with previous results, genetic deletion of ATM caused cell death specifically in cells migrating across constrictions (Figure 19C).

Although we observed a reduction in cell movement in ATM KO HeLa, this result does not count as statistically significant, thus require additional experiments.

Collectively, these data suggest that lack of ATM activity negatively influences the ability of cells to survive during interstitial migration.

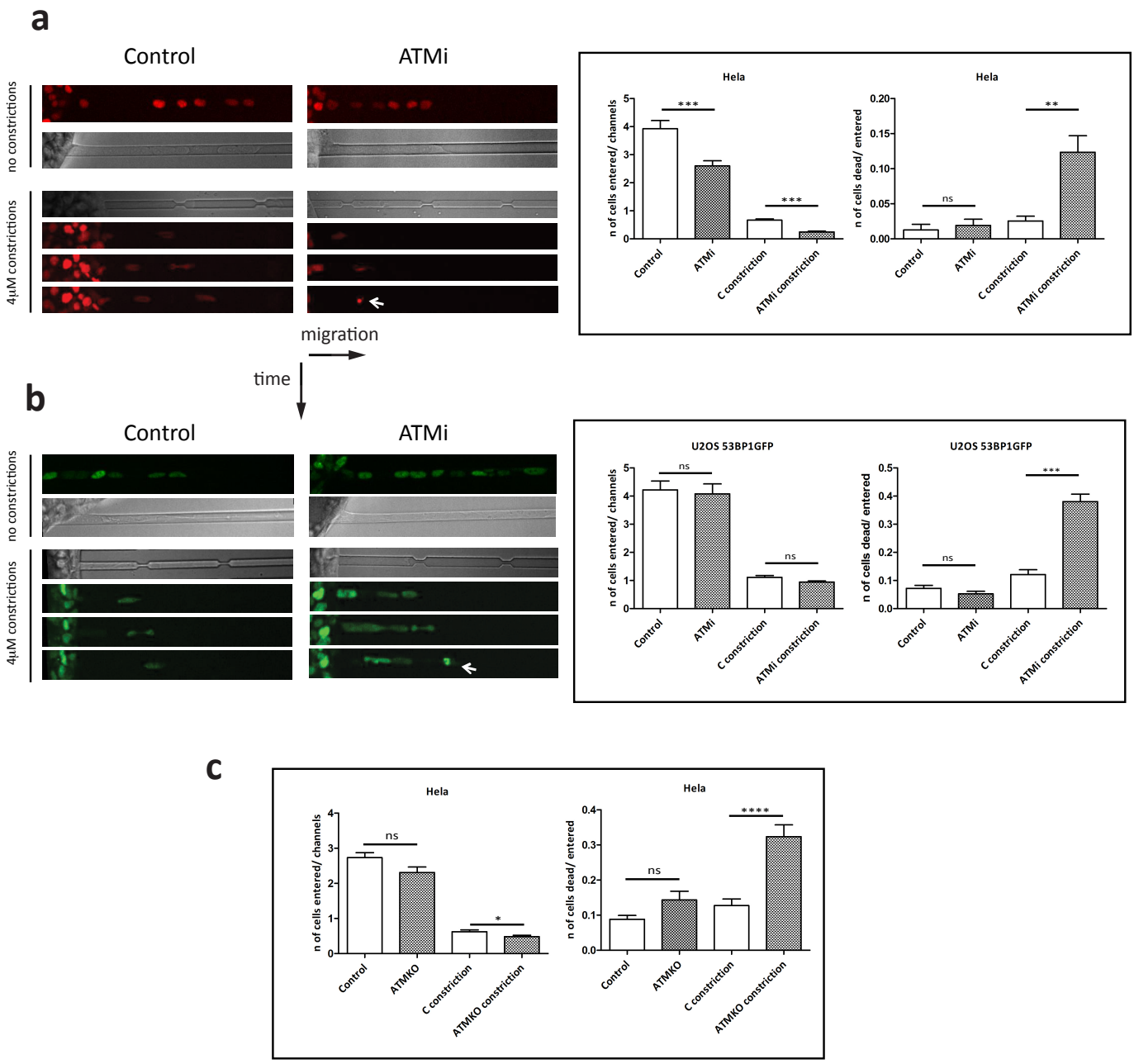


Figure 19. ATM is required for cell movement and survival during interstitial migration.
a) ATMi causes a reduction of migration and increases cell death in HeLa H2B-mCherry.
b) ATMi affects cell survival of U2OS 53BP1GFP cells migrating across constrictions. In both cases the phenotype of cell death is observed only in the presence of constrictions. Left panels: representative examples of control and ATMi cells migrating through micro-channels without constrictions and with 4mM constrictions, the white arrow points to dead cells with condensed chromatin. Cells were seeded as described in material and methods. ATMi: KU-60019 3µM. Right panels: bar plots summarize the results obtained from two independent experiments for each cell line and condition tested, error bars: SEM.
c) The migration phenotype was confirmed by the genetic depletion of ATM in Hela ATM KO Cas9 cells. Bar plots show the results for two independent experiments for each cell line.
Statistical analysis was performed with the one-way ANOVA Tukey's Multiple Comparison Test using PRISM to compare all pairs of columns. *= P value<0.05, **= P value<0,01, ***= P value<0.001, ****= P value<0.0001.

4.7 ATM is activated in cells migrating across constrictions.

ATM inhibition resulted in defective interstitial migration suggesting that ATM could play a role during this process. We decided to investigate whether ATM could be activated in cell squeezing across small pores.

We coupled the micro-channel device system to a fluorescence resonance energy transfer (FRET) reporter designed to detect ATM kinase activity in live cell imaging.

This reporter was constructed by the group of Tony Hunter (Johnson et al, 2007) and is based on a plasmid expressing a 12 amino acid peptide of CHK2 encompassing the T68 usually phosphorylated by ATM in the presence of DNA damage. The CHK2 peptide is linked to the phosphothreonine-binding domain of Rad53, FHA2. The CHK2-FHA2 fusion product is placed between CFP (donor fluorophore) and YFP (acceptor fluorophore) (Figure 20).

When ATM is activated, it phosphorylates the CHK2 peptide causing the intra-molecular association with the FHA domain (Figure 20). This conformational change alters the efficiency of energy transfer between CFP and YFP resulting in a reduction of the ratio of yellow and cyan fluorescence intensities (mY/mC). This change can be measured by fluorescence microscopy to monitor the activity of ATM kinase in living cells.

A cytoplasmic and H2B-fused version of the reporter were generated to visualize ATM activity in the whole cell or in the nucleus (Figure 20).

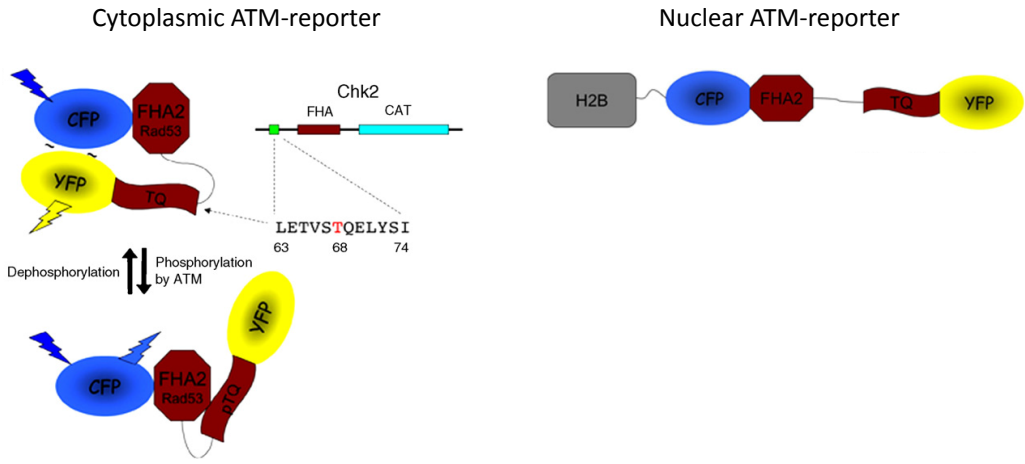


Figure 20. Schematic representations of the cytoplasmic and H2B-fused ATM reporters (images adapted from Johnson et al., 2007).

At first, we tested the activation of ATM using the H2B-fused reporter.

The reporter was transfected into U2OS cells and 48 hours after transfection we performed a control experiment in cells treated with etoposide 30μg/ml to test the reporter in our imaging conditions. The efficiency of transfection was high and transfected cells were growing normally.

We confirmed that DNA damage caused by etoposide treatment was activating ATM causing a decrease in the FRET signal visualized as a shift of the nuclei towards a violet color (Figure 21A), as previously published (Johnson et al, 2007).

Then we tested the H2B-reporter in cells migrating inside straight channels and channels with constrictions (Figure 21B). U2OS cells were transfected with the reporter, cultured for 48 hours and seeded in the channels 4 hour before imaging. We found that cells passing through constrictions were showing ATM activation in the nucleus while cells moving inside straight channels were showing a constant FRET signal (Figure 21B).

Cells were analyzed in the different type of channels during the same experiment using two-chambers slide glasses to avoid possible discrepancies associated with

imaging conditions or cell transfection efficiency. The FRET signal was measured in selected areas of the nuclei in 30 cells/condition as described in figure 21C. Two independent experiments were carried for each condition.

Cells facing constrictions showed a decrease in FRET signal that was significantly higher compared to the background (Figure 21C). Moreover, the number of cells experiencing such variation of FRET was strongly increased in cells migrating in channels with constrictions (Figure 21C).

The same experiment was performed transfecting U2OS cells with the cytoplasmic reporter and showed identical results (Figure 22).

These data suggest that ATM is activated during interstitial migration in cells subjected to mechanical deformation.

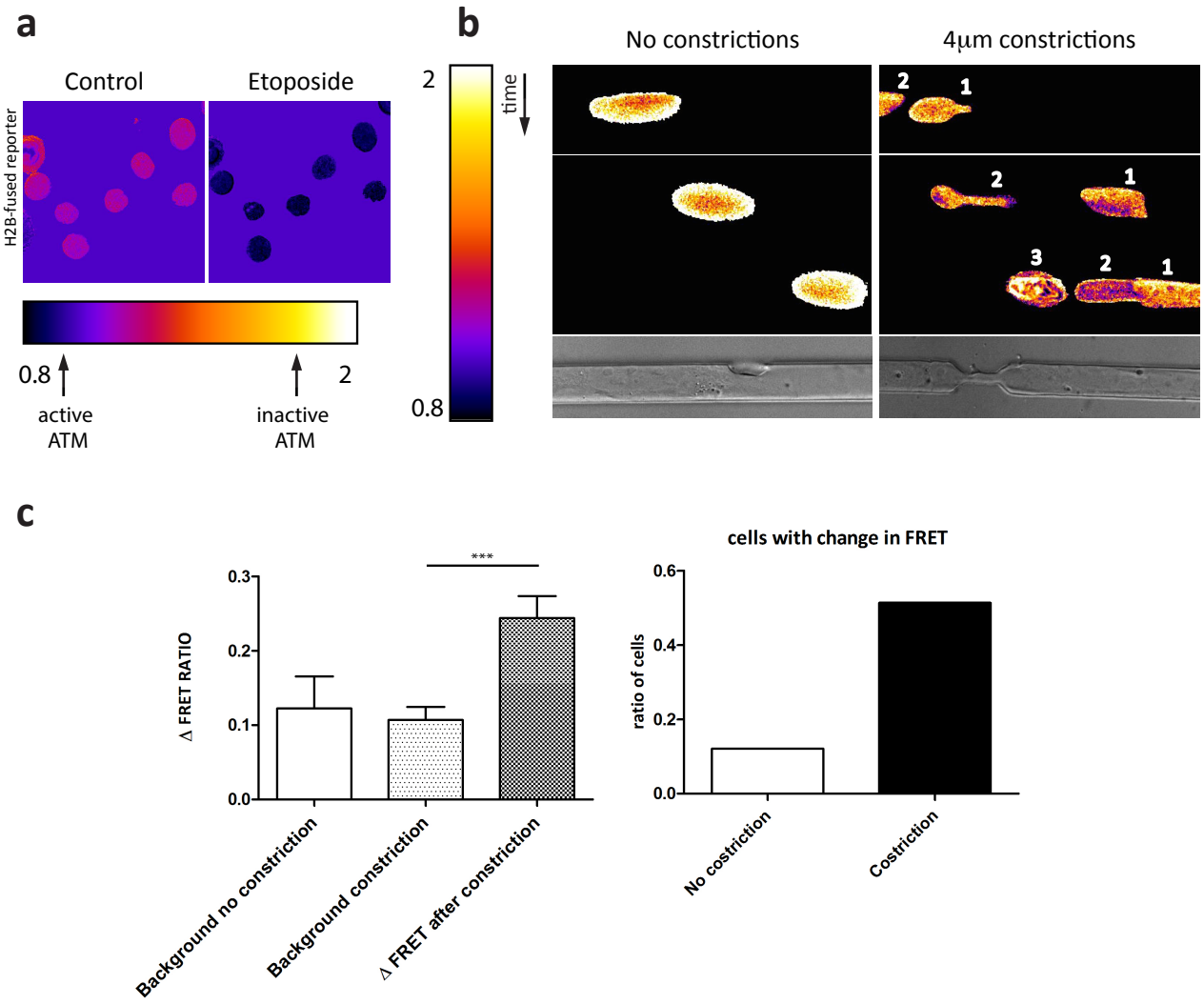


Figure 21. ATM is activated during interstitial migration (H2B-fused ATM reporter).
a) Images showing the change in fluorescence ratio of the H2B-fused FRET sensor upon stimulation with etoposide 30µg/ml for 1hour. The activation of ATM can be visualized in live cell imaging following the decrease of yellow to cyan emission ratio, the appearance of violet color in the images indicates that ATM is active. The upper and lower limits of the FRET: CFP ratio range, are shown on the bottom RATIO colored key (ImageJ software). b) Projection of three different time points of FRET live cell imaging of U2OS cells transfected with the H2B-fused ATM reporter. The nuclear activation of ATM at the constrictions are illustrated (violet spots). The upper and lower limits of the FRET: CFP ratio range are shown on the left in the RATIO colored key (ImageJ software).
Cells were transfected with the ATM reporter 48 hours before the experiment and were seeded inside channels as already described. Images were acquired every 15 minutes for 18 hours (white numbers identify each single cell during time). c) Summary of FRET analysis for two independent experiments. Left panel: the graph shows that the FRET signal is altered in cells that migrate through constrictions (DFRET after constriction) compared to cells in channels without constrictions (background no constriction) or cells in channels with constrictions that do not migrate (background constriction).
The decrease of yellow to cyan emission ratio is significantly higher in such cells compare to the background signal that, instead, is probably due to imaging/samples conditions. Right panel: the number of cells that experience a significant change in FRET ratio is higher inside the 4µm constriction channels. Approximately 30 cells/condition were analyzed for each experiment.

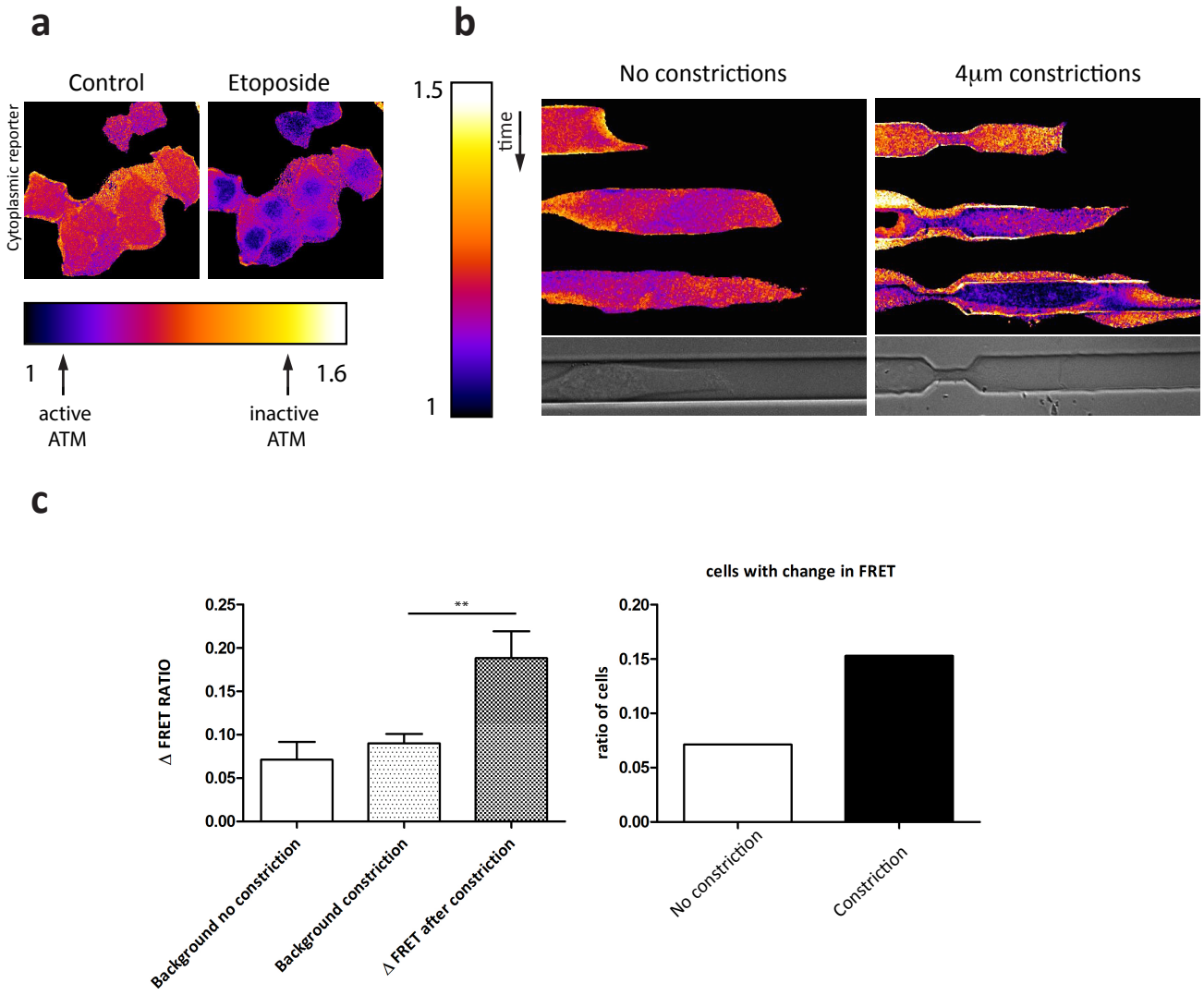


Figure 22. ATM is activated during interstitial migration (Cytoplasmic ATM reporter).

a) Images showing the change in fluorescence ratio of the cytoplasmic FRET sensor upon stimulation with etoposide 30µg/ml for 1hour. Activation of ATM can be visualized in live cell imaging following the decrease of yellow to cyan emission ratio; the appearance of violet color in the images indicates that ATM is active. b) FRET live cell imaging of U2OS cells transfected with the cytoplasmic ATM reporter during migration across channels. In this case, we also detected ATM activation across constrictions (violet spots). The experiment was carried out as described in figure 21 b. c) Summary of FRET analysis for two independent experiments. The analysis was performed as described in figure 21c.

4.8 ATM deficiency impairs survival during interstitial migration independently of the cell cycle phase.

One possible interpretation of our data is that ATM gets activated during interstitial migration and plays a role in the regulation of cell plasticity to assist successful squeezing of cells.

However, ATM is known to regulate the cell cycle checkpoints G1-S, intra-S and G2-M. The depletion of ATM could have altered the distribution of cell cycle phases in the cell population migrating inside the channels. Alternatively, the increased cell death observed in the absence of ATM activity could be restricted to a specific cell cycle phase.

These considerations are more relevant in light of a recent study showing that the ability of cells to deform changes according to the cell cycle phase (Panagiotakopoulou et al, 2016).

To address the consequences of ATM depletion on the cell cycle phase of migrating cells, we used the fluorescent ubiquitination-based cell cycle indicator (FUCCI) (Macurek et al, 2013; Sakaue-Sawano et al, 2008).

This system relies on a pair of fluorescent probes (red and green) fused to degrons derived from Cdt1 and Geminin. Geminin is targeted by the APC/C ubiquitin ligase to degradation in G1 phase, while Cdt1 is degraded only during S and G2 phase. The fluorescent probes fused with the degrons are destabilized in a similar fashion thus the nucleus of cells expressing these constructs appears red in G1 and green in S-G2-M (Figure 23A).

This system allows the recording of cell cycle stages during live cell imaging.

U2OS cells stably expressing the FUCCI reporter were seeded inside micro-channels with 4μm constrictions and analyzed for migration in the presence or absence of ATMi KU-60019 3μM (Figure 23B).

The average percentage of G1, G1-S and S-G2-M migrating cells was compared in control and ATMi-treated cells. We did not observe a significant difference in the overall cell cycle distribution after ATM inhibition (Figure 23C). Moreover, we found that ATM inhibition increased cell death in all the cell cycle phases detected by the FUCCI probe (Figure 23D).

The standard deviation of G1-S transition cells (yellow cells) was higher, likely because these cells are in low number compared to the total population and the red-yellow transition is sometimes more difficult to detect (Figure 23D).

In conclusion, our phenotype does not seem to be related to an effect of ATM on the cell cycle.

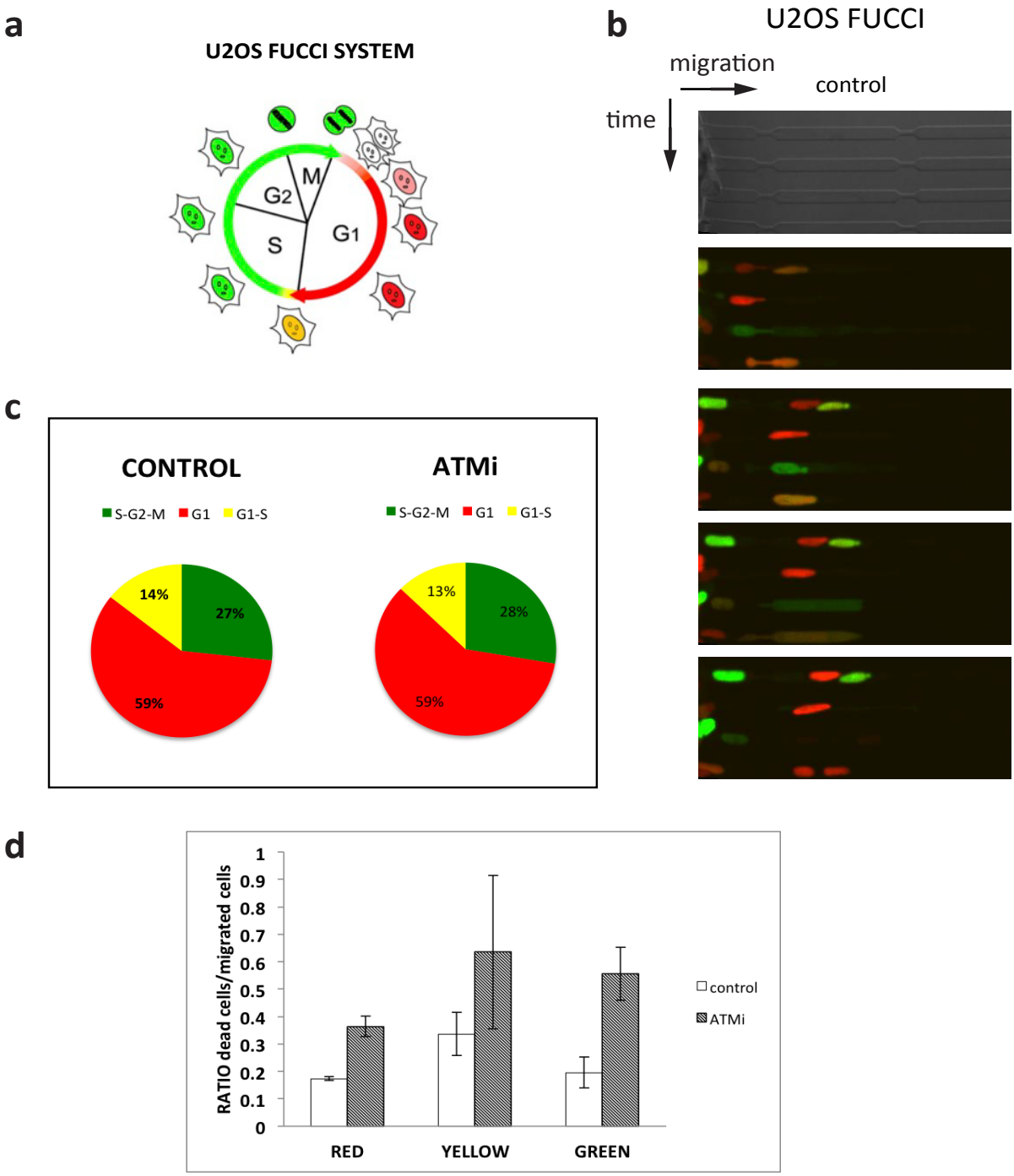


Figure 23. ATMi-induced cell death during 3D migration is not associated to a specific cell cycle phase.

a) Figure adapted from (Sakaue-Sawano et al, 2008) showing the principle of FUCCI system. The fluorescent probe labels G1 phase nuclei in red, nuclei undergoing G1-S transition in yellow and S/G2/M nuclei in green. b) Projections of four different time points of U2OS stable transfectants expressing the FUCCI probe analyzed during migration across constrictions. Cells were seeded as previously described in the presence or absence of ATMi KU-60019 3μM.Images were acquired every 15 minutes for 18 hours. c) Pie charts summarize the average percentages of G1, G1-S and S/G2/M cells counted in two independent experiments for control and ATMi-treated cells. ATMi does not significantly alter the cell cycle distribution of cells entering the channels. d) ATMi-treated cells show increased cell death in all cell cycle phases detected with the fluorescent probe.

4.9 ATM deficiency reduces the migration speed of single cells.

Following the hypothesis that absence of ATM could result in alterations of the cytoskeleton we tested the effect of ATM depletion on 2D locomotion.

2D migration assays study the movement of adherent cells on a plane substrate in the absence of geometric limitations.

We performed manual tracking of single cells moving on fibronectin-coated glass-bottom culture dishes that can be used for live cell imaging.

The experiment was carried out using U2OS cells because they migrate more compared to HeLa. ATM was depleted by short-hairpin RNA.

Glass-bottom cell culture dishes were coated with fibronectin and cells were seeded immediately before imaging acquisition as described in materials and methods. Images were acquired with a bright-field microscope every 2 minutes for 16 hours to follow the spreading and movement of single cells in multiple fields of view. The experiment was performed three times.

The movement of single cells was analyzed manually using the plugin MtrackJ of imageJ. This tool allows the reconstruction of the trajectory covered by each cell from the beginning to the end of the imaging acquisition following the position of the cell in each frame (Figure 24A).

Each track is characterized by four parameters that describe the migration of the cell (Figure 24B).

We found that ATM depletion was affecting all parameters and in particular the speed of migration was reduced in the absence of ATM (Figure 24B, C).

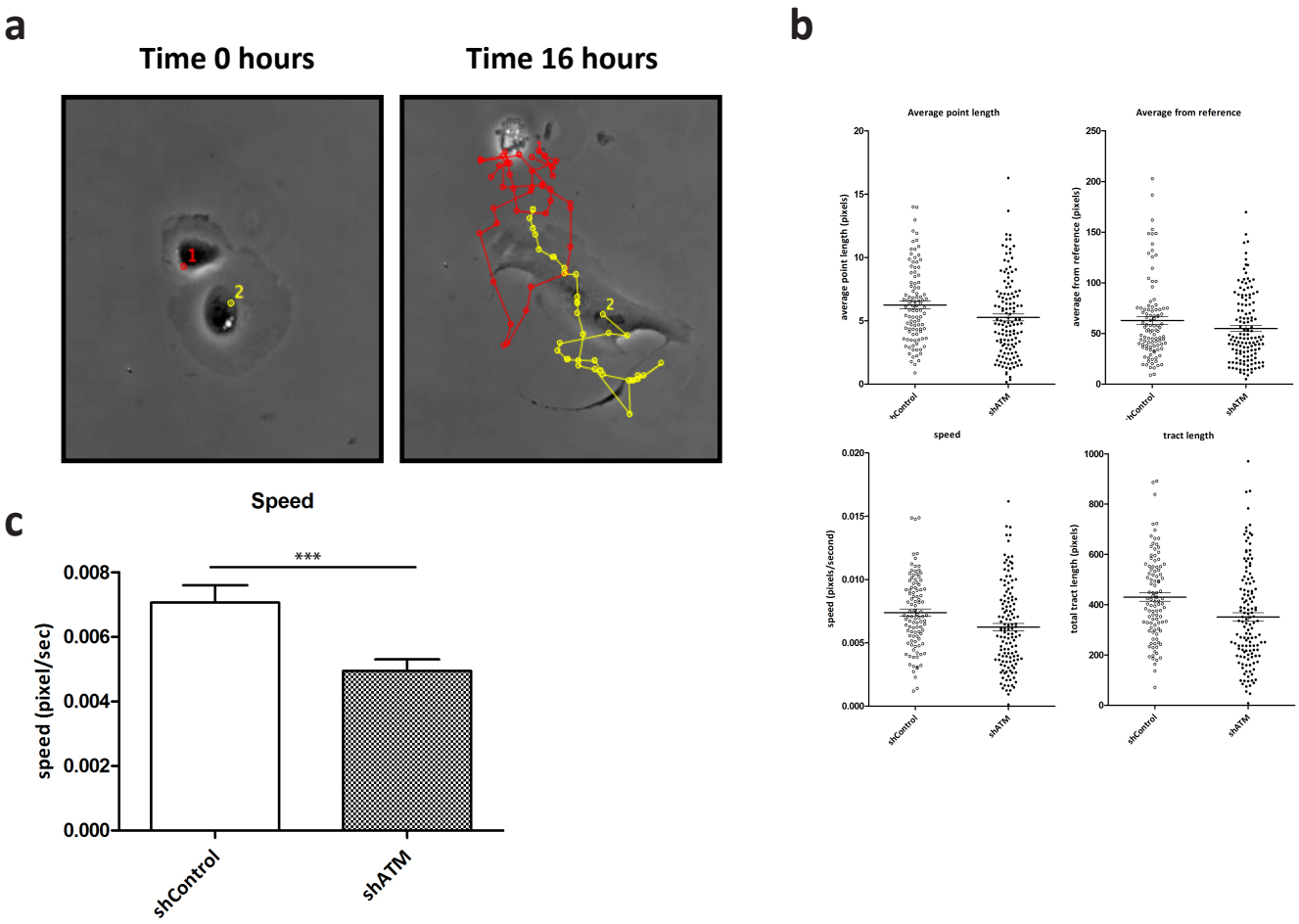


Figure 24. ATM depletion affects the 2D migration of single cells.
a) An example of manual tracking of U2OS cells using the plugin MTrackJ of imageJ. U2OS cells were used for this analysis because they migrate more compared to HeLa cells. Cells were plated on fibronectin-coated round bottom slideglasses at low density and immediately imaged overnight for 16 hours to follow the spreading and movement of each single cell. Images were acquired every 2 minutes with a bright-field microscope and cell tracking was performed manually with MTrackJ with a time step size of 10 frames (20 minutes).
b) The graphs show different parameters measured with MTrackJ in control and shATM cells.
Average point length: average distance of each point to the previous point.
Tract length: total distance from the start point to the end of the movie.
Average from reference: average distance of each point to the reference point.
Speed: measured as pixels/second.
The results suggest that ATM depletion impairs migration.
c) Summary graph of three independent experiments, shATM U2OS are slower compared to control cells.

4.10 ATM physically interacts with several proteins involved in membrane trafficking and cytoskeletal regulation.

To investigate the potential interaction between ATM and cytoskeletal-related proteins we performed mass spectrometry analysis in HeLa cells.

We used the 9E6 anti-ATM mouse monoclonal antibody to immunoprecipitate ATM in whole cell protein extracts derived from control and HeLa ATM KO cells. Immunoprecipitation (IP) was performed as described in materials and methods. HeLa ATM KO cells were used as a negative control to exclude all the factors resulting from non-specific interactions with the antibody or the beads used for the immunoprecipitation. The immunoprecipitation was performed using the antibody against the endogenous ATM, thus we did not overexpress the protein nor we used tagged versions of the protein. We optimized the conditions for the immunoprecipitation and we were able to efficiently pull down ATM in control cells, while the protein was almost absent in the IP of HeLa ATM KO (Figure 25A).

Mass spectrometry was performed twice, in cells growing in normal medium and in cells treated with 10Gy of IR. ATM KO cells were used as a negative control for each experiment.

We speculated that activation of ATM could increase the number of interactors detected by mass spectrometry or reveal specific interactions with active ATM. ATM was activated by IR treatment as shown by S1981 phosphorylation detected by WB with the anti-pS1981 ATM antibody, and the signal was almost absent in ATM KO HeLa (Figure 25A). Cells were grown on normal medium, subjected to

IR treatment when needed, whole cell protein extracts were prepared one hour after treatment to immunoprecipitate ATM (Figure 25C). The immunoprecipitates were subjected to SDS-page electrophoresis using 4-12% gradient acrylamide gels. As shown on Figure 25B, the band of the predicted molecular size of ATM appeared only in the IP of control cells, and not in the ATM KO lane, as indicated on gel stained with Coomassie blue. Following Coomassie blue staining, the polyacrylamide gels of the IP samples were processed for mass spectrometry analysis as described in materials and methods.

Several proteins were immunoprecipitated in the presence or absence of IR.

The scatter plots on Figure 26A summarize the results of the two experiments. On the Y-axis, the intensity of the signal related to each protein, measured by the mass spectrometry instrument, indicates how frequently the protein was identified in the sample, this parameter is normalized to the total input of proteins present in the sample (Label Free Quantification, LFQ). On the X-axis, the ratio between control/ATM KO LFQ intensities of each protein is shown. A ratio>1 indicates that the protein is enriched in the IP of control cells expressing ATM (Figure 26A); such proteins were considered as putative ATM interactors. The factors with a ratio<1 were instead excluded from the analysis. Some proteins were present only in the control IP ATM thus the ratio could not be calculated since the ATM KO intensity was 0 and they are not included in the graph, however they were still considered as putative ATM interactors. Since we know that ATM was still expressed at very low levels in ATM KO cells (Figure 25A), it is possible that some interactors were pulled-down in the negative control as well. We selected specifically the ones enriched in ATM-expressing cells.

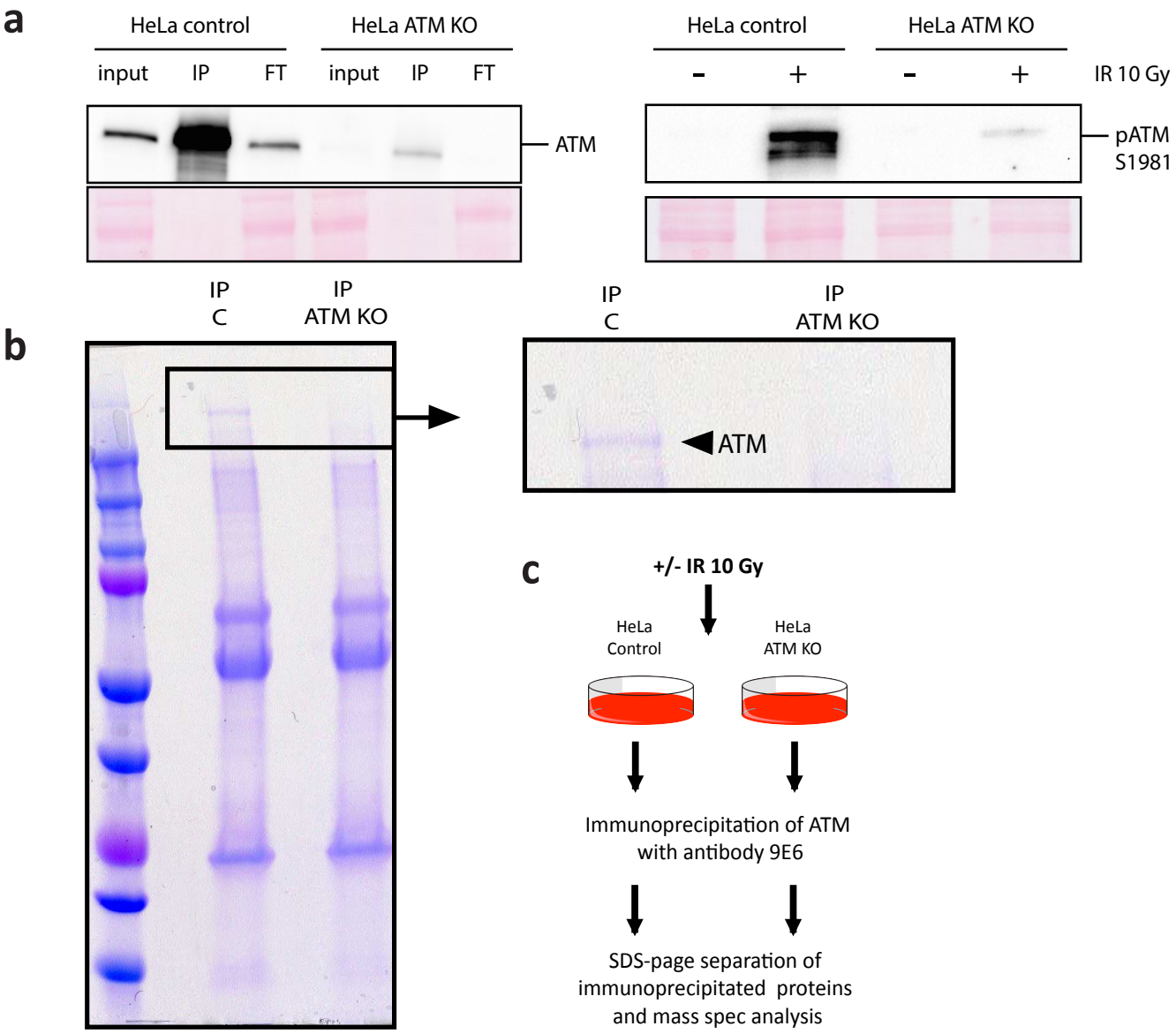
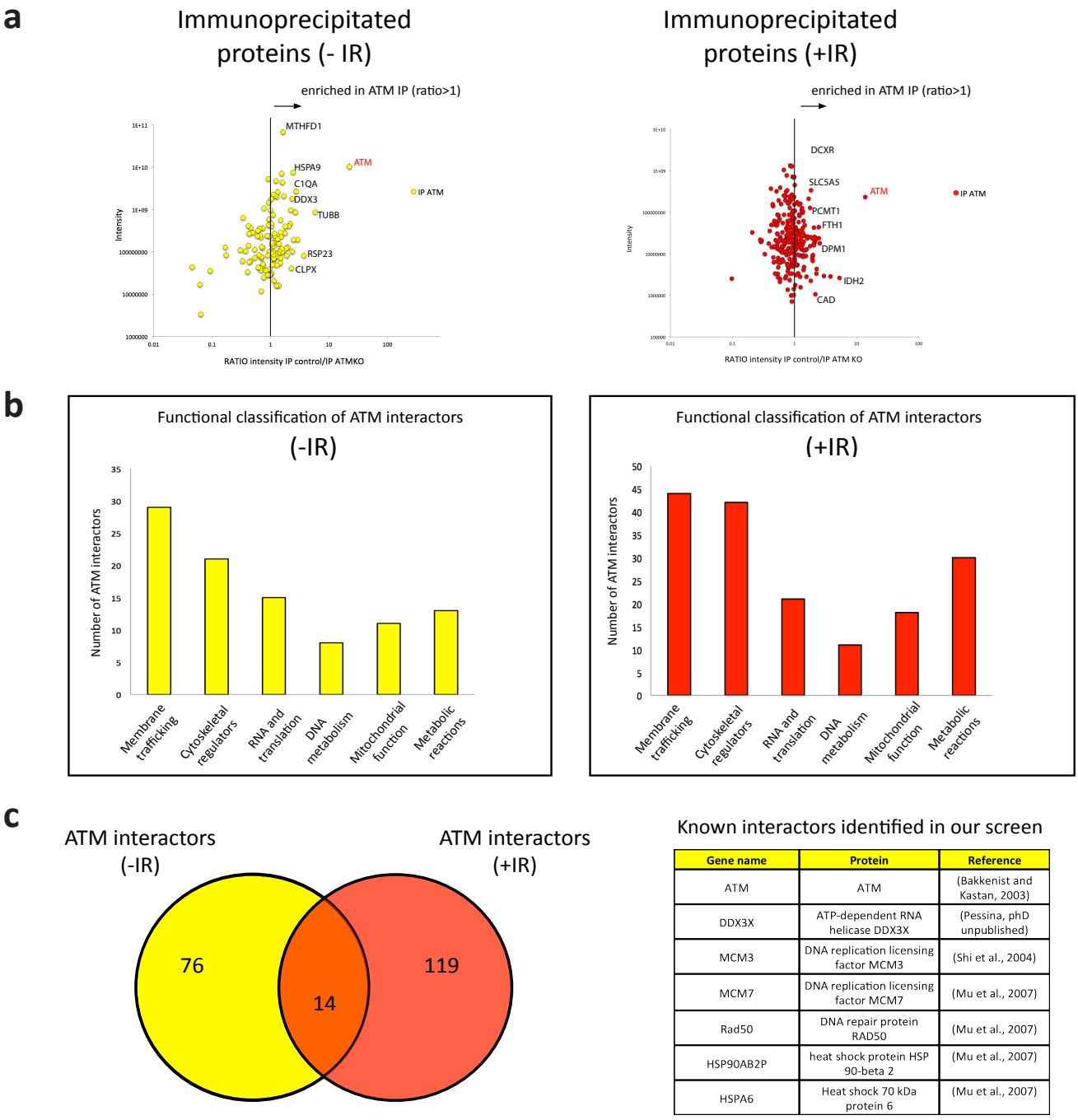


Figure 25. Description of the experimental conditions used for ATM immunoprecipitation and mass spectrometry analysis of ATM physical interactors. (a) Western blot showing the efficient pull down of ATM with anti-ATM 9E6 mouse monoclonal antibody in HeLa cells. Input: ATM protein levels in the whole cell extract before immunoprecipitation. IP: ATM protein levels enriched in the immunoprecipitate. FT: flow-through, residual ATM protein levels in the protein extracts after immunoprecipitation. ATM KO HeLa cells were used as negative control, ATM is almost absent and only a very faint band is detected in the immunoprecipitate. The right panel shows ATM activation (detected with anti-pS1981 ATM mouse monoclonal antibody) 1 hour after 10 Gy of IR. A faint band appears in the ATM KO cells. We used this condition to identify physical interactions with active ATM. (b) An image of an SDS-page electrophoresis gel stained with Coomassie Blue where the immunoprecipated samples of control and ATM KO HeLa cells were separated before mass spectrometry analysis. A band corresponding to ATM molecular weight appears only in the pulled-down of control cells. (c) Experimental flow adopted for the sample preparation of the two mass spectrometry analysis performed in control and IR-treated cells.



Known interactors identified in our screen

Gene name	Protein	Reference
ATM	ATM	(Bakkenist and Kastan, 2003)
DDX3X	ATP-dependent RNA helicase DDX3X	(Pessina, phD unpublished)
MCM3	DNA replication licensing factor MCM3	(Shi et al., 2004)
MCM7	DNA replication licensing factor MCM7	(Mu et al., 2007)
Rad50	DNA repair protein RAD50	(Mu et al., 2007)
HSP90AB2P	heat shock protein HSP 90-beta 2	(Mu et al., 2007)
HSPA6	Heat shock 70 kDa protein 6	(Mu et al., 2007)

Figure 26. Mass spectrometry analysis of ATM physical interactions in control and IR-treated HeLa cells.

(a)Scatter plots showing all the immunoprecipitated proteins identified by mass spectrometry in control and IR-treated cells. ATM is indicated together with other factors as representative examples. On the Y-axis, the intensity of the protein signal detected by mass spectrometry, while on the X-axis, the control/ATM KO ratio of the signal. Factors specifically enriched in the ATM pull-down of control cells were considered as putative ATM interactors (ratio>1) (b) Functional classification of the selected ATM interactors (proteins were classified with the software Enrichr and further grouped to simplify the graph). (c) The number of ATM interactions found in the two sets of experiments together with the common interactors is shown. On the right panel, the table summarizes a list of known ATM interactors identified in previous screens and confirmed in our analysis.

We identified proteins that were already known to interact with ATM in previous screens (Figure 26C), suggesting that we could pull-down ATM interactors in our conditions. Using the software Enrichr, we carried out functional classification of the interactors (Figure 26B). Most of the proteins were involved in membrane trafficking and in regulation of cytoskeleton. In addition, we found interactors involved in RNA and DNA metabolism, mitochondrial function and metabolic reactions.

ATM is known to localize mainly into the nucleus to mediate DSB repair, thus it can be surprising that the number of interactors related to DNA metabolism was a minor portion of the total interactome. However, the conditions we used for the protein extractions were chosen to extract preferentially cytoplasmic proteins while specific protocols are usually required to extract nuclear proteins.

We focused our interest on the interactors that could explain our phenotypes in relation to cell mechanics and migration and we selected all the proteins with structural functions involved in cytoskeletal regulation or membrane trafficking, comprehensively listed in table 3.

Many of these proteins were found as putative targets phosphorylated by ATM in previous proteomic screens (Bensimon et al, 2010; Kozlov et al, 2016; Matsuoka et al, 2007; Mu et al, 2007; Siddoway et al, 2014), although none of them have been studied before. Moreover, previous screens were mostly performed using an antibody against phospho-SQ/TQ, thus these targets could have been phosphorylated by ATR or DNA-PK as well under DNA damage. Our results suggest that ATM physically interacts with these factors (table 3), thus ATM might regulate them by direct phosphorylation.

In conclusion, ATM potentially regulates a plethora of cytoskeletal regulators and factors involved in membrane trafficking that might affect cell plasticity and migration.

Gene name	Protein	Function
IQGAP1	Ras GTPase-activating-like protein IQGAP1	Scaffold protein, interacts with cytoskeleton and adhesion molecules
CFL1	cofilin-1	F-actin depolymerization
FN1	Fibronectin	ECM protein, binds to integrins
TUBB4A	Tubulin alpha-4A chain	Microtubules component
DSP	Desmoplakin	Component of desmosomes
FGB	Fibrinogen beta chain	Cell adhesion and spreading
VIM	Vimentin	Intermediate filament protein
TUBB	Tubulin beta-8 chain	Microtubules component
VTN	Vitronectin	ECM protein, binds to integrins
ANXA2	Annexin A2	Phospholipid-binding protein, functions in cell motility, exocytosis, endocytosis,
PKP4	Plakophilin-4	Cell adhesion
S100A7	Protein S100-A7	Calcium-binding protein
FLN	Filamin-C;Filamin-B	Actin-binding protein, filament actin crosslinking
DKFZp781O2021; CTNND1	catenin-delta 1	Cell-cell adhesion
RAB11A	Ras-related protein Rab-11A	Intracellular membrane trafficking
RHOC	Transforming protein RhoA	Rho GTPase, reorganization of actin cytoskeleton
SEMA4B	Semaphorin-4B	Secreted and membrane proteins, role in axon guidance
DYNC1H1	Cytoplasmic dynein 1 heavy chain 1	Microtubule-activated ATPase, intracellular motility, organelle movement
CNTN1	Contactin-1	Cell adhesion molecule
ARPC2	Actin-related protein 2/3 complex subunit 2	Regulation of actin cytoskeleton
COPZ1	Coatomer subunit zeta-1	autophagy
RAB13	Ras-related protein Rab-13	Membrane trafficking and assembly of tight junctions
ACTC1	Actin, alpha cardiac muscle 1	Actin filaments component
DSTN	Destrin	Actin depolymerizing protein
RAP1A	Ras-related protein Rap-1A	Cell proliferation and adhesion
RAB7A	Ras-related protein Rab-7a	Endocytosis and vesicles trafficking
LAMB1	Laminin subunit beta-1	ECM glycoprotein, role in cell adhesion, migration, differentiation
ACTN4	Alpha-actinin-4	Actin filaments component
ARPC3	Actin-related protein 2/3 complex subunit 3	Regulation of actin cytoskeleton
ARPC4	Actin-related protein 2/3 complex subunit 4	Regulation of actin cytoskeleton
TUBB2B	Tubulin beta-2B chain;Tubulin beta-2A chain	Component of microtubules
POSTN	Periostin	Binds to integrins and supports cell adhesion and migration
GDI2	Rab GDP dissociation inhibitor beta	GDP dissociation inhibitor, vesicular trafficking of molecules between organelles
ARHGDIA	Rho GDP-dissociation inhibitor 1	Modulation of Rho proteins, role in cell motility
MOB1A	MOB kinase activator 1A	Activator of LATS1/2, transcriptional regulation, cell proliferation, cell death and cell migration

Table 3. ATM interactors involved in the regulation of cytoskeleton and cell structure.
A list summarizing cytoskeleton-related ATM interactors identified by mass spectrometry in control (black characters) and IR-treated HeLa cells (red characters). The light yellow underlines proteins found as putative ATM targets, phosphorylated at SQ/TQ sites, in previous proteomic screens (Bensimon et al, 2010; Kozlov et al, 2016; Matsuoka et al, 2007; Mu et al, 2007; Siddoway et al, 2014).

5. DISCUSSION

Growing pieces of evidence indicate novel functions of DDR in the regulation of cytoplasmic pathways. More recently, the relationship between DDR proteins and cytoskeleton is coming into light. In this study we attempted to shed light on the connection between DDR and cell mechanics, focusing specifically on ATM.

5.1 ATM regulates cell plasticity.

In the first part of this study, we showed that ATM has an impact on cell plasticity. We took advantage of the AFM instrument to measure the mechanical behavior of cells in the absence of ATM. ATM inhibition or ATM depletion resulted in increased cell stiffness. Similarly, primary fibroblasts derived from A-T patient reproduced the same phenotype.

We showed that this phenotype is not due to altered plasticity of the nucleus since isolated nuclei were not stiffer in the absence of ATM. Although ATM-defective cells had deformed nuclear shape, this was not correlating with altered lamin proteins expression nor with different plasticity of the nuclei. Ultrastructural analysis of the cells by electron microscopy confirmed these observations; most of the abnormalities that we observed in ATM deficient cells were related to the cytosolic compartment. These included accumulation of lipid droplets, autophagosomes and actin stress fibers.

Additional AFM analyses were recently carried out in our lab to study the role of the different DDR pathways in cell plasticity. Increased stiffness was a specific phenotype of ATM depletion, and was not observed in the case of DNA-PK or ATR. DNA-PK did not show a significant effect on cell plasticity. Interestingly, ATR depletion had an opposite effect compared to ATM. Indeed, ATR-deficient cells were softer compared to control cells. While the ATM phenotype is restricted to the cytosol compartment, ATR was found to profoundly alter the nuclear plasticity. The absence of ATR resulted in softer nuclei measured by AFM and caused nuclear membrane invaginations bound to condensed chromatin. Nuclear membrane invaginations were also observed in ATM deficient cells but these were minor, less marked and not associated with condensed chromatin. Our results indicate that ATM and ATR play diverse roles, in the cytoplasm and in the nucleus, respectively.

Moreover, the increased stiffness observed in the absence of ATM is not associated with general defective DDR response, since each kinase, ATM, ATR and DNA-PK, showed different contributions to cell plasticity.

Short-term inhibition of ATM did not cause increased cell stiffness. This result can be interpreted in different ways. If the phenotype is due to the direct phosphorylation of substrates involved in cell mechanics, longer time of ATM inhibition might be required to achieve their complete de-phosphorylation resulting in a detectable phenotype.

Alternatively, the altered plasticity could be an indirect consequence of ATM depletion, and might be triggered in response to other cell stresses caused by ATM deficiency or by transcriptional regulation. In this scenario, it is possible to speculate whether the phenotype could arise following the deregulation of other

DDR kinases, ATR or DNA-PK, which might take over the function of ATM for a compensation mechanism. In particular, it will be interesting to investigate whether ATR deregulation following ATM deletion could be responsible for the increased stiffness. ATR and ATM might act on different cytoskeletal pathways to maintain the cellular homeostasis, with this equilibrium being altered in the absence of one of the two kinases.

One of the major consequences of ATM loss on the cellular homeostasis is the accumulation of ROS (Ditch & Paull, 2012; Rotman & Shiloh, 1997b). This raises the question whether the increased stiffness could derive from oxidative stress. Although we did not directly test this hypothesis, it is published that oxidative stress causes a drop of cell stiffness (Sun et al, 2014; Vileno et al, 2007). Thus, accumulation of ROS per se, is unlikely the reason behind the increased stiffness observed in ATM deficient cells. It is important to note that the effect of ROS on cell stiffness was measured in cells expressing ATM (Sun et al, 2014; Vileno et al, 2007). Since ATM is known to be activated by ROS (Guo et al, 2010), activation of ATM could have caused a decrease in stiffness in that condition, contrary to what we observed by inhibiting ATM. Thus, the reported observations will be in line with our results. It is still possible that the ROS accumulated in the absence of ATM, could generate a different cell response leading to increased stiffness. This can be addressed by combining ATMi treatment with N-acetyl-cysteine (NAC) in AFM experiments.

Previously reported AFM indentation analyses showed that the major contribution to cell stiffness is dictated by the cytoskeletal organization of the cells (Haase & Pelling, 2015). Actin filaments, intermediate filaments and microtubules are the

three major components of the cytoskeleton. Diverse studies investigated the relative contribution of each cytoskeletal component to the cellular stiffness. It was shown that depolymerization of microtubules has no impact on cell stiffness (Rotsch & Radmacher, 2000). On the other hand, actin filaments, and especially actomyosin stress fibers, have been shown to modulate cell stiffness and internal tension at a greater extent (Ketene et al, 2012; Rotsch & Radmacher, 2000). Stress fibers are composed of antiparallel arrays of F-actin bundles and non-muscle myosin II, and are stabilized by actin-binding proteins. A recent study investigated the relationship between cell stiffness and stress fiber amounts (Gavara & Chadwick, 2016). By combining AFM measurements with fluorescence imaging, the authors demonstrated that the amount of myosin and actin assembled in stress fibers directly correlated with cell stiffness, moreover the spatial organization of fibers influenced the elasticity of cells.

More recently, the role of intermediate filaments (IF) in cell mechanics has been investigated. The most widely distributed of all IF proteins is vimentin. Independent studies showed that depletion of vimentin reduces the stiffness of the cytoplasm as well as alters the intracellular movement of vesicles (Buehler, 2013; Guo et al, 2013; Wang & Stamenovic, 2000; Wang & Stamenovic, 2002).

We found that ATM depletion increased cell stiffness and resulted in accumulation of stress fibers (by electron microscopy analysis). The most straightforward interpretation of our results is that ATM might be involved, directly or indirectly, in the regulation of cytoskeletal dynamics, and in particular might affect the organization of actin or intermediate filaments.

In support of direct regulation of the cytoskeleton by ATM, we identified a plethora of actin regulatory proteins interacting with ATM by mass spectrometry analysis, both in proliferating cells and in cells treated with ionizing radiations.

Arp2, Arp3 and Arp4, three subunits of the Arp2/3 complex, co-immunoprecipitated with ATM. Arp2/3 is involved in the nucleation of actin filaments and plays a major role in the regulation of the actin cytoskeleton (Goley & Welch, 2006). Cofilin-1, which depolymerizes actin filaments and was implicated in the DDR response (Lee et al, 2005; Leu et al, 2013; Yan et al, 2012), was also found to interact with ATM. Also actin filaments components such as ACTC1, ACTN4 and the actin filament crosslinker Filamin C, were immunoprecipitated with ATM. In addition, ATM interacts with the Rho GTPase Rho C; this protein belongs to the family of Rho GTPases and participates in the formation of actin stress fibers and focal adhesions. Rho interacts and activates Rho kinase that regulate the myosin II regulatory chain (MLC) phosphorylation, at S19 (Amano et al, 2010). In both muscle and non-muscle cells, MLC phosphorylation is critical to control actomyosin contractility. Interestingly, ATM also interacted with the Rho-GDP dissociation inhibitor 1, a factor that controls several Rho family proteins and maintains them in an inactive state (Olofsson, 1999). Among the intermediate filament components, vimentin interacts with ATM and was previously found as a putative ATM target phosphorylated upon DNA damage (Bensimon et al, 2010; Kozlov et al, 2016; Matsuoka et al, 2007; Mu et al, 2007; Siddoway et al, 2014).

Vimentin is phosphorylated by DNA-PK at S456 (Kotula et al, 2013), this phosphorylation was proposed to play an inhibitory effect on cell migration and adhesion. Although this phosphorylation site was specific for DNA-PK, vimentin

is phosphorylated in mitosis in a DNA-PK-independent manner. Because ATM was found to interact with vimentin, it is also possible that ATM might be involved in the phosphorylation of this protein, perhaps on other residues. The absence of ATM might alter the phosphorylation status of vimentin, or increment the activity of DNA-PK, affecting the overall structure of vimentin filaments.

We plan to verify whether the increased stiffness observed in the absence of ATM is rescued by the inhibition of actomyosin contractility combining the AFM experiments with treatments that counteract actin polymerization.

We will monitor the status of cofilin-1 expression and phosphorylation in ATM-deficient cells, as well as the level of myosin II regulatory chain phosphorylation.

Moreover, we will investigate the role of vimentin in ATM-mediated mechanical regulation. According to the results, we will further validate the most interesting interactors and investigate the mechanism that drives their regulation by ATM.

We cannot exclude that other ATM-regulated pathways might be relevant to our phenotype. By electron microscopy analysis, we observed accumulation of lipid droplets and autophagosomes in ATM-defective cells. Less is known about the role of autophagosomes and lipid droplets in cell stiffness and morphology and currently we cannot exclude that such alterations might contribute, directly or indirectly, to our phenotype.

5.2 ATM influences 2D locomotion and interstitial migration

In the second part of this study, we explored the physiological consequences of the altered mechanical properties caused by ATM deficiency. The deformability of cells has been shown to affect a number of cell functions including cell differentiation, aging and disease states (Haase & Pelling, 2015; Wozniak & Chen, 2009).

The transmission of mechanical forces within the cells largely relies on the cytoskeleton. Cells are able to sense and respond to a variety of mechanical stimuli, a phenomenon known as “mechanotransduction”. This process involves the transmission of forces between cells as well as between cells and extracellular matrix.

Importantly, cell-cell adhesion, cell-matrix interactions, and intracellular organization of the cytoskeleton play a major role in the control of cell migration.

The process of cell migration is involved in several biological processes, such as embryonic development, immune responses and cancer progression. Cancer cells evolved a broad spectrum of migration and invasion mechanisms (Friedl & Wolf, 2003), thus understanding the cellular and molecular basis of the different invasion strategies will help to develop new treatments to block the generation of metastasis in cancer therapy.

We hypothesized that ATM regulation of cell plasticity could have an impact on cell migration at the physiological level.

ATM has been shown to influence migration of breast cancer cells through the regulation of the transcription factor SNAIL involved in the expression of cadherins (Boohaker et al, 2013; Sun et al, 2012; Yin et al, 2016). More recently, Chen and coworkers showed that oxidative stress promote tumor invasion and migration of MDA-MB-231 cells by transcriptional regulation of IL-8, through ATM (Chen et al, 2015).

Following our original hypothesis that ATM could regulate cell plasticity through cytoskeletal targets we performed manual tracking analysis of single cells and we found that ATM depletion impairs 2D locomotion of U2OS cells.

We believe that ATM could also play additional functions, along with the published ones, in cell migration, especially through direct regulation of cytoskeletal targets.

In vivo migration is supposed to occur in complex 3D environments. Many cells adopt different mechanisms for 3D migration, which are classified according to the relative contribution of actomyosin contractility and cell-matrix adhesion (Petrie & Yamada, 2016).

Three-dimensional migration has different requirements compared to 2D locomotion; indeed cells are subjected to strong deformations, especially of the cell nucleus.

We investigated the role of ATM in 3D migration. We found that ATM inhibition in HeLa or U2OS cells impaired the survival of cells during interstitial migration. This phenotype was reproduced by the genetic deletion of ATM in HeLa cells.

Parallel studies carried out on ATR-defective cells in our lab showed that ATR also plays a role in the three-dimensional migration, affecting the survival of cells entering inside constrictions. We know that ATR regulates nuclear plasticity and one hypothesis is that alteration of the mechanical properties of the nucleus could cause the cell death in 3D migration in ATR defective cells.

Interestingly, ATR and ATM have opposite roles with respect to cell mechanics, nevertheless both kinases contribute to the process of interstitial migration.

Recent studies showed that cells migrating in confined spaces experience strong deformations of the nuclei causing ruptures of the nuclear envelope and DNA damage (Denais et al, 2016; Raab et al, 2016).

The amount of nuclear membrane ruptures increased with the reduction of constriction sizes. Moreover, this phenomenon was enhanced by depletion of lamin proteins, and was partially rescued by inhibition of actomyosin contractility (Denais et al, 2016).

Both studies showed that ESCRT III components were recruited to the site of membrane ruptures and participated in nuclear envelope repair. Depletion of ESCRT III components slowed down the membrane repair process and caused an increase in cell death during migration, especially when combined with inhibition of DNA repair (through ATMi treatment).

Thus, preserving nuclear integrity is crucial for this type of migration and it can be challenged by several factors. On one side, factors that alter the nuclear plasticity, such as lamin proteins, destabilize the nuclear envelope, inducing

ruptures of the membrane, DNA damage and cell death. Indeed, the impact of lamin protein levels on 3D migration has been already documented (Harada et al, 2014).

On the other side, cytoplasmic forces acting on the nuclear membrane during migration can contribute to nuclear pressurization. One candidate is the actomyosin contraction at the rear of the nucleus. Myosin II B was found to play a central role in the nuclear translocation during 3D migration, being responsible for the force generation necessary to squeeze the nucleus through narrow constrictions in 3D environments (Thomas et al, 2015). Thus, actomyosin contractility exerts tension on the nuclear membrane; this tension is necessary to allow the squeezing of the nucleus but at the same time constitutes a source of mechanical stress at the nuclear envelope. Alterations in the actomyosin cytoskeleton are thus expected to have an impact on the 3D migration of cells.

Important hints derive from the study of naturally-migrating cells, such as immune cells. Immune cells physiologically migrate toward sites of infection to exert their function. These cells evolved different strategies to facilitate the movement of stiff nuclei across complex body environments. Neutrophils display high deformable nuclei due to the lack of lamin A/C expression; these cells have a short lifespan (Rowat et al, 2013).

Dendritic cells combine high migration capacity with long-term survival; these cells express higher level of lamin A/C compared to neutrophils, nevertheless they can easily deform their nuclei. Nuclei deformation is achieved by the nucleation of an Arp2/3-dependent actin network around the nucleus (Thiam et al, 2016).

The actin network causes the transient rupture of nuclear lamina facilitating the nuclear squeezing across small constrictions (Thiam et al, 2016).

Interestingly, the nucleation of actin around the nucleus was not required in cells with low level of lamin A/C expression and softer nuclei (Thiam et al, 2016).

Thus, a delicate balance, between internal and external forces, regulates the process of deformation at the nuclear membrane boundary during 3D migration.

Our results suggest that ATM affects cytoplasmic plasticity and increases actin stress fibers; we also showed that ATM was activated in cells subjected to mechanical deformation of the nucleus, suggesting an active role of the kinase in this process. Moreover, the phenotype was not due to an effect of ATM on the cell cycle.

We hypothesize that lack of ATM could alter the structure of the cytoskeleton with negative impact on the ability of cells to survive upon migration. We plan to combine the micro-channel device system with electron microscopy analysis to observe the morphological features of ATM-defective cells migrating inside channels, focusing on the cytoskeletal apparatus. Indeed, our preliminary observations indicate that the movement of nuclei across constrictions is slower in ATM-defective cells (data not shown).

Constricted migration is associated with DNA damage (Irianto et al.,2015; Denais et al, 2016; Raab et al, 2016).

Therefore, inhibition of ATM in migrating cells could compromise DNA damage repair, leading to cell death. We will attempt to address this point by measuring 53BP1-GFP or Ku70-GFP foci formation in cells passing through constrictions in the presence or absence of ATM.

Previously published data suggested that DNA repair inhibition alone does not significantly affect cell survival in 3D migration (Denais et al, 2016; Raab et al, 2016). The authors suggested that DNA damage, and consequent cell death, are strongly increased only when depletion of ESCRT III is combined with ATMi treatment.

In particular, Raab and coworkers showed that ATMi alone does not significantly increase cell death during 3D migration in RPE-1 cells. Denais and colleagues proposed a similar interpretation of their results, although according to their data, ATMi treatment caused a 2-fold increase of cell death, although this was strongly increased by combining ATMi treatment with inhibition of ESCRT III leading to a 6-fold increase of cell death.

Our results suggested that ATM inhibition or depletion was sufficient to induce a 6-fold increase of cell death in HeLa cells, and a 3-fold increase in U2OS cells.

Genetic deletion of ATM in HeLa cells also increased cell death 2.6-fold times.

The discrepancies with the results of Raab publication might be related to the model cell line, indeed RPE-1 cells are highly migratory compared to HeLa or U2OS. Thus, these cells might overcome ATM inhibition. Denais also showed a 2-fold increase of cell death in cells migrating in the presence of ATMi, similarly to our observations.

We believe that a 4-fold increment of cell mortality, obtained as an average of our experimental data, is sufficient to be considered physiologically-relevant.

The findings suggesting that ATM depletion increased cell death during constricted migration open two alternative interpretations: 1) ATM is required to repair DSBs occurring in nuclei subjected to mechanical deformations 2) ATM regulates the cytoskeleton to preserve nuclear integrity during interstitial migration.

Likely defective ATM could contribute to cell death by impairing the cytoskeletal functions leading to unrepaired DSBs inside the nuclei.

We propose a model in which ATM and ATR collaborate to assist three-dimensional migration. ATR controls nuclear plasticity and chromatin-nuclear membrane dynamics. ATM regulates cytoplasmic pathways involved in the regulation of cytoskeleton and, possibly, its interaction with the nucleus.

Moreover, both kinases will contribute to the repair of DNA damage induced by mechanical stress.

Altogether, our observations point to a novel role of the ATM pathway in the regulation of cell plasticity. ATM might achieve this function controlling cytoskeletal regulators and will be subject to future investigations. Our results suggest potential implications of ATM in the development of tumor metastasis with relevance to cancer therapy. Moreover, we will unveil novel targets of ATM in relation to the cytoskeleton, which is still an unexplored area of action for this kinase. Our discoveries might help understanding the complex scenario of ATM functions that lead to the occurrence of multisystem abnormalities in patients affected by Ataxia-Telangiectasia disease.

7. REFERENCES

Abraham RT (2001) Cell cycle checkpoint signaling through the ATM and ATR kinases. *Genes Dev* **15:** 2177-2196

Abraham RT (2004) PI 3-kinase related kinases: 'big' players in stress-induced signaling pathways. *DNA Repair (Amst)* **3:** 883-887

Alexander A, Cai SL, Kim J, Nanez A, Sahin M, MacLean KH, Inoki K, Guan KL, Shen J, Person MD, Kusewitt D, Mills GB, Kastan MB, Walker CL (2010) ATM signals to TSC2 in the cytoplasm to regulate mTORC1 in response to ROS. *Proc Natl Acad Sci U S A* **107:** 4153-4158

Ali A, Zhang J, Bao S, Liu I, Otterness D, Dean NM, Abraham RT, Wang XF (2004) Requirement of protein phosphatase 5 in DNA-damage-induced ATM activation. *Genes Dev* **18:** 249-254

Amano M, Nakayama M, Kaibuchi K (2010) Rho-kinase/ROCK: A key regulator of the cytoskeleton and cell polarity. *Cytoskeleton (Hoboken)* **67:** 545-554

Ambrose M, Goldstine JV, Gatti RA (2007) Intrinsic mitochondrial dysfunction in ATM-deficient lymphoblastoid cells. *Hum Mol Genet* **16:** 2154-2164

Andegeko Y, Moyal L, Mittelman L, Tsarfaty I, Shiloh Y, Rotman G (2001) Nuclear retention of ATM at sites of DNA double strand breaks. *J Biol Chem* **276:** 38224-38230

Andrin C, McDonald D, Attwood KM, Rodrigue A, Ghosh S, Mirzayans R, Masson JY, Dellaire G, Hendzel MJ (2012) A requirement for polymerized actin in DNA double-strand break repair. *Nucleus* **3:** 384-395

Awasthi P, Foiani M, Kumar A (2016) ATM and ATR signaling at a glance. *J Cell Sci* **129:** 1285

Aylett CH, Sauer E, Imseng S, Boehringer D, Hall MN, Ban N, Maier T (2016) Architecture of human mTOR complex 1. *Science* **351:** 48-52

Bakkenist CJ, Kastan MB (2003) DNA damage activates ATM through intermolecular autophosphorylation and dimer dissociation. *Nature* **421:** 499-506

Bar RS, Levis WR, Rechler MM, Harrison LC, Siebert C, Podskalny J, Roth J, Muggeo M (1978) Extreme insulin resistance in ataxia telangiectasia: defect in affinity of insulin receptors. *N Engl J Med* **298:** 1164-1171

Barascu A, Le Chalony C, Pennarun G, Genet D, Imam N, Lopez B, Bertrand P (2012) Oxidative stress induces an ATM-independent senescence pathway through p38 MAPK-mediated lamin B1 accumulation. *EMBO J* **31:** 1080-1094

Baretic D, Williams RL (2014) PIKKs--the solenoid nest where partners and kinases meet. *Curr Opin Struct Biol* **29:** 134-142

Barlow C, Hirotsune S, Paylor R, Liyanage M, Eckhaus M, Collins F, Shiloh Y, Crawley JN, Ried T, Tagle D, Wynshaw-Boris A (1996) Atm-deficient mice: a paradigm of ataxia telangiectasia. *Cell* **86:** 159-171

Barlow C, Ribaut-Barassin C, Zwingman TA, Pope AJ, Brown KD, Owens JW, Larson D, Harrington EA, Haeberle AM, Mariani J, Eckhaus M, Herrup K, Bailly Y, Wynshaw-Boris A (2000) ATM is a cytoplasmic protein in mouse brain required to prevent lysosomal accumulation. *Proc Natl Acad Sci U S A* **97:** 871-876

Bartek J, Falck J, Lukas J (2001) CHK2 kinase--a busy messenger. *Nat Rev Mol Cell Biol* **2:** 877-886

Bartkova J, Horejsi Z, Koed K, Kramer A, Tort F, Zieger K, Guldberg P, Sehested M, Nesland JM, Lukas C, Orntoft T, Lukas J, Bartek J (2005) DNA damage response as a candidate anti-cancer barrier in early human tumorigenesis. *Nature* **434:** 864-870

Barzilai A, Biton S, Shiloh Y (2008) The role of the DNA damage response in neuronal development, organization and maintenance. *DNA Repair (Amst)* **7:** 1010-1027

Barzilai A, Rotman G, Shiloh Y (2002) ATM deficiency and oxidative stress: a new dimension of defective response to DNA damage. *DNA Repair (Amst)* **1:** 3-25

Bassing CH, Alt FW (2004) H2AX may function as an anchor to hold broken chromosomal DNA ends in close proximity. *Cell Cycle* **3:** 149-153

Baumann K (2014) Nuclear envelope: ATR senses mechanical stress. *Nat Rev Mol Cell Biol* **15:** 559

Belin BJ, Lee T, Mullins RD (2015) DNA damage induces nuclear actin filament assembly by Formin -2 and Spire-(1/2) that promotes efficient DNA repair. [corrected]. *Elife* **4:** e07735

Bencokova Z, Kaufmann MR, Pires IM, Lecane PS, Giaccia AJ, Hammond EM (2009) ATM activation and signaling under hypoxic conditions. *Mol Cell Biol* **29:** 526-537

Bensimon A, Schmidt A, Ziv Y, Elkon R, Wang SY, Chen DJ, Aebersold R, Shiloh Y (2010) ATM-dependent and -independent dynamics of the nuclear phosphoproteome after DNA damage. *Sci Signal* **3:** rs3

Berchtold D, Piccolis M, Chiaruttini N, Riezman I, Riezman H, Roux A, Walther TC, Loewith R (2012) Plasma membrane stress induces relocalization of Slm proteins and activation of TORC2 to promote sphingolipid synthesis. *Nat Cell Biol* **14:** 542-547

Bermejo R, Capra T, Jossen R, Colosio A, Frattini C, Carotenuto W, Cocito A, Doksani Y, Klein H, Gomez-Gonzalez B, Aguilera A, Katou Y, Shirahige K, Foiani M (2011) The replication checkpoint protects fork stability by releasing transcribed genes from nuclear pores. *Cell* **146:** 233-246

Beznoussenko GV, Dolgikh VV, Seliverstova EV, Semenov PB, Tokarev YS, Trucco A, Micaroni M, Di Giandomenico D, Auinger P, Senderskiy IV, Skarlato SO, Snigirevskaya ES, Komissarchik YY, Pavelka M, De Matteis MA, Luini A, Sokolova YY, Mironov AA (2007) Analogs of the Golgi complex in microsporidia: structure and avesicular mechanisms of function. *J Cell Sci* **120:** 1288-1298

Boder E, Sedgwick RP (1958) Ataxia-telangiectasia; a familial syndrome of progressive cerebellar ataxia, oculocutaneous telangiectasia and frequent pulmonary infection. *Pediatrics* **21:** 526-554

Boehrs JK, He J, Halaby MJ, Yang DQ (2007) Constitutive expression and cytoplasmic compartmentalization of ATM protein in differentiated human neuron-like SH-SY5Y cells. *J Neurochem* **100:** 337-345

Boohaker RJ, Cui X, Stackhouse M, Xu B (2013) ATM-mediated Snail Serine 100 phosphorylation regulates cellular radiosensitivity. *Radiother Oncol* **108:** 403-408

Borghesani PR, Alt FW, Bottaro A, Davidson L, Aksoy S, Rathbun GA, Roberts TM, Swat W, Segal RA, Gu Y (2000) Abnormal development of Purkinje cells and lymphocytes in Atm mutant mice. *Proc Natl Acad Sci U S A* **97:** 3336-3341

Bosotti R, Isacchi A, Sonnhammer EL (2000) FAT: a novel domain in PIK-related kinases. *Trends Biochem Sci* **25:** 225-227

Brandt A, Krohne G, Grosshans J (2008) The farnesylated nuclear proteins KUGELKERN and LAMIN B promote aging-like phenotypes in Drosophila flies. *Aging Cell* **7:** 541-551

Buehler MJ (2013) Mechanical players-The role of intermediate filaments in cell mechanics and organization. *Biophys J* **105:** 1733-1734

Burgess RC, Misteli T (2015) Not All DDRs Are Created Equal: Non-Canonical DNA Damage Responses. *Cell* **162:** 944-947

Cameron RS, Liu C, Pihkala JP (2013) Myosin 16 levels fluctuate during the cell cycle and are downregulated in response to DNA replication stress. *Cytoskeleton (Hoboken)* **70:** 328-348

Canman CE, Lim DS (1998) The role of ATM in DNA damage responses and cancer. *Oncogene* **17:** 3301-3308

Capell BC, Collins FS (2006) Human laminopathies: nuclei gone genetically awry. *Nat Rev Genet* **7:** 940-952

Carlessi L, De Filippis L, Lecis D, Vescovi A, Delia D (2009) DNA-damage response, survival and differentiation in vitro of a human neural stem cell line in relation to ATM expression. *Cell Death Differ* **16:** 795-806

Carlessi L, Fusar Poli E, De Filippis L, Delia D (2013) ATM-deficient human neural stem cells as an in vitro model system to study neurodegeneration. *DNA Repair (Amst)* **12:** 605-611

Case N, Thomas J, Sen B, Styner M, Xie Z, Galior K, Rubin J (2011) Mechanical regulation of glycogen synthase kinase 3beta (GSK3beta) in mesenchymal stem cells is dependent on Akt protein serine 473 phosphorylation via mTORC2 protein. *J Biol Chem* **286:** 39450-39456

Chen S, Paul P, Price BD (2003) ATM's leucine-rich domain and adjacent sequences are essential for ATM to regulate the DNA damage response. *Oncogene* **22:** 6332-6339

Chen WT, Ebelt ND, Stracker TH, Xhemalce B, Van Den Berg CL, Miller KM (2015) ATM regulation of IL-8 links oxidative stress to cancer cell migration and invasion. *Elife* **4**

Cheng TH, Hsu PK, Li AF, Hung IC, Huang MH, Hsu HS (2009) Correlation of p53, MDM2 and p14(ARF) protein expression in human esophageal squamous cell carcinoma. *J Cancer Res Clin Oncol* **135:** 1577-1582

Chiesa N, Barlow C, Wynshaw-Boris A, Strata P, Tempia F (2000) Atm-deficient mice Purkinje cells show age-dependent defects in calcium spike bursts and calcium currents. *Neuroscience* **96:** 575-583

Cimprich KA, Cortez D (2008) ATR: an essential regulator of genome integrity. *Nat Rev Mol Cell Biol* **9:** 616-627

Cortes-Bratti X, Chaves-Olarte E, Lagergard T, Thelestam M (1999) The cytolethal distending toxin from the chancroid bacterium Haemophilus ducreyi induces cell-cycle arrest in the G2 phase. *J Clin Invest* **103:** 107-115

Cosentino C, Grieco D, Costanzo V (2011) ATM activates the pentose phosphate pathway promoting anti-oxidant defence and DNA repair. *EMBO J* **30:** 546-555

Costanzo V, Paull T, Gottesman M, Gautier J (2004) Mre11 assembles linear DNA fragments into DNA damage signaling complexes. *PLoS Biol* **2:** E110

Coutts AS, Weston L, La Thangue NB (2009) A transcription co-factor integrates cell adhesion and motility with the p53 response. *Proc Natl Acad Sci U S A* **106:** 19872-19877

Coutts AS, Weston L, La Thangue NB (2010) Actin nucleation by a transcription co-factor that links cytoskeletal events with the p53 response. *Cell Cycle* **9:** 1511-1515

Crawford TO, Skolasky RL, Fernandez R, Rosquist KJ, Lederman HM (2006) Survival probability in ataxia telangiectasia. *Arch Dis Child* **91:** 610-611

Cremaschi P, Oliverio M, Leva V, Bione S, Carriero R, Mazzucco G, Palamidessi A, Scita G, Biamonti G, Montecucco A (2015) Chronic Replication Problems Impact Cell Morphology and Adhesion of DNA Ligase I Defective Cells. *PLoS One* **10:** e0130561

Croft DR, Crighton D, Samuel MS, Lourenco FC, Munro J, Wood J, Bensaad K, Vousden KH, Sansom OJ, Ryan KM, Olson MF (2011) p53-mediated transcriptional regulation and activation of the actin cytoskeleton regulatory RhoC to LIMK2 signaling pathway promotes cell survival. *Cell Res* **21:** 666-682

Cross SE, Kreth J, Zhu L, Sullivan R, Shi W, Qi F, Gimzewski JK (2007) Nanomechanical properties of glucans and associated cell-surface adhesion of Streptococcus mutans probed by atomic force microscopy under in situ conditions. *Microbiology* **153:** 3124-3132

Dahl KN, Ribeiro AJ, Lammerding J (2008) Nuclear shape, mechanics, and mechanotransduction. *Circ Res* **102:** 1307-1318

Davidson PM, Denais C, Bakshi MC, Lammerding J (2014) Nuclear deformability constitutes a rate-limiting step during cell migration in 3-D environments. *Cell Mol Bioeng* **7:** 293-306

De Cicco M, Rahim MS, Dames SA (2015) Regulation of the Target of Rapamycin and Other Phosphatidylinositol 3-Kinase-Related Kinases by Membrane Targeting. *Membranes (Basel)* **5:** 553-575

de Jager M, van Noort J, van Gent DC, Dekker C, Kanaar R, Wyman C (2001) Human Rad50/Mre11 is a flexible complex that can tether DNA ends. *Mol Cell* **8:** 1129-1135

Denais CM, Gilbert RM, Isermann P, McGregor AL, te Lindert M, Weigelin B, Davidson PM, Friedl P, Wolf K, Lammerding J (2016) Nuclear envelope rupture and repair during cancer cell migration. *Science* **352:** 353-358

Ditch S, Paull TT (2012) The ATM protein kinase and cellular redox signaling: beyond the DNA damage response. *Trends Biochem Sci* **37:** 15-22

Doil C, Mailand N, Bekker-Jensen S, Menard P, Larsen DH, Pepperkok R, Ellenberg J, Panier S, Durocher D, Bartek J, Lukas J, Lukas C (2009) RNF168 binds and amplifies ubiquitin conjugates on damaged chromosomes to allow accumulation of repair proteins. *Cell* **136:** 435-446

Dubash AD, Guilluy C, Srougi MC, Boulter E, Burridge K, Garcia-Mata R (2011) The small GTPase RhoA localizes to the nucleus and is activated by Net1 and DNA damage signals. *PLoS One* **6:** e17380

Durocher D, Jackson SP (2001) DNA-PK, ATM and ATR as sensors of DNA damage: variations on a theme? *Curr Opin Cell Biol* **13:** 225-231

E AH, Heinz WF, Antonik MD, D'Costa NP, Nageswaran S, Schoenenberger CA, Hoh JH (1998) Relative microelastic mapping of living cells by atomic force microscopy. *Biophys J* **74:** 1564-1578

Eaton JS, Lin ZP, Sartorelli AC, Bonawitz ND, Shadel GS (2007) Ataxia-telangiectasia mutated kinase regulates ribonucleotide reductase and mitochondrial homeostasis. *J Clin Invest* **117:** 2723-2734

Elson A, Wang Y, Daugherty CJ, Morton CC, Zhou F, Campos-Torres J, Leder P (1996) Pleiotropic defects in ataxia-telangiectasia protein-deficient mice. *Proc Natl Acad Sci U S A* **93:** 13084-13089

Eriksson M, Brown WT, Gordon LB, Glynn MW, Singer J, Scott L, Erdos MR, Robbins CM, Moses TY, Berglund P, Dutra A, Pak E, Durkin S, Csoka AB, Boehnke M, Glover TW, Collins FS (2003) Recurrent de novo point mutations in lamin A cause Hutchinson-Gilford progeria syndrome. *Nature* **423:** 293-298

Espinha G, Osaki JH, Costa ET, Forti FL (2016) Inhibition of the RhoA GTPase Activity Increases Sensitivity of Melanoma Cells to UV Radiation Effects. *Oxid Med Cell Longev* **2016:** 2696952

Famulski KS, Al-Hijailan RS, Dobler K, Pienkowska M, Al-Mohanna F, Paterson MC (2003) Aberrant sensing of extracellular Ca2+ by cultured ataxia telangiectasia fibroblasts. *Oncogene* **22:** 471-475

Fernandes N, Sun Y, Chen S, Paul P, Shaw RJ, Cantley LC, Price BD (2005) DNA damage-induced association of ATM with its target proteins requires a protein interaction domain in the N terminus of ATM. *J Biol Chem* **280:** 15158-15164

Ferrera D, Canale C, Marotta R, Mazzaro N, Gritti M, Mazzanti M, Capellari S, Cortelli P, Gasparini L (2014) Lamin B1 overexpression increases nuclear rigidity in autosomal dominant leukodystrophy fibroblasts. *FASEB J* **28:** 3906-3918

Flatt PM, Tang LJ, Scatena CD, Szak ST, Pietenpol JA (2000) p53 regulation of G(2) checkpoint is retinoblastoma protein dependent. *Mol Cell Biol* **20:** 4210-4223

Frappart PO, Tong WM, Demuth I, Radovanovic I, Herceg Z, Aguzzi A, Digweed M, Wang ZQ (2005) An essential function for NBS1 in the prevention of ataxia and cerebellar defects. *Nat Med* **11:** 538-544

Friedl P, Wolf K (2003) Tumour-cell invasion and migration: diversity and escape mechanisms. *Nat Rev Cancer* **3:** 362-374

Frisan T, Cortes-Bratti X, Chaves-Olarte E, Stenerlow B, Thelestam M (2003) The Haemophilus ducreyi cytolethal distending toxin induces DNA double-strand breaks and promotes ATM-dependent activation of RhoA. *Cell Microbiol* **5:** 695-707

Gavara N, Chadwick RS (2016) Relationship between cell stiffness and stress fiber amount, assessed by simultaneous atomic force microscopy and live-cell fluorescence imaging. *Biomech Model Mechanobiol* **15:** 511-523

Gelfanova V, Hansen EJ, Spinola SM (1999) Cytolethal distending toxin of Haemophilus ducreyi induces apoptotic death of Jurkat T cells. *Infect Immun* **67:** 6394-6402

Golden A, Liu J, Cohen-Fix O (2009) Inactivation of the C. elegans lipin homolog leads to ER disorganization and to defects in the breakdown and reassembly of the nuclear envelope. *J Cell Sci* **122:** 1970-1978

Goley ED, Welch MD (2006) The ARP2/3 complex: an actin nucleator comes of age. *Nat Rev Mol Cell Biol* **7:** 713-726

Goodarzi AA, Douglas P, Moorhead GB, Lees-Miller SP (2007) Utilizing protein phosphatase inhibitors to define PP2A as a regulator of ataxia-telangiectasia mutated. *Methods Mol Biol* **365:** 47-59

Gorgoulis VG, Vassiliou LV, Karakaidos P, Zacharatos P, Kotsinas A, Liloglou T, Venere M, Ditullio RA, Jr., Kastrinakis NG, Levy B, Kletsas D, Yoneta A, Herlyn

M, Kittas C, Halazonetis TD (2005) Activation of the DNA damage checkpoint and genomic instability in human precancerous lesions. *Nature* **434:** 907-913

Gotoff SP, Amirmokri E, Liebner EJ (1967) Ataxia telangiectasia. Neoplasia, untoward response to x-irradiation, and tuberous sclerosis. *Am J Dis Child* **114:** 617-625

Grinthal A, Adamovic I, Weiner B, Karplus M, Kleckner N (2010) PR65, the HEAT-repeat scaffold of phosphatase PP2A, is an elastic connector that links force and catalysis. *Proc Natl Acad Sci U S A* **107:** 2467-2472

Guck J, Schinkinger S, Lincoln B, Wottawah F, Ebert S, Romeyke M, Lenz D, Erickson HM, Ananthakrishnan R, Mitchell D, Kas J, Ulvick S, Bilby C (2005) Optical deformability as an inherent cell marker for testing malignant transformation and metastatic competence. *Biophys J* **88:** 3689-3698

Guleria A, Chandna S (2016) ATM kinase: Much more than a DNA damage responsive protein. *DNA Repair (Amst)* **39:** 1-20

Guo M, Ehrlicher AJ, Mahammad S, Fabich H, Jensen MH, Moore JR, Fredberg JJ, Goldman RD, Weitz DA (2013) The role of vimentin intermediate filaments in cortical and cytoplasmic mechanics. *Biophys J* **105:** 1562-1568

Guo Z, Deshpande R, Paull TT (2010) ATM activation in the presence of oxidative stress. *Cell Cycle* **9:** 4805-4811

Haase K, Pelling AE (2015) Investigating cell mechanics with atomic force microscopy. *J R Soc Interface* **12:** 20140970

Halaby MJ, Hibma JC, He J, Yang DQ (2008) ATM protein kinase mediates full activation of Akt and regulates glucose transporter 4 translocation by insulin in muscle cells. *Cell Signal* **20:** 1555-1563

Halazonetis TD, Gorgoulis VG, Bartek J (2008) An oncogene-induced DNA damage model for cancer development. *Science* **319:** 1352-1355

Hall AE, Lu WT, Godfrey JD, Antonov AV, Paicu C, Moxon S, Dalmay T, Wilczynska A, Muller PA, Bushell M (2016) The cytoskeleton adaptor protein ankyrin-1 is upregulated by p53 following DNA damage and alters cell migration. *Cell Death Dis* **7:** e2184

Hammond EM, Kaufmann MR, Giaccia AJ (2007) Oxygen sensing and the DNA-damage response. *Curr Opin Cell Biol* **19:** 680-684

Harada T, Swift J, Irianto J, Shin JW, Spinler KR, Athirasala A, Diegmiller R, Dingal PC, Ivanovska IL, Discher DE (2014) Nuclear lamin stiffness is a barrier to 3D migration, but softness can limit survival. *J Cell Biol* **204:** 669-682

Harper JW, Elledge SJ (2007) The DNA damage response: ten years after. *Mol Cell* **28:** 739-745

Herzog KH, Chong MJ, Kapsetaki M, Morgan JI, McKinnon PJ (1998) Requirement for Atm in ionizing radiation-induced cell death in the developing central nervous system. *Science* **280:** 1089-1091

Heuze ML, Collin O, Terriac E, Lennon-Dumenil AM, Piel M (2011) Cell migration in confinement: a micro-channel-based assay. *Methods Mol Biol* **769:** 415-434

Hirao A, Kong YY, Matsuoka S, Wakeham A, Ruland J, Yoshida H, Liu D, Elledge SJ, Mak TW (2000) DNA damage-induced activation of p53 by the checkpoint kinase Chk2. *Science* **287:** 1824-1827

Hoche F, Seidel K, Theis M, Vlaho S, Schubert R, Zielen S, Kieslich M (2012) Neurodegeneration in ataxia telangiectasia: what is new? What is evident? *Neuropediatrics* **43:** 119-129

Hsu FF, Lin TY, Chen JY, Shieh SY (2010) p53-Mediated transactivation of LIMK2b links actin dynamics to cell cycle checkpoint control. *Oncogene* **29:** 2864-2876

Huen MS, Chen J (2008) The DNA damage response pathways: at the crossroad of protein modifications. *Cell Res* **18:** 8-16

Hunt CR, Pandita RK, Laszlo A, Higashikubo R, Agarwal M, Kitamura T, Gupta A, Rief N, Horikoshi N, Baskaran R, Lee JH, Lobrich M, Paull TT, Roti Roti JL, Pandita TK (2007) Hyperthermia activates a subset of ataxia-telangiectasia mutated effectors independent of DNA strand breaks and heat shock protein 70 status. *Cancer Res* **67:** 3010-3017

Innocente SA, Abrahamson JL, Cogswell JP, Lee JM (1999) p53 regulates a G2 checkpoint through cyclin B1. *Proc Natl Acad Sci U S A* **96:** 2147-2152

Irianto J, Pfeifer C R, Xia Y, Athirasala A, Ivanovska I L, Greenberg R E, Discher D E (2015) Constricted cell migration causes nuclear lamina damage, DNA breaks, and squeeze-out of repair factors. *bioRXiv.*

Jackson SP, Bartek J (2009) The DNA-damage response in human biology and disease. *Nature* **461:** 1071-1078

Jazayeri A, Balestrini A, Garner E, Haber JE, Costanzo V (2008) Mre11-Rad50-Nbs1-dependent processing of DNA breaks generates oligonucleotides that stimulate ATM activity. *EMBO J* **27:** 1953-1962

Jeong I, Patel AY, Zhang Z, Patil PB, Nadella ST, Nair S, Ralston L, Hoormann JK, Fisher JS (2010) Role of ataxia telangiectasia mutated in insulin signalling of muscle-derived cell lines and mouse soleus. *Acta Physiol (Oxf)* **198:** 465-475

Johnson SA, You Z, Hunter T (2007) Monitoring ATM kinase activity in living cells. *DNA Repair (Amst)* **6:** 1277-1284

Kanu N, Behrens A (2007) ATMIN defines an NBS1-independent pathway of ATM signalling. *EMBO J* **26:** 2933-2941

Kardash E, Bandemer J, Raz E (2011) Imaging protein activity in live embryos using fluorescence resonance energy transfer biosensors. *Nat Protoc* **6:** 1835-1846

Kastan MB (2008) DNA damage responses: mechanisms and roles in human disease: 2007 G.H.A. Clowes Memorial Award Lecture. *Mol Cancer Res* **6:** 517-524

Kastan MB, Bartek J (2004) Cell-cycle checkpoints and cancer. *Nature* **432:** 316-323

Ketene AN, Roberts PC, Shea AA, Schmelz EM, Agah M (2012) Actin filaments play a primary role for structural integrity and viscoelastic response in cells. *Integr Biol (Camb)* **4:** 540-549

Khanna KK, Jackson SP (2001) DNA double-strand breaks: signaling, repair and the cancer connection. *Nat Genet* **27:** 247-254

Kidiyoor GR, Kumar A, Foiani M (2016) ATR-mediated regulation of nuclear and cellular plasticity. *DNA Repair (Amst)* **44:** 143-150

Kim TS, Kawaguchi M, Suzuki M, Jung CG, Asai K, Shibamoto Y, Lavin MF, Khanna KK, Miura Y (2010) The ZFHX3 (ATBF1) transcription factor induces PDGFRB, which activates ATM in the cytoplasm to protect cerebellar neurons from oxidative stress. *Dis Model Mech* **3:** 752-762

Kippenberger S, Loitsch S, Guschel M, Muller J, Kaufmann R, Bernd A (2005) Hypotonic stress induces E-cadherin expression in cultured human keratinocytes. *FEBS Lett* **579:** 207-214

Kitagawa R, Bakkenist CJ, McKinnon PJ, Kastan MB (2004) Phosphorylation of SMC1 is a critical downstream event in the ATM-NBS1-BRCA1 pathway. *Genes Dev* **18:** 1423-1438

Kitayama K, Kamo M, Oma Y, Matsuda R, Uchida T, Ikura T, Tashiro S, Ohyama T, Winsor B, Harata M (2009) The human actin-related protein

hArp5: nucleo-cytoplasmic shuttling and involvement in DNA repair. *Exp Cell Res* **315:** 206-217

Kolas NK, Chapman JR, Nakada S, Ylanko J, Chahwan R, Sweeney FD, Panier S, Mendez M, Wildenhain J, Thomson TM, Pelletier L, Jackson SP, Durocher D (2007) Orchestration of the DNA-damage response by the RNF8 ubiquitin ligase. *Science* **318:** 1637-1640

Kotula E, Faigle W, Berthault N, Dingli F, Loew D, Sun JS, Dutreix M, Quanz M (2013) DNA-PK target identification reveals novel links between DNA repair signaling and cytoskeletal regulation. *PLoS One* **8:** e80313

Kozlov S, Gueven N, Keating K, Ramsay J, Lavin MF (2003) ATP activates ataxia-telangiectasia mutated (ATM) in vitro. Importance of autophosphorylation. *J Biol Chem* **278:** 9309-9317

Kozlov SV, Graham ME, Jakob B, Tobias F, Kijas AW, Tanuji M, Chen P, Robinson PJ, Taucher-Scholz G, Suzuki K, So S, Chen D, Lavin MF (2011) Autophosphorylation and ATM activation: additional sites add to the complexity. *J Biol Chem* **286:** 9107-9119

Kozlov SV, Graham ME, Peng C, Chen P, Robinson PJ, Lavin MF (2006) Involvement of novel autophosphorylation sites in ATM activation. *EMBO J* **25:** 3504-3514

Kozlov SV, Waardenberg AJ, Engholm-Keller K, Arthur JW, Graham ME, Lavin M (2016) Reactive Oxygen Species (ROS)-Activated ATM-Dependent Phosphorylation of Cytoplasmic Substrates Identified by Large-Scale Phosphoproteomics Screen. *Mol Cell Proteomics* **15:** 1032-1047

Kuljis RO, Chen G, Lee EY, Aguila MC, Xu Y (1999) ATM immunolocalization in mouse neuronal endosomes: implications for ataxia-telangiectasia. *Brain Res* **842:** 351-358

Kuljis RO, Xu Y, Aguila MC, Baltimore D (1997) Degeneration of neurons, synapses, and neuropil and glial activation in a murine Atm knockout model of ataxia-telangiectasia. *Proc Natl Acad Sci U S A* **94:** 12688-12693

Kulkarni A, McNeill DR, Gleichmann M, Mattson MP, Wilson DM, 3rd (2008) XRCC1 protects against the lethality of induced oxidative DNA damage in nondividing neural cells. *Nucleic Acids Res* **36:** 5111-5121

Kumar A, Mazzanti M, Mistrik M, Kosar M, Beznoussenko GV, Mironov AA, Garre M, Parazzoli D, Shivashankar GV, Scita G, Bartek J, Foiani M (2014) ATR mediates a checkpoint at the nuclear envelope in response to mechanical stress. *Cell* **158:** 633-646

Kweon HS, Beznoussenko GV, Micaroni M, Polishchuk RS, Trucco A, Martella O, Di Giandomenico D, Marra P, Fusella A, Di Pentima A, Berger EG, Geerts WJ, Koster AJ, Burger KN, Luini A, Mironov AA (2004) Golgi enzymes are enriched in perforated zones of golgi cisternae but are depleted in COPI vesicles. *Mol Biol Cell* **15:** 4710-4724

Lange JR, Fabry B (2013) Cell and tissue mechanics in cell migration. *Exp Cell Res* **319:** 2418-2423

Lavin MF (2008) Ataxia-telangiectasia: from a rare disorder to a paradigm for cell signalling and cancer. *Nat Rev Mol Cell Biol* **9:** 759-769

Lavin MF (2013) The appropriateness of the mouse model for ataxia-telangiectasia: neurological defects but no neurodegeneration. *DNA Repair (Amst)* **12:** 612-619

Lee JH, Paull TT (2005) ATM activation by DNA double-strand breaks through the Mre11-Rad50-Nbs1 complex. *Science* **308:** 551-554

Lee JH, Paull TT (2007) Activation and regulation of ATM kinase activity in response to DNA double-strand breaks. *Oncogene* **26:** 7741-7748

Lee YJ, Sheu TJ, Keng PC (2005) Enhancement of radiosensitivity in H1299 cancer cells by actin-associated protein cofilin. *Biochem Biophys Res Commun* **335:** 286-291

Lekka M, Laidler P, Gil D, Lekki J, Stachura Z, Hrynkiewicz AZ (1999) Elasticity of normal and cancerous human bladder cells studied by scanning force microscopy. *Eur Biophys J* **28:** 312-316

Leu JD, Chiu YW, Lo CC, Chiang PH, Chiu SJ, Tsai CH, Hwang JJ, Chen RC, Gorbunova V, Lee YJ (2013) Enhanced cellular radiosensitivity induced by cofilin-1 over-expression is associated with reduced DNA repair capacity. *Int J Radiat Biol* **89:** 433-444

Li J, Chen J, Ricupero CL, Hart RP, Schwartz MS, Kusnecov A, Herrup K (2012) Nuclear accumulation of HDAC4 in ATM deficiency promotes neurodegeneration in ataxia telangiectasia. *Nat Med* **18:** 783-790

Li J, Han YR, Plummer MR, Herrup K (2009) Cytoplasmic ATM in neurons modulates synaptic function. *Curr Biol* **19:** 2091-2096

Li QS, Lee GY, Ong CN, Lim CT (2008) AFM indentation study of breast cancer cells. *Biochem Biophys Res Commun* **374:** 609-613

Liao WC, Haimovitz-Friedman A, Persaud RS, McLoughlin M, Ehleiter D, Zhang N, Gatei M, Lavin M, Kolesnick R, Fuks Z (1999) Ataxia telangiectasia-

mutated gene product inhibits DNA damage-induced apoptosis via ceramide synthase. *J Biol Chem* **274:** 17908-17917

Lilley CE, Schwartz RA, Weitzman MD (2007) Using or abusing: viruses and the cellular DNA damage response. *Trends Microbiol* **15:** 119-126

Lim DS, Kim ST, Xu B, Maser RS, Lin J, Petrini JH, Kastan MB (2000) ATM phosphorylates p95/nbs1 in an S-phase checkpoint pathway. *Nature* **404:** 613-617

Lim DS, Kirsch DG, Canman CE, Ahn JH, Ziv Y, Newman LS, Darnell RB, Shiloh Y, Kastan MB (1998) ATM binds to beta-adaptin in cytoplasmic vesicles. *Proc Natl Acad Sci U S A* **95:** 10146-10151

Lindahl T, Barnes DE (2000) Repair of endogenous DNA damage. *Cold Spring Harb Symp Quant Biol* **65:** 127-133

Liu H, Wen J, Xiao Y, Liu J, Hopyan S, Radisic M, Simmons CA, Sun Y (2014) In situ mechanical characterization of the cell nucleus by atomic force microscopy. *ACS Nano* **8:** 3821-3828

Liu L, Luo Q, Sun J, Song G (2016) Nucleus and nucleus-cytoskeleton connections in 3D cell migration. *Exp Cell Res*

Liu N, Stoica G, Yan M, Scofield VL, Qiang W, Lynn WS, Wong PK (2005) ATM deficiency induces oxidative stress and endoplasmic reticulum stress in astrocytes. *Lab Invest* **85:** 1471-1480

Llorca O, Rivera-Calzada A, Grantham J, Willison KR (2003) Electron microscopy and 3D reconstructions reveal that human ATM kinase uses an arm-like domain to clamp around double-stranded DNA. *Oncogene* **22:** 3867-3874

Longhese MP (2008) DNA damage response at functional and dysfunctional telomeres. *Genes Dev* **22:** 125-140

Lottersberger F, Karssemeijer RA, Dimitrova N, de Lange T (2015) 53BP1 and the LINC Complex Promote Microtubule-Dependent DSB Mobility and DNA Repair. *Cell* **163:** 880-893

Lukas C, Savic V, Bekker-Jensen S, Doil C, Neumann B, Pedersen RS, Grofte M, Chan KL, Hickson ID, Bartek J, Lukas J (2011) 53BP1 nuclear bodies form around DNA lesions generated by mitotic transmission of chromosomes under replication stress. *Nat Cell Biol* **13:** 243-253

Macurek L, Benada J, Mullers E, Halim VA, Krejcikova K, Burdova K, Pechackova S, Hodny Z, Lindqvist A, Medema RH, Bartek J (2013)

Downregulation of Wip1 phosphatase modulates the cellular threshold of DNA damage signaling in mitosis. *Cell Cycle* **12:** 251-262

Mahmoudi M, Mercer J, Bennett M (2006) DNA damage and repair in atherosclerosis. *Cardiovasc Res* **71:** 259-268

Mailand N, Bekker-Jensen S, Faustrup H, Melander F, Bartek J, Lukas C, Lukas J (2007) RNF8 ubiquitylates histones at DNA double-strand breaks and promotes assembly of repair proteins. *Cell* **131:** 887-900

Mailand N, Diffley JF (2005) CDKs promote DNA replication origin licensing in human cells by protecting Cdc6 from APC/C-dependent proteolysis. *Cell* **122:** 915-926

Matei IR, Gladdy RA, Nutter LM, Canty A, Guidos CJ, Danska JS (2007) ATM deficiency disrupts Tcra locus integrity and the maturation of CD4+CD8+ thymocytes. *Blood* **109:** 1887-1896

Matsuoka S, Ballif BA, Smogorzewska A, McDonald ER, 3rd, Hurov KE, Luo J, Bakalarski CE, Zhao Z, Solimini N, Lerenthal Y, Shiloh Y, Gygi SP, Elledge SJ (2007) ATM and ATR substrate analysis reveals extensive protein networks responsive to DNA damage. *Science* **316:** 1160-1166

Matsuoka S, Rotman G, Ogawa A, Shiloh Y, Tamai K, Elledge SJ (2000) Ataxia telangiectasia-mutated phosphorylates Chk2 in vivo and in vitro. *Proc Natl Acad Sci U S A* **97:** 10389-10394

Matynia A, Salus SS, Sazer S (2002) Three proteins required for early steps in the protein secretory pathway also affect nuclear envelope structure and cell cycle progression in fission yeast. *J Cell Sci* **115:** 421-431

Matzuk MM, Lamb DJ (2008) The biology of infertility: research advances and clinical challenges. *Nat Med* **14:** 1197-1213

Melero R, Uchiyama A, Castano R, Kataoka N, Kurosawa H, Ohno S, Yamashita A, Llorca O (2014) Structures of SMG1-UPFs complexes: SMG1 contributes to regulate UPF2-dependent activation of UPF1 in NMD. *Structure* **22:** 1105-1119

Melixetian M, Klein DK, Sorensen CS, Helin K (2009) NEK11 regulates CDC25A degradation and the IR-induced G2/M checkpoint. *Nat Cell Biol* **11:** 1247-1253

Metcalfe S, Weeds A, Okorokov AL, Milner J, Cockman M, Pope B (1999) Wild-type p53 protein shows calcium-dependent binding to F-actin. *Oncogene* **18:** 2351-2355

Moon SH, Nguyen TA, Darlington Y, Lu X, Donehower LA (2010) Dephosphorylation of gamma-H2AX by WIP1: an important homeostatic regulatory event in DNA repair and cell cycle control. *Cell Cycle* **9:** 2092-2096

Morrison AJ, Highland J, Krogan NJ, Arbel-Eden A, Greenblatt JF, Haber JE, Shen X (2004) INO80 and gamma-H2AX interaction links ATP-dependent chromatin remodeling to DNA damage repair. *Cell* **119:** 767-775

Mu JJ, Wang Y, Luo H, Leng M, Zhang J, Yang T, Besusso D, Jung SY, Qin J (2007) A proteomic analysis of ataxia telangiectasia-mutated (ATM)/ATM-Rad3-related (ATR) substrates identifies the ubiquitin-proteasome system as a regulator for DNA damage checkpoints. *J Biol Chem* **282:** 17330-17334

Nayler S, Gatei M, Kozlov S, Gatti R, Mar JC, Wells CA, Lavin M, Wolvetang E (2012) Induced pluripotent stem cells from ataxia-telangiectasia recapitulate the cellular phenotype. *Stem Cells Transl Med* **1:** 523-535

Olofsson B (1999) Rho guanine dissociation inhibitors: pivotal molecules in cellular signalling. *Cell Signal* **11:** 545-554

Osaki JH, Espinha G, Magalhaes YT, Forti FL (2016) Modulation of RhoA GTPase Activity Sensitizes Human Cervix Carcinoma Cells to gamma-Radiation by Attenuating DNA Repair Pathways. *Oxid Med Cell Longev* **2016:** 6012642

Panagiotakopoulou M, Bergert M, Taubenberger A, Guck J, Poulikakos D, Ferrari A (2016) A Nanoprinted Model of Interstitial Cancer Migration Reveals a Link between Cell Deformability and Proliferation. *ACS Nano* **10:** 6437-6448

Paull TT, Gellert M (1998) The 3' to 5' exonuclease activity of Mre 11 facilitates repair of DNA double-strand breaks. *Mol Cell* **1:** 969-979

Pederson T, Aebi U (2002) Actin in the nucleus: what form and what for? *J Struct Biol* **140:** 3-9

Perkins EJ, Nair A, Cowley DO, Van Dyke T, Chang Y, Ramsden DA (2002) Sensing of intermediates in V(D)J recombination by ATM. *Genes Dev* **16:** 159-164

Perry J, Kleckner N (2003) The ATRs, ATMs, and TORs are giant HEAT repeat proteins. *Cell* **112:** 151-155

Petrie RJ, Yamada KM (2016) Multiple mechanisms of 3D migration: the origins of plasticity. *Curr Opin Cell Biol* **42:** 7-12

Plans V, Scheper J, Soler M, Loukili N, Okano Y, Thomson TM (2006) The RING finger protein RNF8 recruits UBC13 for lysine 63-based self polyubiquitylation. *J Cell Biochem* **97:** 572-582

Poruchynsky MS, Komlodi-Pasztor E, Trostel S, Wilkerson J, Regairaz M, Pommier Y, Zhang X, Kumar Maity T, Robey R, Burotto M, Sackett D, Guha U, Fojo AT (2015) Microtubule-targeting agents augment the toxicity of DNA-damaging agents by disrupting intracellular trafficking of DNA repair proteins. *Proc Natl Acad Sci U S A* **112:** 1571-1576

Raab M, Gentili M, de Belly H, Thiam HR, Vargas P, Jimenez AJ, Lautenschlaeger F, Voituriez R, Lennon-Dumenil AM, Manel N, Piel M (2016) ESCRT III repairs nuclear envelope ruptures during cell migration to limit DNA damage and cell death. *Science* **352:** 359-362

Rappsilber J, Mann M, Ishihama Y (2007) Protocol for micro-purification, enrichment, pre-fractionation and storage of peptides for proteomics using StageTips. *Nat Protoc* **2:** 1896-1906

Reaper PM, di Fagagna F, Jackson SP (2004) Activation of the DNA damage response by telomere attrition: a passage to cellular senescence. *Cell Cycle* **3:** 543-546

Rhodes N, D'Souza T, Foster CD, Ziv Y, Kirsch DG, Shiloh Y, Kastan MB, Reinhart PH, Gilmer TM (1998) Defective potassium currents in ataxia telangiectasia fibroblasts. *Genes Dev* **12:** 3686-3692

Richardson C, Horikoshi N, Pandita TK (2004) The role of the DNA double-strand break response network in meiosis. *DNA Repair (Amst)* **3:** 1149-1164

Rogakou EP, Pilch DR, Orr AH, Ivanova VS, Bonner WM (1998) DNA double-stranded breaks induce histone H2AX phosphorylation on serine 139. *J Biol Chem* **273:** 5858-5868

Rotman G, Shiloh Y (1997a) Ataxia-telangiectasia: is ATM a sensor of oxidative damage and stress? *Bioessays* **19:** 911-917

Rotman G, Shiloh Y (1997b) The ATM gene and protein: possible roles in genome surveillance, checkpoint controls and cellular defence against oxidative stress. *Cancer Surv* **29:** 285-304

Rotsch C, Radmacher M (2000) Drug-induced changes of cytoskeletal structure and mechanics in fibroblasts: an atomic force microscopy study. *Biophys J* **78:** 520-535

Rowat AC, Jaalouk DE, Zwerger M, Ung WL, Eydelnant IA, Olins DE, Olins AL, Herrmann H, Weitz DA, Lammerding J (2013) Nuclear envelope composition

determines the ability of neutrophil-type cells to passage through micron-scale constrictions. *J Biol Chem* **288:** 8610-8618

Saito S, Goodarzi AA, Higashimoto Y, Noda Y, Lees-Miller SP, Appella E, Anderson CW (2002) ATM mediates phosphorylation at multiple p53 sites, including Ser(46), in response to ionizing radiation. *J Biol Chem* **277:** 12491-12494

Sakaue-Sawano A, Kurokawa H, Morimura T, Hanyu A, Hama H, Osawa H, Kashiwagi S, Fukami K, Miyata T, Miyoshi H, Imamura T, Ogawa M, Masai H, Miyawaki A (2008) Visualizing spatiotemporal dynamics of multicellular cell-cycle progression. *Cell* **132:** 487-498

Sarkaria JN, Busby EC, Tibbetts RS, Roos P, Taya Y, Karnitz LM, Abraham RT (1999) Inhibition of ATM and ATR kinase activities by the radiosensitizing agent, caffeine. *Cancer Res* **59:** 4375-4382

Savic V, Yin B, Maas NL, Bredemeyer AL, Carpenter AC, Helmink BA, Yang-Iott KS, Sleckman BP, Bassing CH (2009) Formation of dynamic gamma-H2AX domains along broken DNA strands is distinctly regulated by ATM and MDC1 and dependent upon H2AX densities in chromatin. *Mol Cell* **34:** 298-310

Savitsky K, Sfez S, Tagle DA, Ziv Y, Sartiel A, Collins FS, Shiloh Y, Rotman G (1995) The complete sequence of the coding region of the ATM gene reveals similarity to cell cycle regulators in different species. *Hum Mol Genet* **4:** 2025-2032

Schalch DS, McFarlin DE, Barlow MH (1970) An unusual form of diabetes mellitus in ataxia telangiectasia. *N Engl J Med* **282:** 1396-1402

Schiebe M, Ohneseit P, Hoffmann W, Meyermann R, Rodemann HP, Bamberg M (2000) Analysis of mdm2 and p53 gene alterations in glioblastomas and its correlation with clinical factors. *J Neurooncol* **49:** 197-203

Schneider JG, Finck BN, Ren J, Standley KN, Takagi M, Maclean KH, Bernal-Mizrachi C, Muslin AJ, Kastan MB, Semenkovich CF (2006) ATM-dependent suppression of stress signaling reduces vascular disease in metabolic syndrome. *Cell Metab* **4:** 377-389

Schon O, Friedler A, Bycroft M, Freund SM, Fersht AR (2002) Molecular mechanism of the interaction between MDM2 and p53. *J Mol Biol* **323:** 491-501

Schumacher B, Hoeijmakers JH, Garinis GA (2009) Sealing the gap between nuclear DNA damage and longevity. *Mol Cell Endocrinol* **299:** 112-117

Sen B, Xie Z, Case N, Thompson WR, Uzer G, Styner M, Rubin J (2014) mTORC2 regulates mechanically induced cytoskeletal reorganization and

lineage selection in marrow-derived mesenchymal stem cells. *J Bone Miner Res* **29:** 78-89

Shao G, Lilli DR, Patterson-Fortin J, Coleman KA, Morrissey DE, Greenberg RA (2009) The Rap80-BRCC36 de-ubiquitinating enzyme complex antagonizes RNF8-Ubc13-dependent ubiquitination events at DNA double strand breaks. *Proc Natl Acad Sci U S A* **106:** 3166-3171

Sharpless NE, DePinho RA (2007) How stem cells age and why this makes us grow old. *Nat Rev Mol Cell Biol* **8:** 703-713

Shevchenko A, Wilm M, Vorm O, Mann M (1996) Mass spectrometric sequencing of proteins silver-stained polyacrylamide gels. *Anal Chem* **68:** 850-858

Shiloh Y (2003) ATM and related protein kinases: safeguarding genome integrity. *Nat Rev Cancer* **3:** 155-168

Shiloh Y, Lederman HM (2016) Ataxia-telangiectasia (A-T): An emerging dimension of premature ageing. *Ageing Res Rev*

Shimada K, Filipuzzi I, Stahl M, Helliwell SB, Studer C, Hoepfner D, Seeber A, Loewith R, Movva NR, Gasser SM (2013) TORC2 signaling pathway guarantees genome stability in the face of DNA strand breaks. *Mol Cell* **51:** 829-839

Shreeram S, Hee WK, Demidov ON, Kek C, Yamaguchi H, Fornace AJ, Jr., Anderson CW, Appella E, Bulavin DV (2006) Regulation of ATM/p53-dependent suppression of myc-induced lymphomas by Wip1 phosphatase. *J Exp Med* **203:** 2793-2799

Sibanda BL, Chirgadze DY, Blundell TL (2010) Crystal structure of DNA-PKcs reveals a large open-ring cradle comprised of HEAT repeats. *Nature* **463:** 118-121

Siddoway B, Hou H, Yang H, Petralia R, Xia H (2014) Synaptic activity bidirectionally regulates a novel sequence-specific S-Q phosphoproteome in neurons. *J Neurochem* **128:** 841-851

Siniossoglou S, Santos-Rosa H, Rappsilber J, Mann M, Hurt E (1998) A novel complex of membrane proteins required for formation of a spherical nucleus. *EMBO J* **17:** 6449-6464

Smith GC, d'Adda di Fagagna F, Lakin ND, Jackson SP (1999) Cleavage and inactivation of ATM during apoptosis. *Mol Cell Biol* **19:** 6076-6084

Sommer LA, Schaad M, Dames SA (2013) NMR- and circular dichroism-monitored lipid binding studies suggest a general role for the FATC domain

as membrane anchor of phosphatidylinositol 3-kinase-related kinases (PIKK). *J Biol Chem* **288:** 20046-20063

Soza S, Leva V, Vago R, Ferrari G, Mazzini G, Biamonti G, Montecucco A (2009) DNA ligase I deficiency leads to replication-dependent DNA damage and impacts cell morphology without blocking cell cycle progression. *Mol Cell Biol* **29:** 2032-2041

Spring K, Cross S, Li C, Watters D, Ben-Senior L, Waring P, Ahangari F, Lu SL, Chen P, Misko I, Paterson C, Kay G, Smorodinsky NI, Shiloh Y, Lavin MF (2001) Atm knock-in mice harboring an in-frame deletion corresponding to the human ATM 7636del9 common mutation exhibit a variant phenotype. *Cancer Res* **61:** 4561-4568

Stewart GS, Maser RS, Stankovic T, Bressan DA, Kaplan MI, Jaspers NG, Raams A, Byrd PJ, Petrini JH, Taylor AM (1999) The DNA double-strand break repair gene hMRE11 is mutated in individuals with an ataxia-telangiectasia-like disorder. *Cell* **99:** 577-587

Stucki M, Clapperton JA, Mohammad D, Yaffe MB, Smerdon SJ, Jackson SP (2005) MDC1 directly binds phosphorylated histone H2AX to regulate cellular responses to DNA double-strand breaks. *Cell* **123:** 1213-1226

Sun M, Guo X, Qian X, Wang H, Yang C, Brinkman KL, Serrano-Gonzalez M, Jope RS, Zhou B, Engler DA, Zhan M, Wong ST, Fu L, Xu B (2012) Activation of the ATM-Snail pathway promotes breast cancer metastasis. *J Mol Cell Biol* **4:** 304-315

Sun S, Wong S, Mak A, Cho M (2014) Impact of oxidative stress on cellular biomechanics and rho signaling in C2C12 myoblasts. *J Biomech* **47:** 3650-3656

Sur I, Neumann S, Noegel AA (2014) Nesprin-1 role in DNA damage response. *Nucleus* **5:** 173-191

Swift M, Morrell D, Massey RB, Chase CL (1991) Incidence of cancer in 161 families affected by ataxia-telangiectasia. *N Engl J Med* **325:** 1831-1836

Takeuchi H, Ara G, Sausville EA, Teicher B (1998) Jasplakinolide: interaction with radiation and hyperthermia in human prostate carcinoma and Lewis lung carcinoma. *Cancer Chemother Pharmacol* **42:** 491-496

Taniguchi T, Garcia-Higuera I, Andreassen PR, Gregory RC, Grompe M, D'Andrea AD (2002) S-phase-specific interaction of the Fanconi anemia protein, FANCD2, with BRCA1 and RAD51. *Blood* **100:** 2414-2420

Taylor AM, Harnden DG, Arlett CF, Harcourt SA, Lehmann AR, Stevens S, Bridges BA (1975) Ataxia telangiectasia: a human mutation with abnormal radiation sensitivity. *Nature* **258:** 427-429

Thiam HR, Vargas P, Carpi N, Crespo CL, Raab M, Terriac E, King MC, Jacobelli J, Alberts AS, Stradal T, Lennon-Dumenil AM, Piel M (2016) Perinuclear Arp2/3-driven actin polymerization enables nuclear deformation to facilitate cell migration through complex environments. *Nat Commun* **7:** 10997

Thomas DG, Yenepalli A, Denais CM, Rape A, Beach JR, Wang YL, Schiemann WP, Baskaran H, Lammerding J, Egelhoff TT (2015) Non-muscle myosin IIB is critical for nuclear translocation during 3D invasion. *J Cell Biol* **210:** 583-594

Tian B, Yang Q, Mao Z (2009) Phosphorylation of ATM by Cdk5 mediates DNA damage signalling and regulates neuronal death. *Nat Cell Biol* **11:** 211-218

Trache A, Meininger GA (2008) Atomic force microscopy (AFM). *Curr Protoc Microbiol* **Chapter 2:** Unit 2C 2

Tripathi DN, Zhang J, Jing J, Dere R, Walker CL (2016) A new role for ATM in selective autophagy of peroxisomes (pexophagy). *Autophagy* **12:** 711-712

Uziel T, Lerenthal Y, Moyal L, Andegeko Y, Mittelman L, Shiloh Y (2003) Requirement of the MRN complex for ATM activation by DNA damage. *EMBO J* **22:** 5612-5621

Vail G, Cheng A, Han YR, Zhao T, Du S, Loy MM, Herrup K, Plummer MR (2016) ATM protein is located on presynaptic vesicles and its deficit leads to failures in synaptic plasticity. *J Neurophysiol* **116:** 201-209

Valentin-Vega YA, Maclean KH, Tait-Mulder J, Milasta S, Steeves M, Dorsey FC, Cleveland JL, Green DR, Kastan MB (2012) Mitochondrial dysfunction in ataxia-telangiectasia. *Blood* **119:** 1490-1500

Valko M, Rhodes CJ, Moncol J, Izakovic M, Mazur M (2006) Free radicals, metals and antioxidants in oxidative stress-induced cancer. *Chem Biol Interact* **160:** 1-40

van Attikum H, Fritsch O, Hohn B, Gasser SM (2004) Recruitment of the INO80 complex by H2A phosphorylation links ATP-dependent chromatin remodeling with DNA double-strand break repair. *Cell* **119:** 777-788

Varon R, Vissinga C, Platzer M, Cerosaletti KM, Chrzanowska KH, Saar K, Beckmann G, Seemanova E, Cooper PR, Nowak NJ, Stumm M, Weemaes CM, Gatti RA, Wilson RK, Digweed M, Rosenthal A, Sperling K, Concannon P, Reis A (1998) Nibrin, a novel DNA double-strand break repair protein, is mutated in Nijmegen breakage syndrome. *Cell* **93:** 467-476

Velkova A, Carvalho MA, Johnson JO, Tavtigian SV, Monteiro AN (2010) Identification of Filamin A as a BRCA1-interacting protein required for efficient DNA repair. *Cell Cycle* **9:** 1421-1433

Vileno B, Lekka M, Sienkiewicz A, Jeney S, Stoessel G, Lekki J, Forro L, Stachura Z (2007) Stiffness alterations of single cells induced by UV in the presence of nanoTiO2. *Environ Sci Technol* **41:** 5149-5153

Viniegra JG, Martinez N, Modirassari P, Hernandez Losa J, Parada Cobo C, Sanchez-Arevalo Lobo VJ, Aceves Luquero CI, Alvarez-Vallina L, Ramon y Cajal S, Rojas JM, Sanchez-Prieto R (2005) Full activation of PKB/Akt in response to insulin or ionizing radiation is mediated through ATM. *J Biol Chem* **280:** 4029-4036

Wang L, Wang M, Wang S, Qi T, Guo L, Li J, Qi W, Ampah KK, Ba X, Zeng X (2013) Actin polymerization negatively regulates p53 function by impairing its nuclear import in response to DNA damage. *PLoS One* **8:** e60179

Wang N, Stamenovic D (2000) Contribution of intermediate filaments to cell stiffness, stiffening, and growth. *Am J Physiol Cell Physiol* **279:** C188-194

Wang N, Stamenovic D (2002) Mechanics of vimentin intermediate filaments. *J Muscle Res Cell Motil* **23:** 535-540

Ward KA, Li WI, Zimmer S, Davis T (1991) Viscoelastic properties of transformed cells: role in tumor cell progression and metastasis formation. *Biorheology* **28:** 301-313

Watters D, Kedar P, Spring K, Bjorkman J, Chen P, Gatei M, Birrell G, Garrone B, Srinivasa P, Crane DI, Lavin MF (1999) Localization of a portion of extranuclear ATM to peroxisomes. *J Biol Chem* **274:** 34277-34282

Wogan GN, Hecht SS, Felton JS, Conney AH, Loeb LA (2004) Environmental and chemical carcinogenesis. *Semin Cancer Biol* **14:** 473-486

Wozniak MA, Chen CS (2009) Mechanotransduction in development: a growing role for contractility. *Nat Rev Mol Cell Biol* **10:** 34-43

Xu B, Kim S, Kastan MB (2001) Involvement of Brca1 in S-phase and G(2)-phase checkpoints after ionizing irradiation. *Mol Cell Biol* **21:** 3445-3450

Xu Y, Baltimore D (1996) Dual roles of ATM in the cellular response to radiation and in cell growth control. *Genes Dev* **10:** 2401-2410

Yallapu MM, Katti KS, Katti DR, Mishra SR, Khan S, Jaggi M, Chauhan SC (2015) The roles of cellular nanomechanics in cancer. *Med Res Rev* **35:** 198-223

Yamazaki Y, Tsuruga M, Zhou D, Fujita Y, Shang X, Dang Y, Kawasaki K, Oka S (2000) Cytoskeletal disruption accelerates caspase-3 activation and alters the intracellular membrane reorganization in DNA damage-induced apoptosis. *Exp Cell Res* **259:** 64-78

Yan H, Yang K, Xiao H, Zou YJ, Zhang WB, Liu HY (2012) Over-expression of cofilin-1 and phosphoglycerate kinase 1 in astrocytomas involved in pathogenesis of radioresistance. *CNS Neurosci Ther* **18:** 729-736

Yang C, Tang X, Guo X, Niikura Y, Kitagawa K, Cui K, Wong ST, Fu L, Xu B (2011) Aurora-B mediated ATM serine 1403 phosphorylation is required for mitotic ATM activation and the spindle checkpoint. *Mol Cell* **44:** 597-608

Yang C, Wang H, Xu Y, Brinkman KL, Ishiyama H, Wong ST, Xu B (2012) The kinetochore protein Bub1 participates in the DNA damage response. *DNA Repair (Amst)* **11:** 185-191

Yang DQ, Kastan MB (2000) Participation of ATM in insulin signalling through phosphorylation of eIF-4E-binding protein 1. *Nat Cell Biol* **2:** 893-898

Yang H, Rudge DG, Koos JD, Vaidialingam B, Yang HJ, Pavletich NP (2013) mTOR kinase structure, mechanism and regulation. *Nature* **497:** 217-223

Yarden RI, Pardo-Reoyo S, Sgagias M, Cowan KH, Brody LC (2002) BRCA1 regulates the G2/M checkpoint by activating Chk1 kinase upon DNA damage. *Nat Genet* **30:** 285-289

Yin S, Wang P, Yang L, Liu Y, Wang Y, Liu M, Qi Z, Meng J, Shi TY, Yang G, Zang R (2016) Wip1 suppresses ovarian cancer metastasis through the ATM/AKT/Snail mediated signaling. *Oncotarget* **7:** 29359-29370

You Z, Chahwan C, Bailis J, Hunter T, Russell P (2005) ATM activation and its recruitment to damaged DNA require binding to the C terminus of Nbs1. *Mol Cell Biol* **25:** 5363-5379

Young DB, Jonnalagadda J, Gatei M, Jans DA, Meyn S, Khanna KK (2005) Identification of domains of ataxia-telangiectasia mutated required for nuclear localization and chromatin association. *J Biol Chem* **280:** 27587-27594

Yu X, Fu S, Lai M, Baer R, Chen J (2006) BRCA1 ubiquitinates its phosphorylation-dependent binding partner CtIP. *Genes Dev* **20:** 1721-1726

Yuan Y, Shen Z (2001) Interaction with BRCA2 suggests a role for filamin-1 (hsFLNa) in DNA damage response. *J Biol Chem* **276:** 48318-48324

Yue J, Huhn S, Shen Z (2013) Complex roles of filamin-A mediated cytoskeleton network in cancer progression. *Cell Biosci* **3:** 7

Yue J, Wang Q, Lu H, Brenneman M, Fan F, Shen Z (2009) The cytoskeleton protein filamin-A is required for an efficient recombinational DNA double strand break repair. *Cancer Res* **69:** 7978-7985

Zhang J, Tripathi DN, Jing J, Alexander A, Kim J, Powell RT, Dere R, Tait-Mulder J, Lee JH, Paull TT, Pandita RK, Charaka VK, Pandita TK, Kastan MB, Walker CL (2015) ATM functions at the peroxisome to induce pexophagy in response to ROS. *Nat Cell Biol* **17:** 1259-1269

Zhang T, Penicud K, Bruhn C, Loizou JI, Kanu N, Wang ZQ, Behrens A (2012) Competition between NBS1 and ATMIN controls ATM signaling pathway choice. *Cell Rep* **2:** 1498-1504

Zhao H, Piwnica-Worms H (2001) ATR-mediated checkpoint pathways regulate phosphorylation and activation of human Chk1. *Mol Cell Biol* **21:** 4129-4139

Zink D, Fischer AH, Nickerson JA (2004) Nuclear structure in cancer cells. *Nat Rev Cancer* **4:** 677-687

Zinkel SS, Yin XM, Gross A (2013) Rejuvenating Bi(d)ology. *Oncogene* **32:** 3213-3219

Zou L, Elledge SJ (2003) Sensing DNA damage through ATRIP recognition of RPA-ssDNA complexes. *Science* **300:** 1542-1548

Zuchero JB, Coutts AS, Quinlan ME, Thangue NB, Mullins RD (2009) p53-cofactor JMY is a multifunctional actin nucleation factor. *Nat Cell Biol* **11:** 451-459

8. APPENDIX

This section includes one project focused on DSB repair at the immunoglobulin locus. This work was recently published in Nucleic Acid Research and is presented in a paper-like version.

Title of the project:

"A double-strand break can trigger immunoglobulin gene conversion"

8.1 ABSTRACT

The enzyme activation-induced cytidine deaminase (AID) is essential for all three B cell-specific activities of the immunoglobulin (Ig) gene re-modeling system— gene conversion, somatic hypermutation, and class switch recombination.

At the immunoglobulin (Ig) locus, AID introduces uracil bases by cytosine deamination, these uracils are further processed into DNA lesions that are dissected into different DNA recombination pathways. Immunoglobulin gene conversion is the favored pathway in chickens and many other animals and it is possibly activated by the introduction of a single strand break (SSB) or a double strand break (DSB) at the locus.

In order to characterize the potential intermediates for Ig gene conversion, we inserted an I-SceI recognition site into the complementarity determining region 1 (CDR1) of the Ig light chain locus of the AID knockout DT40 cell line, and conditionally expressed the I-SceI endonuclease. We found that a DSB in CDR1 is sufficient to trigger Ig gene conversion in the absence of AID. DSB induced gene conversion shows similar features with the one mediated by AID, suggesting that a DSB in the CDR1 can be an intermediate for gene conversion. Interestingly the DSB was also repaired by non-homologous end joining events (NHEJ) in the absence of AID, although NHEJ was a second choice compared to gene conversion.

We propose a model where physiological gene conversion is mediated by a tightly regulated DSB that is locally protected from non-homologous end joining (NHEJ) or other non-homologous DNA recombination machineries.

8.2 INTRODUCTION

The adaptive immune system protects our organism against infectious agents like bacteria, viruses, fungi and parasites. An individual born with a defective adaptive immune response is soon exposed to high risk of death unless he is isolated from pathogens.

B lymphocytes are one of the major player of the adaptive immune response, these cells secrete the antibodies (or immunoglobulins Ig) that bind and inactivate antigens in a very specific way (Parkin & Cohen, 2001).

Immunoglobulins are Y-shaped molecules composed by a tail region, harboring the functional properties of the protein, and two antigen binding sites involved in the antigen recognition. Four polypeptide chains constitute the antibody, one pair of Ig heavy chains and one pair of Ig light chains.

Different genomic loci encode for the heavy and light chains and each locus contains a variable region (V) and a constant region (C).

The V regions of both heavy and light chains are located at the N terminus of the protein and together form the antigen-binding site.

To build an appropriate immune response against the different pathogens has to be recognized by the antigen-binding site of the antibodies that is diversified at the genomic level through multiple mechanisms of recombination.

Several strategies have been employed by the different species of vertebrates to achieve a large antigen receptor repertoire.

Human and mice adopted V(D)J recombination, a mechanism based on the assembly of multiple V D and J segments catalyzed by the recombination-activating genes 1 and 2 (RAG1 and RAG2) enzymes (Matthews & Oettinger, 2009).

Chickens have only one pair of functional V and J segments in both Ig light and heavy chain gene loci (Reynaud et al, 1987a); therefore, the diversity generated by V (D) J recombination is limited. Chickens diversify the single functional V gene by gene conversion (Reynaud et al, 1987a; Reynaud et al, 1989). Gene conversion is based on the presence of a set of 25 pseudo V (ψV) genes in the upstream of the functional V gene in the Ig light chain locus (Reynaud et al, 1987a) and more than 100 ψV genes in the Ig heavy chain locus (Reynaud et al, 1989). The ψV genes share high homology of sequence with the functional V

gene and are used as templates to copy and paste fragments of sequences into the V region.

During gene conversion, genetic information is unidirectionally transferred from the ψV gene to the rearranged V (D) J gene on the same chromosome The length of the copied ψV DNA fragments range from a few bp to more than 200 bp (McCormack & Thompson, 1990). Because gene conversion is a "copy and paste" genetic reaction, the ψV templates are preserved during gene conversion (Reynaud et al, 1987b). ψV genes have been under strong selective pressure over the course of evolution, and are even more conserved than the single functional V gene (McCormack et al, 1993). Since gene conversion is based on homologous recombination, ψV genes that are more homologous to the acceptor V gene sequence are more frequently used, and contribute to the stepwise editing of the acceptor V gene (Arakawa et al, 1996). Although the number of ψV genes is limited, gene conversion is predicted to create more potential diversity of the Ig gene than V (D) J recombination due to the flexibility of ψV gene assembly in the gene conversion system (Arakawa & Buerstedde, 2004).

Although originally discovered in chickens, immunoglobulin gene conversion is common to many other birds and domestic mammals.

Rabbit, cattle, swine and horses use gene conversion (Becker & Knight, 1990; Butler, 1998) and more recently, the guinea pig (Guo et al, 2012), Tasmanian devil (Ujvari & Belov, 2015), and prairie vole (Qin et al, 2015b) have also been added to the list.

The V region of immunoglobulins is also diversified through somatic hypermutation, a mechanism where point mutations are accumulated in the

sequence. It is still unclear how cells regulate the pathway choice between somatic hypermutation and gene conversion, although it has been shown that in chickens immunoglobulin gene conversion is preferred, and somatic hypermutation significantly increases when ψV genes or homologous recombination factors are deleted (Qin et al, 2015a; Sale et al, 2001).

Activation-induced cytidine deaminase (AID) is essential for both gene conversion and somatic hypermutation (Arakawa et al, 2002).

AID catalyzes cytosine deamination (Di Noia & Neuberger, 2002a; Petersen-Mahrt et al, 2002a) introducing uracil bases. It was shown that uracils are removed by the uracil glycosylase UNG-2 (Di Noia & Neuberger, 2002b; Saribasak et al, 2006). UNG converts uracils into abasic sites leading to single strand breaks (SSBs) that are substrates for successive recombination events. Consecutive deaminations on opposite strands of DNA are supposed to cause DSBs. Uracils can be also processed by mismatch repair factors (Xue et al, 2006), or simply replicated, leading to mutations at C/G (somatic hypermutation).

AID-induced SSBs or DSBs are candidates for intermediates of immunoglobulin gene conversion. Whether AID functions mainly to introduce the lesion or plays additional roles in the regulation of gene conversion is still unclear. Similarly, no conclusive reports claimed SSB or DSB as the intermediate of gene conversion.

In attempt to address these questions we directly introduced SSB or DSB at the Ig locus in the absence of AID.

We took advantage of the highly recombinogenic DT40 cell line. DT40 cells are a chicken B cell line intensely used to study DNA repair and recombination mechanisms due to their ability to perform gene conversion and somatic hypermutation during in vitro culture. Moreover DT40 can be genetically

modified by targeted integration to mutate any locus of interest (Buerstedde et al, 1990a; Buerstedde & Takeda, 1991; Kim et al, 1990; Winding & Berchtold, 2001). We artificially introduced an I-SceI recognition site at a fixed position of the Ig light chain gene and conditionally expressed I-SceI in AID knockout DT40 cells. The mega endonuclease I-SceI has been widely used to induce DSBs at genomic regions of interest (Abe & Branzei, 2014; Puchta et al, 1993). A DSB induced by I-SceI can activate switch recombination in mouse B cells (Zarrin et al, 2007) and enhance the gene conversion of variant surface glycoprotein coat genes in Trypanosoma (Boothroyd et al, 2009).

We expressed I-SceI and its nickase mutants K122I and K223I to study the effect of DSB or SSB at the Ig locus. We found that a single DSB is sufficient to trigger immunoglobulin gene conversion in the absence of AID. To our knowledge, there has been no report describing Ig gene conversion events in the absence of AID. We further investigate the features of DSB induced gene conversion and found high similarity with the one mediated by AID.

Finally we addressed the nature of the repair pathways triggered by a DSB targeted to the Ig locus.

8.3 MATERIALS AND METHODS

8.3.1 Cell culture and reverse genetics

DT40 cells were cultured in chicken medium (DMEM/F-12 with 10% fetal bovine serum, 2% chicken serum, 2 mM L-glutamine, 0.1 mM β-mercaptoethanol, and penicillin/streptomycin) at 39.5 ˚C with 5% CO2. Cells were transfected by electroporation using the Gene Pulser II (BIO-RAD) at 25 μF and 700 V, as previously described (Saribasak & Arakawa, 2006). Targeted integration was screened by PCR using PrimeSTAR GXL DNA Polymerase (Takara) with the following cycling parameters: 35 cycles of 98 ˚C for 10 s and 68 ˚C for 4 min. In order to activate the Tet-inducible promoter, cell lines were cultured in presence of 100ng/ml doxycycline (dox) (Sigma) for two weeks.

8.3.2 Vectors

The gene conversion reporter vector was designed as follows: 1) an I-SceI site was integrated into the CDR1; 2) a hydrophobic array of 5 amino acids, LLLAV, was deleted from the leader sequence to functionally disrupt the leader sequence (ΔL); and 3) VJ was fused to GFP, followed by the internal ribosome entry site (IRES), a blasticidin-S resistance (bsr) gene, and a SV40 polyA signal. Dr. Holger Puchta kindly provided a vector containing the I-SceI coding sequence. The K122I and K223I mutant I-SceI was generated by PCR-based site-directed mutagenesis of the I-SceI coding sequence. The I-SceI coding sequence was

cloned into multiple cloning sites of pTRE3G-mCherry (Clontech) to generate pTre3gMcherrySce (Figure 29). The I-SceI mutants with K122I or K223I were also cloned in the same manner. The Tet-On 3G expression vector, pChr2RsvProTetOn3gPuro (Figure 29), was generated by cloning the Tet-On 3G coding sequence, which is driven by a RSV promoter, into a targeted integration vector directed to an intergenic locus on the chicken chromosome 2.

8.3.3 Cell lines

The I-SceI reporter cell lines $IgL^{Sce\ GFP}$ and $AID^{-/-}$ $IgL^{Sce\ GFP}$ were generated by targeted integration of the reporter into $DT40^{Cre1}$ (Arakawa et al, 2001) and $AID^{-/-}$ DT40 (Arakawa et al, 2002) cell lines, respectively. Integration of the I-SceI reporter vector into the rearranged Ig light chain locus was screened using the PS148/VL533 primer pairs and was further verified by PCR amplification of the VJ intervening sequence of the un-rearranged locus using the VL513/VL514 primer pairs as previously described (Arakawa et al, 2008). $AID^{-/-}$ $IgL^{Sce\ GFP}$ was transfected with a Tet-On 3G expression vector, pChr2RsvProTetOn3gPuro, and integration of the vector into the target locus was screened using the CHR0208/ RS16 primer pairs. This cell line, $AID^{-/-}$ $IgL^{Sce\ GFP}$ Tet-On, was further co-transfected by pLoxGpt (Arakawa et al, 2001) with pTre3gMcherrySce to generate the $AID^{-/-}$ $IgL^{Sce\ GFP}$ $Tet\text{-}On^{I\text{-}SceI}$ cell line. Alternatively, the $AID^{-/-}$ $IgL^{Sce\ GFP}$ Tet-On cell line was co-transfected by pLoxPuro (Arakawa et al, 2001) with either pTre3gMcherrySceK122i or pTre3gMcherrySceK223i to generate the $AID^{-/-}$ $IgL^{Sce\ GFP}$ $Tet\text{-}On^{I\text{-}SceI\ K122I}$ or $AID^{-/-}$ $IgL^{Sce\ GFP}$ $Tet\text{-}On^{I\text{-}SceI\ K223I}$ cell lines, respectively.

8.3.4 Sorting, cloning, and sequencing

The analytical FACS was performed using FACS Calibur (BD Biosciences) (Arakawa, 2006), and preparative FACS sorting for the GFP (+) population was performed using FACS Aria (BD Biosciences). The GFP (+) population was sorted from either the $AID^{-/-}$ $IgL^{Sce\ GFP}$ $Tet\text{-}On^{I\text{-}SceI}$ cell line cultured in the presence of 100 ng/ml for two weeks or the $IgL^{Sce\ GFP}$ cell line two weeks after subcloning. The $AID^{-/-}$ $IgL^{Sce\ GFP}$ cell line was used as negative control for sequencing. These cells were further expanded and used for genomic DNA extraction using Easy-DNA kit (Invitrogen). The rearranged Ig light chain reporter gene was amplified via PCR, using the VL242/GF70 primer pair and Q5 high-fidelity DNA polymerase (NEB), with the following cycling parameters: 30 s of initial incubation at 98 ˚C; 35 cycles consisting of 10 s at 98 ˚C and 2 min at 72 ˚C; and a final elongation step of 2 min at 72 ˚C. The PCR product was purified using the QIAquick Gel Extraction Kit (Qiagen), digested with HindIII (NEB) and XbaI (NEB), and cloned into the pUC119 plasmid vector. Approximately 100 plasmid clones were sequenced using the VL154 primer. Although a quarter of sequences from the sorted GFP (+) population did not have sequence changes, they were considered to be derived from a contaminated GFP (-) population and were excluded from further analysis. In order to identify possible gene conversion donors, mutated sequences were aligned with a ψV gene table from a CB inbred strain chicken (Reynaud et al, 1987b), since the ψV genes of the rearranged Ig light chain allele of the DT40 cell line appeared to be nearly identical to those of the CB inbred strain chicken (Arakawa et al, 2002).

The rearranged Ig heavy chain gene was amplified from AID$^{-/-}$ IgL$^{Sce\ GFP}$ Tet-On$^{I\text{-}SceI}$ DT40 cells cultured in the presence or absence of 100 ng/ml dox. The duration of dox induction was two weeks. PCR, cloning, and sequencing were performed as described above, except that the VH48/VH49 primer pair was used for PCR and the UC1 primer was used for sequencing. Twenty-two and 23 plasmid clones were sequenced for the rearranged Ig heavy chain gene before and after dox treatment, respectively.

8.3.5 Oligonucleotides

CHR0208	CCTCACTGAACAGGATGGCCAAGAGATGCT
GF70	TTACGTCGCCGTCCAGCTCGACCAGGATGG
PS148	TGCAGGCACAGGTGGCAGTGGGGGTCTCTG
RS16	TGTAGCTTAAATTTTGCTCGCGCACTACTC
UC1	AGCGGATAACAATTTCACACAGGA
VL154	GTGCGTGCGGGGCCGTCACTGATTGCCGTT
VL242	GGGAAGCTTAAAGGGCATCGAGGTCCCCGGCACA
VL513	CACGGTGACACAAAGCAATGGGGAAATGAT
VL514	GTGACCGGTGCAAGTGATAGAAACTCATTG
VL533	GTACCAGCCATAATTACCCTGTTATCCCTA
VH48	TCTCCGAAAGCTTCGGAGGAGCACCAGTCGGCTCCGCA
VH49	GCCGCGGTCTAGACAATTTTGGGGGGGGTTGAAGACTC

8.3.6 Western blotting

The DT40 cell lines were grown in the presence or absence of 100 ng/ml dox for the described time. Total cell lysates were prepared in radioimmunoprecipitation assay (RIPA) lysis buffer [50 mM TRIS-HCL (pH 8.0), 1 mM $MgCl_2$, 200 mM NaCl, 1 mM $CaCl_2$, 10% Glycerol, 1% NP-40, complete protease inhibitors (1:100; Roche), and phosphatase inhibitor cocktail 2 (1:200; Sigma)]. Cells were harvested and then washed with PBS buffer. The pellet was resuspended in RIPA buffer, incubated on ice for 30 minutes, and centrifuged at maximum speed for 30 minutes. Laemmli buffer (1x) was added to the supernatant and the samples were boiled for 10 minutes at 95˚C. Samples were separated on a 4-20% CRITERION SFX gradient precast gel (BIO-RAD). The membrane was incubated with anti-α-tubulin monoclonal antibody B-5-1-2 (1:10000; SIGMA) and anti-I-SceI polyclonal antibody FL-86 (1:500; Santa Cruz) followed by horseradish peroxidase-conjugated anti-rabbit or anti-mouse IgG secondary antibodies (BIO-RAD). Proteins were visualized using SuperSignal West Dura Extended Duration Substrate (Thermo Scientific).

8.4 RESULTS

8.4.1 GFP reporter to assay DSB-induced Ig reversion

In DT40 cells the hotspot of gene conversion and somatic hypermutation is at the complementarity-determining region 1 (CDR1) (Arakawa et al, 2002; Arakawa et al, 2004b). CDR 1, 2 and 3 are the regions of Ig light and heavy chains that fold to form the antigen binding sites of the antibody.

To investigate whether a DNA break can substitute for the function of AID, we inserted an I-SceI site into the CDR1 of the Ig light chain locus of the DT40^{Cre1} cell line (Arakawa et al, 2001) (Figure 28A). The I-SceI site, harboring a frameshift mutation, was linked to a GFP reporter fused in frame to the V region (Figure 28B) and this construct was named IgV-GFP. Gene conversion events occurring at the CDR1 are supposed to repair the frameshift mutation restoring the expression of GFP cDNA and can be measured by FACS as appearance of a GFP+ population (Figure 28C). This assay is called "Ig reversion".

Our first experimental design failed to detect GFP signals in the presence of AID. Considering the possibility that the leader sequence could have caused extracellular release of the antibody-GFP fusion protein, we disrupted the leader sequence of the GFP reporter gene (ΔL in Figure 28A). This modification was successful as we could detect 0.88% of a GFP(+) population in DT40 cells transfected with the reporter and maintained in culture for two weeks (Figure 28D).

This result also indicated that AID was able to efficiently induce Ig reversion regardless the insertion of I-SceI recognition sequence at the CDR1. The same construct transfected in AID knockout DT40 cells did not show any GFP+ signal after two weeks of culture suggesting that the GFP signal was specific for AID induced modifications (Figure 28D).

The generated cell line was named IgL$^{Sce\ GFP}$.

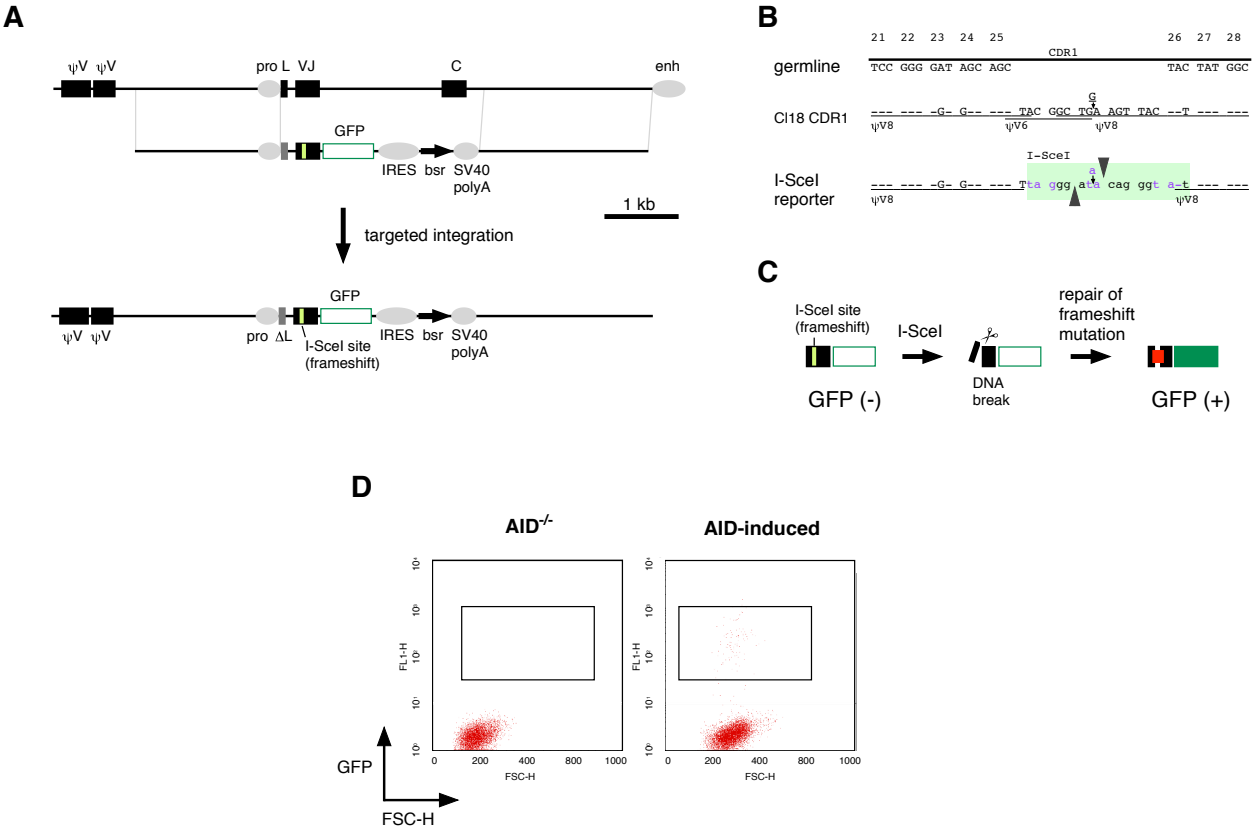


Figure 28. Ig reversion assay to analyze DSB repair in the rearranged immunoglobulin light chain gene.
(A) Targeted integration of the IgV-GFP reporter in the V region of the Ig light chain locus. In this reporter, the leader sequence was functionally disrupted (ΔL), and VJ was fused to GFP to visualize frame-shift reversion. (B) Sequence of the CDR1 region harboring the I-SceI site. The site was inserted to minimize sequence changes from Cl18-type CDR1 (Buerstedde et al, 1990b) and its position was carefully designed considering the three potential stop codons (purple letters). Differences in ψV genes derived sequences are highlighted (C) Ig reversion assay using GFP. (D) FACS profiles of AID$^{-/-}$ IgL$^{Sce\ GFP}$ and IgL$^{Sce\ GFP}$ cell lines. AID-induced Ig reversion was analyzed two weeks after subcloning. Representative FACS profiles are shown with the GFP (+) gatings.

8.4.2 Ig reversion induced by a DSB or SSB

The I-SceI GFP reporter was inserted into the Ig light chain locus of $AID^{-/-}$ DT40 cells by targeted integration (the $AID^{-/-}$ $IgL^{Sce\ GFP}$ cell line). In order to induce DSB at the reporter we took advantage of the tetracycline-controlled transcriptional activation system to conditionally express I-SceI in these cells. Cells were transfected with the third-generation Tet-On expression vector (Figure 29) and with a vector containing the I-SceI endonuclease gene under the third-generation Tet-inducible promoter, pTre3gMcherrySce (Figure 29).

The coding sequence of I-SceI was substituted with the one of I-SceI K223I and K122I, its nickase mutants, to study the effect of SSB at the Ig locus.

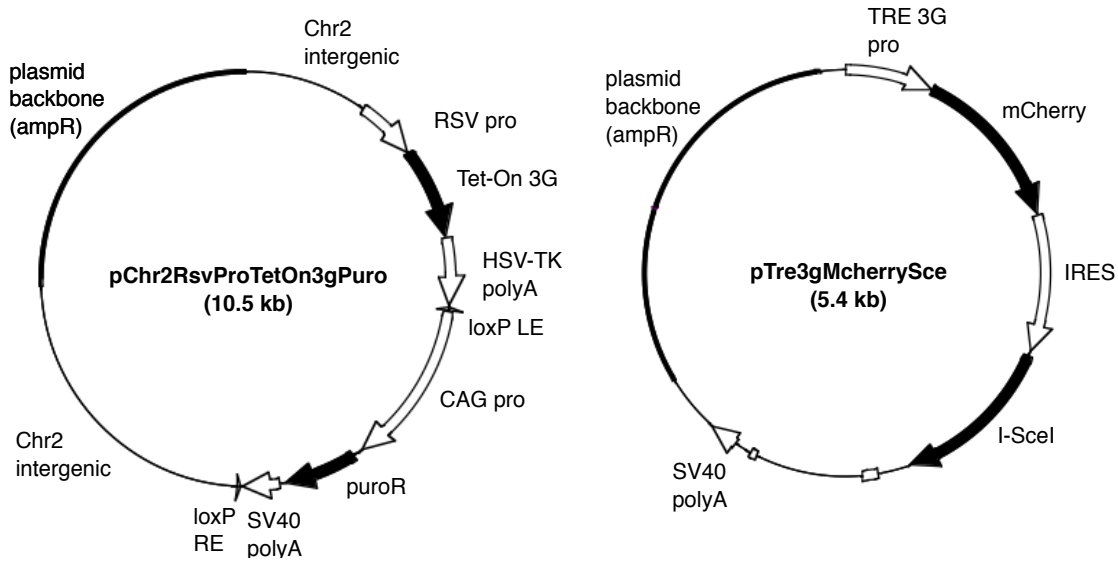


Figure 29. Plasmid maps of the Tet-On 3G expression vector and the Tet-inducible I-SceI expressing vector.
The coding sequence of I-SceI in the pTre3gMcherrySce was replaced with that of I-SceI K122I or K223I for the conditional expression of the nickase mutants.

The pTregMcherrySce vector expresses mCherry and I-SceI in the same cistron, thus we could monitor the I-SceI induction by FACS according to the intensity of the mCherry signal upon dox administration. We successfully established a cell line, $AID^{-/-}$ $IgL^{Sce\ GFP}$ $Tet\text{-}On^{I\text{-}SceI}$, that strongly expressed I-SceI in a dox-dependent manner. In this cell line we performed the Ig reversion assay as previously described for $IgL^{Sce\ GFP}$ cell line. We found that dox induction could generate a GFP(+) population also in this cell line (Figure 30A). This GFP(+) population appeared two days after dox induction and increased to 0.94% after 14 days, which was comparable to the one induced by AID (Figure 30A, B,C).

When we performed the same experiment in cell lines expressing I-SceI K122I or K223I we failed to detect a GFP(+) population after 14 days of dox treatment (Figure 30A, B). These mutants can cleave the opposite sides of the I-SceI site and thus introduce a SSB (Niu et al, 2008). The difference observed between WT I-SceI and the nickase mutants could be due to different level of induction of the proteins upon dox treatment. To exclude this possibility we performed a western blot against I-SceI and found that I-SceI K122I and K223I proteins levels were similar to wt I-SceI (Figure 30D).

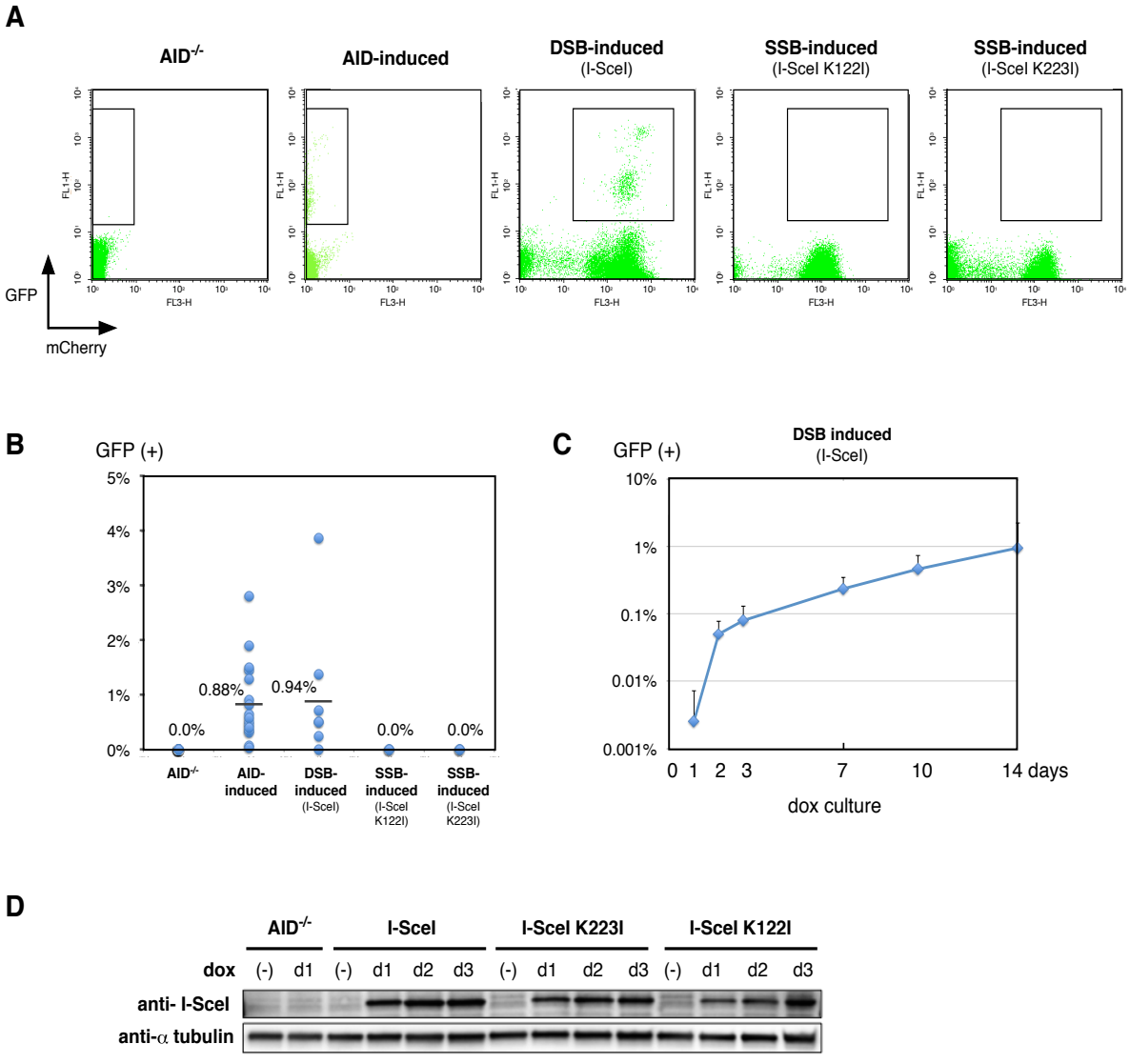


Figure 30. Analysis of Ig reversion induced by AID, DSB and SSB.
(A) FACS profiles of AID$^{-/-}$ IgL$^{Sce\ GFP}$, IgL$^{Sce\ GFP}$, AID$^{-/-}$ IgL$^{Sce\ GFP}$ Tet-On$^{I\text{-}SceI}$, AID$^{-/-}$ IgL$^{Sce\ GFP}$ Tet-On$^{I\text{-}SceI\ K122I}$, and AID$^{-/-}$ IgL$^{Sce\ GFP}$ Tet-On$^{I\text{-}SceI\ K223I}$ cell lines. Representative FACS profiles are shown with the GFP (+) gatings, which were also used for FACS sorting. The expression levels of I-SceI or its nickase mutants were monitored using the intensity of the mCherry signal on the same cistron. (B) Fluctuation analysis of Ig reversion caused by AID, DSB and SSB. AID knockout is shown as negative control. The graph represents the average percentages of GFP(+) cells observed after 14 days of dox culture in different experimental replicates. (C) Time course of Ig reversion of the AID$^{-/-}$ IgL$^{Sce\ GFP}$ Tet-On$^{I\text{-}SceI}$ cell line. Eight experimental replicates of the cell line were independently cultured for two weeks in the presence of dox. (D) Western blot showing the protein levels of I-SceI and I-SceI mutants in the different cell lines upon treatment with dox for the indicated times. Tubulin is shown as loading control.

These results suggest that a DSB at the Ig locus, and not SSB, activates recombination events that contribute to revert the frame-shift mutation as similarly observed for AID. To investigate the nature of the recombination events, the GFP(+) population was isolated by FACS sorting in $IgL^{Sce\ GFP}$ and $AID^{-/-}$ $IgL^{Sce\ GFP}$ Tet-$On^{I\text{-}SceI}$. From this GFP (+) population, the VJ-GFP reporter was amplified by PCR, cloned into a plasmid vector, and sequenced.

8.4.3 Gene conversion induced by AID

We analyzed the sequence of the VJ-GFP reporter of the $IgL^{Sce\ GFP}$ cell line expressing AID. We found that the majority of those sequences had additional sequence changes including some resembling ψV genes (Figure 31A and B), which is a typical feature of Ig gene conversion. Thus, although the 18-bp sequence of the I-SceI site is not homologous to ψV genes, it was efficiently diversified through gene conversion.

We analyzed total 89 sequences of the VJ-GFP amplified from the $IgL^{Sce\ GFP}$ cell line. 86 sequences showed gene conversion events (Figure 31A). A total of 105 gene conversion tracts from 17 of different ψV genes of various lengths were observed (Figure 31A and C). The pattern of ψV usage and tract length resembled the typical gene conversion mediated by AID. The ψV8 gene was most frequently used as a gene conversion donor, probably due to its homology with the ψV8 gene conversion tracts on the reporter (Figure 31B and C).

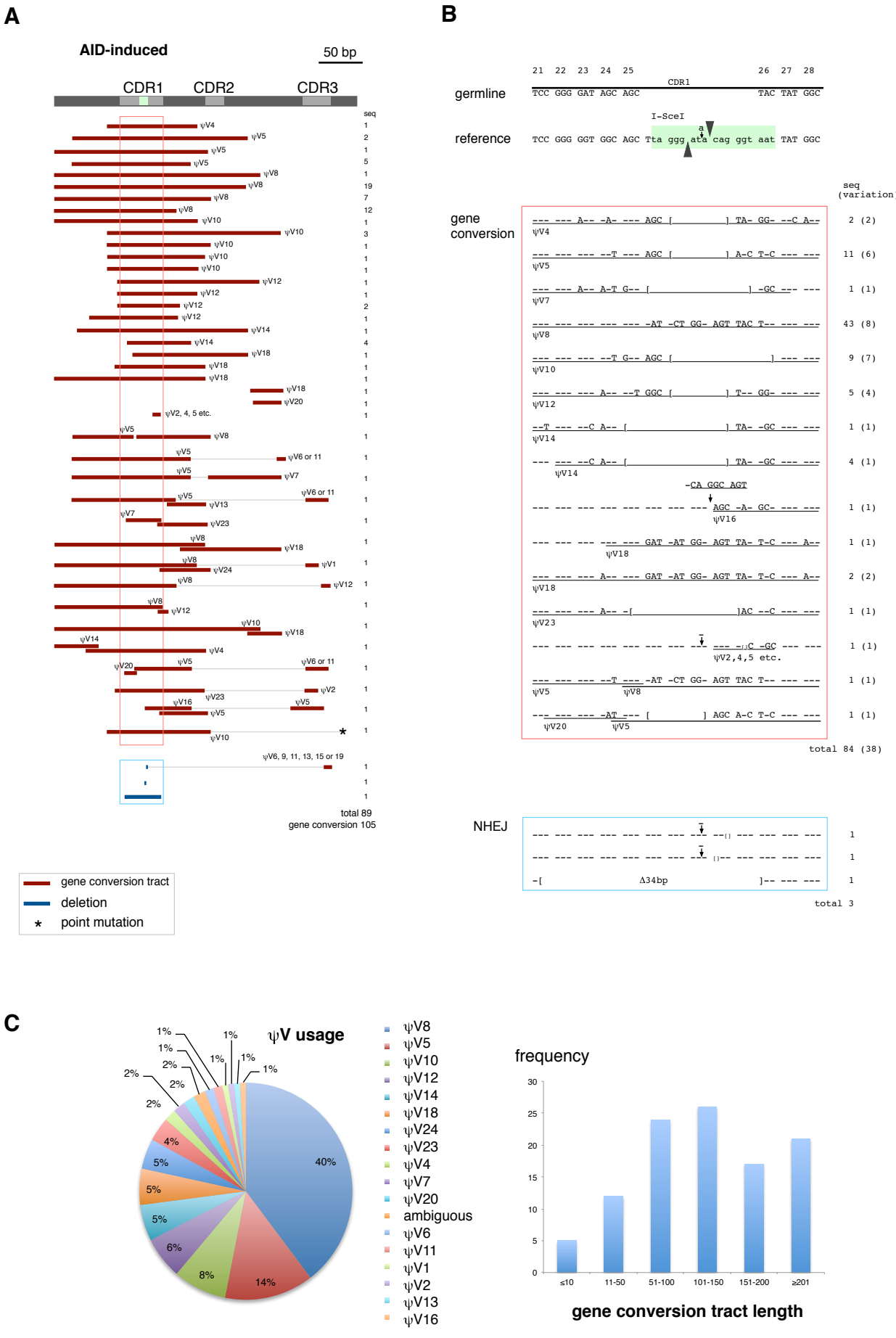

A
AID-induced
50 bp
CDR1
CDR2
CDR3
seq
total 89
gene conversion 105
gene conversion tract
deletion
point mutation
B
germline
reference
I-SceI
CDR1
TCC GGG GAT AGC AGC
TAC TAT GGC
TCC GGG GGT GGC AGC Tta ggg ata cag ggt aat TAT GGC
gene conversion
seq (variation)
total 84 (38)
NHEJ
Δ34bp
total 3
C
ψV usage
ψV8
ψV5
ψV10
ψV12
ψV14
ψV18
ψV24
ψV23
ψV4
ψV7
ψV20
ambiguous
ψV6
ψV11
ψV1
ψV2
ψV13
ψV16
40%
14%
8%
6%
5%
5%
5%
4%
2%
2%
2%
1%
1%
1%
1%
1%
frequency
gene conversion tract length
≤10
11-50
51-100
101-150
151-200
≥201

Figure 31. AID-induced gene conversion at the VJ-GFP reporter.
(A) An overview of the AID-induced DNA sequences modifications analyzed in sorted GFP(+) IgL^{SceGFP} cells. The different types of sequence changes are summarized in the map. (B) Detailed analysis of gene conversion and NHEJ. Brackets indicate region of deletions, dashes represent nucleotides identical to the mother cell line. Gene conversion tracts are marked with lines and the name of the ψV donor is indicated. (C) Pie chart showing the ψV donor usage. The bar plot shows the distribution of gene conversion tract length.

Several ψV genes were used as template and sometimes the same ψV provided different DNA sequence tracts as substrate of gene conversion. For example, gene conversion tracts by ψV8 spanned from 118 bp to 212 bp. While 72 sequences had single gene conversion events, 14 sequences had two or more gene conversion events. As previously reported (Arakawa et al, 2002), CDR1 was the hotspot of gene conversion, as most of the gene conversion events overlapped with CDR1 (Figure 4B), and gene conversion tracts targeting CDR1 were relatively longer than gene conversion events changing CDR2 or 3 sequences (Figure 31A).

Together with gene conversion we detected a minor fraction of NHEJ events.

Three sequences out of 89 carried deletions on the I-SceI site that we interpreted as NHEJ (Figure 31A, B). The frequency of the NHEJ-mediated deletions appeared higher than previously described results (Arakawa et al, 2002), possibly because of the selection for cells that had reverted the in-frame mutation. One event of non-templated C to T point mutations was also observed, which is a common mutation signature of AID (Arakawa et al, 2004a).

As a control we sequenced the VJ-GFP reporter derived from AID knockout DT40 cells and, as expected, the sequence remained unchanged (Arakawa et al, 2002) (Figure 32A, B).



Figure 32. Sequence analysis of VJ-GFP reporter in AID knockout cells.

Overall NHEJ mediated deletions and somatic hypermutation were rare occurrences when compared to gene conversion events and most of the frameshift repair event derived from gene conversion (Figure 33).

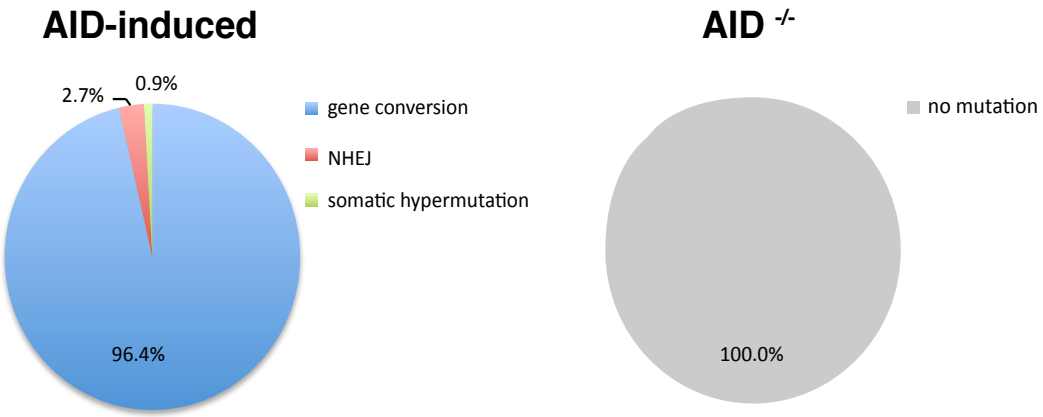


Figure 33. Summary of AID-induced DNA repair pathways.

8.4.4 Gene conversion induced by a DSB

To analyze the nature of the recombination events happening in $AID^{-/-}$ $IgL^{Sce\ GFP}$ Tet-$On^{I\text{-}SceI}$ DT40 cells upon induction of I-SceI we sorted the GFP(+) population arose after 14 days of culture in the presence of dox.

The VJ-GFP sequence was amplified from the sorted population and sequenced as previously done for AID induced gene conversion analysis.

A total of 80 VJ-GFP sequences were analyzed. We found that reversion of the frameshift mutation at the I-SceI site occurred either through deletions or insertions (Figure 34A). While some of the sequences were only repaired by deletion, other sequences had additional sequence changes that were identical to the ψV genes (Figure 34A and B), suggesting the occurrence of gene conversion events.

The DSB-induced gene conversion pattern appeared simpler than that of AID, since most were single gene conversion events per sequence (Figure 34A), and long gene conversion tracts were relatively less frequent (Figure 34C). Single-gene conversion events were observed in 50 sequences, which had 18 variations in gene conversion tracts (Figure 34B).

Differently from AID induced gene conversion, in this case, the ψV12 gene was most frequently used as a gene conversion donor, and ψV8 was the second-most preferential pseudogene donor (Figure 34C). CDR1 was targeted by a variety of ψV donors, such as ψV4, 5, 8, 10, 12, 14, and 18; similarly as for AID induced gene conversion (Figure 31C, 34C). The length of gene conversion tracts spanned up to 212 bp, and they were sometimes extended to around 100 bp upstream and 200 bp downstream of the I-SceI site. Among the ψV donors used, ψV20 was the

most distal pseudogene donor from the functional V gene (Reynaud et al, 1987b). Since ψV20 is located approximately 20 kb upstream of the I-SceI site (Reynaud et al, 1987b), the DNA end of the I-SceI-induced DSB was supposed to interact at a distance of at least 20 kb. Similarly to AID-induced gene conversion, even the same ψV gene produced a variety of gene conversion tracts. Thus, a DSB in the Ig V gene of DT40 cells is sufficient to trigger a diversified set of gene conversion events, comparable in frequency and nature to those induced by AID. The analysis revealed one single event of somatic hypermutation, an A to T mutation, which is rarely observed in the mutational pattern initiated by AID (Arakawa et al, 2004a) (Figure 34A).

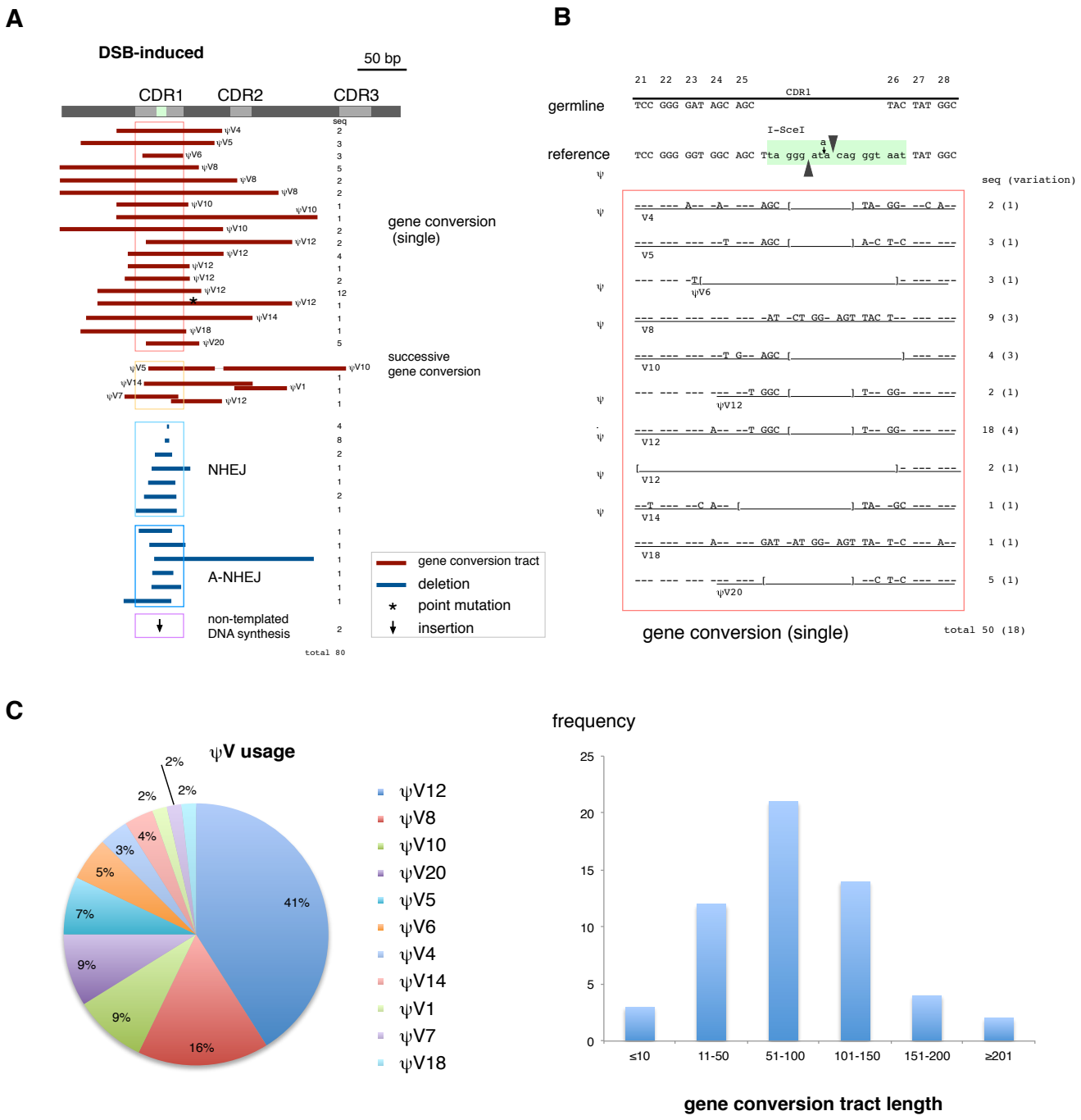


Figure 34. DSB-induced gene conversion.
(A) An overview of the DSB-induced DNA sequences modifications analyzed in sorted AID$^{-/-}$ IgL$^{Sce\ GFP}$ Tet-On$^{I\text{-}SceI}$ DT40 cells. The different types of sequence changes are summarized in the map. (B) Detailed analysis of DSB-induced gene conversion events. (C) ψV donor usage and gene conversion tract length induced by DSB.

To exclude potential off target effects of I-SceI, we sequenced the V region of the rearranged Ig heavy chain gene in the same cell lines treated with dox for two weeks. This sequence contains CDR1 but lacks the I-SceI site. We did not observe any alteration in this sequence despite the induction of I-SceI for two weeks, suggesting that off-target mutation by I-SceI is limited (Figure 35).

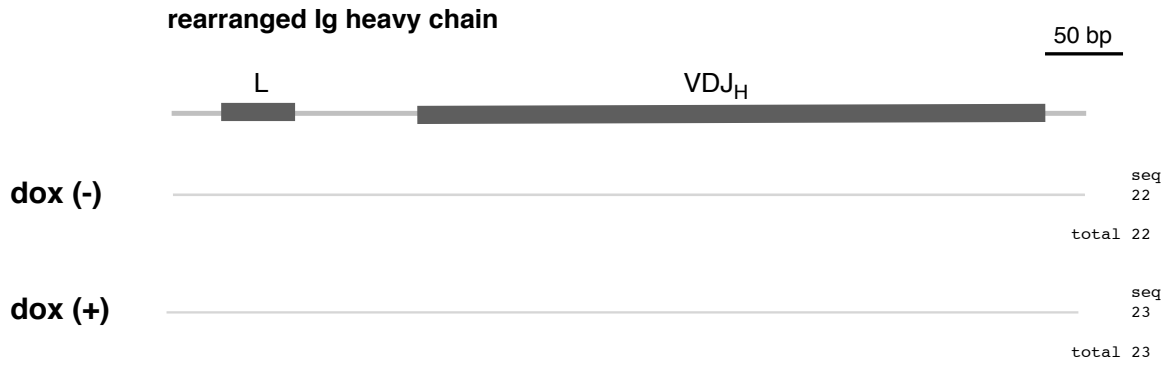


Figure 35. Sequence analysis of the rearranged Ig heavy chain locus.
I-SceI induction does not cause any alteration at the Ig heavy chain after two weeks of dox treatment.

The sequence analysis of DSB-induced gene conversion revealed the occurrence of multiple gene conversion events in three sequences (Figure 36), suggesting that gene conversion can be initiated not only by the DSB but also by the DNA repair processes during the first gene conversion. It is the first time that such event is described for immunoglobulin gene conversion, this finding suggest that some of the multiple gene conversion events generally observed in the presence of AID (Figure 31A) might be initiated by single AID-induced lesions.

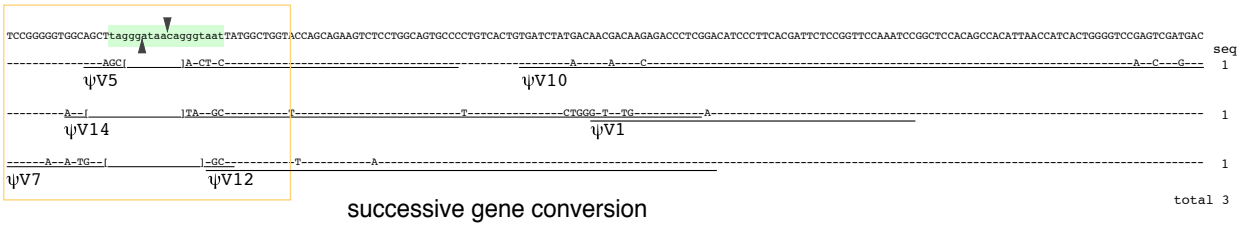


Figure 36. Successive gene conversion events caused by a single DSB.

8.4.5 Non-gene conversion pathways induced by a DSB

Although gene conversion was the favorite pathway identified in the sequence analysis of DSB Ig reversion, we were able to recognize additional repair pathways in higher frequency compared to AID Ig reversion: NHEJ, alternative NHEJ (A-NHEJ), non-templated DNA synthesis.

Sequencing of the VJ-GFP gene in GFP (+) $AID^{-/-}$ $IgL^{Sce\ GFP}$ Tet-$On^{I\text{-}SceI}$ DT40 cells showed deletions from 1 bp to 34 bp around the I-SceI site in 19 sequences (Figure 34A, 37A). These deletions were sometimes extended to 16 bp upstream and 12 bp downstream of the I-SceI site. Since micro-homology was not detected around the breakpoints in those sequences, it is likely that these events are caused by NHEJ, which is the second major pathway for frame-shift reversion induced by a DSB.

6 sequences showed deletions surrounded by micro-homology (Figure 37B). These events can be interpreted as A-NHEJ, which differs from classical NHEJ by its use of micro-homologous sequences to align the broken DNA ends before joining. A-NHEJ is independent of Ku or DNA-PK, and the end-joining is

catalyzed by DNA ligases III and I instead of DNA ligase IV (Paul et al, 2013; Simsek et al, 2011). Deletions by A-NHEJ were relatively larger than those caused by NHEJ and spanned from 10 to 151 bp (Figure 37B).

Finally, we also observed the insertion of a "TATATATT" sequence stretch (Figure 37C) in two sequences. This mutation cannot be explained by gene conversion since such sequence is absent among the pool of ψV genes. We also exclude that the insertion resulted from duplication of the sequence at the breakpoint. Hence, this non-templated DNA synthesis event appears to be caused by an unidentified DNA polymerase.

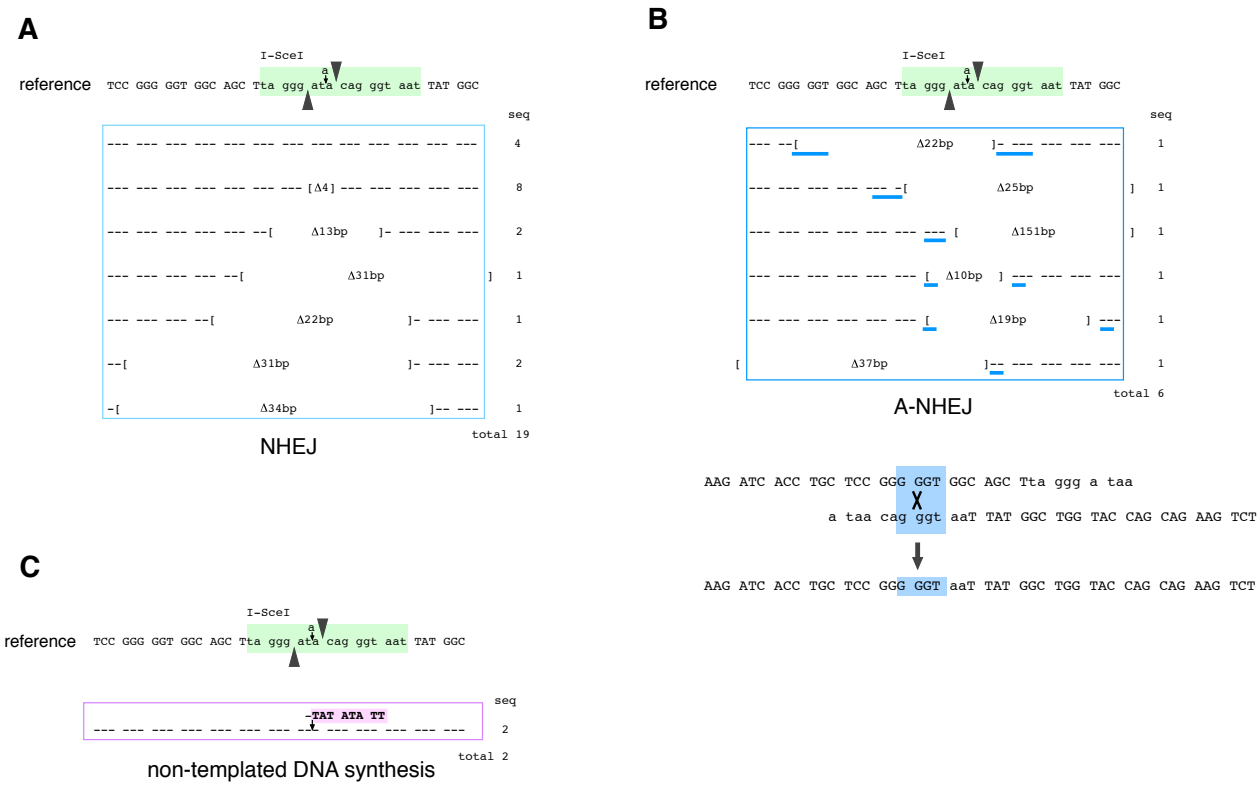


Figure 37. Non-gene conversion pathways induced by a DSB.
(A) NHEJ events. Brackets mark the border of deletions. (B) A-NHEJ. Blue lines highlight regions of micro-homology and one example of A-NHEJ is shown on the bottom panel. (C) Non-templated DNA synthesis.

The figure 38 summarizes the different DNA repair mechanisms triggered by AID or a DSB at the Ig light chain locus. The results show that in the absence of AID, NHEJ occurs at higher frequency at the locus together with other DNA repair pathways, implying that AID-mediated DSBs are tightly regulated to favor gene conversion.

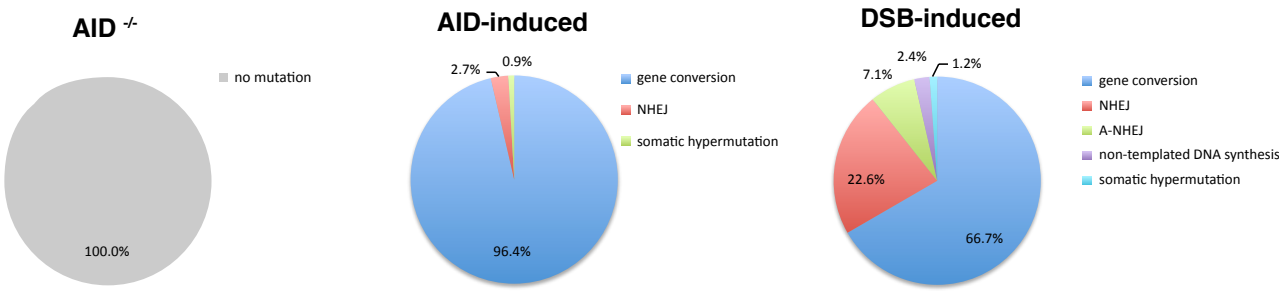


Figure 38. Summary of the DNA repair pathways triggered by AID or a DSB at the Ig light chain locus.

8.5 DISCUSSION

Our results provide evidences that a DSB in CDR1 is sufficient to trigger Ig gene conversion, even in the absence of AID. A single DSB in the same position spurred a variety of gene conversions events, in a similar fashion to those initiated by AID. We propose that a DSB can be an intermediate for physiological gene conversion (Figure 39). DSBs can arise in the Ig locus as a result of consecutive deamination events mediated by AID on opposite DNA strands. AID modifications are mainly processed by gene conversion, suggesting that this process is tightly regulated. AID might control the time and frequency of such

DNA lesions or interact with additional DNA repair factors that favor immunoglobulin gene conversion versus other types of repair.

However, although at very low frequency, we found NHEJ events occurring at the Ig locus in the presence of AID, and this itself suggests the presence of DSBs at the locus.

Our analysis shows that DSB-induced repair offers higher flexibility in pathway choices than AID-induced repair, leading relatively more frequently to NHEJ or A-NHEJ.

Although the I-SceI site does not share significant homology with the ψV genes, this sequence was efficiently diversified by both AID- and DSB-induced gene conversions. This may not be surprising considering that CDRs are often diversified by the poorly homologous gene conversion tracts of different ψV genes (Arakawa et al, 2002; Reynaud et al, 1987b). The preference of ψV8 as a donor, observed in AID induced gene conversion, suggests that this mechanism is influenced by homologous sequences flanking a non-homologous sequence. Indeed the CDR1 sequence flanking the I-SceI site in the mother cell line harbors gene conversion tracts from ψV8.

Most likely, ψV donors align not only in the short regions in CDRs, but also in rather wide regions, including conserved framework regions, based on homology. While long stretches of homologous sequences support alignment between the ψV genes and the functional V gene during gene conversion, the non-homologous regions flanked by long homologies appear to be targeted by gene conversion, contributing to the generation of diversity.

In the case of DSB induced gene conversion, ψV12 was the most frequently used donor, and ψV8 was the second. The preference for ψV donors may have been affected by local deletion of the sequence around the I-SceI site in these cells. Another possibility is that additional factors, usually recruited by AID, could be involved in the choice of the ψV donor, and their absence might affect the ψV usage. For example, ψV12 might be the most accessible donor in the three-dimensional conformation of the local chromatin, thus its choice might be favored to accelerate the repair when DSB is continuously induced by I-SceI.

During the sequence analysis of DSB-induced gene conversion we observed the occurrence of successive gene conversion events.

Interestingly, a single DSB was able to cause even two rounds of gene conversion (Figure 34A, 36). Thus, the double-stranded DNA end can continuously access different loci of the chromosome by using micro-homology during gene conversion, which can be explained by the following model (Figure 39): once the local homology search has been initiated by the DNA end induced by a DSB, this DNA end will copy one of the ψV gene sequences. Usually this DNA end turns back to the rearranged V (D) J locus to complete DNA synthesis, fixing a gene conversion tract (single gene conversion in Figure 34A); however, before completing DNA synthesis at the rearranged V (D) J locus, such a DNA end can be further aligned with another ψV gene to copy the second gene conversion tract. After that the DNA end turns back to the rearranged V (D) J locus and the copied sequences are fixed as multiple gene conversion tracts (successive gene conversion in Figure 34A and model in figure 39).

If multiple rounds of gene conversion can be initiated with a single DSB, such events may also occur under physiological gene conversion by AID.

This has not been documented before since it is usually impossible to distinguish whether multiple gene conversion events are initiated by a single DNA lesion in the case of AID-induced gene conversion.

AID preferentially deaminates cytosines in WRCY motifs (W=adenine or thymine, R=purine, C=cytosine, Y=pyrimidine) that are very common throughout the genome, thus it is impossible to restrict AID activity to a specific site and even to predict the timing and location of the mutated sites.

Hence, successive Ig gene conversion initiated by a DSB was revealed for the first time by this study. During the successive gene conversion, template switching to the second ψV gene may use short regions of homology. This process reminded us of the "copy choice" model for combinatorial assembly of different leucine-rich repeat (LRR) sequences of variable lymphocyte receptor (VLR) genes in the lamprey (Nagawa et al, 2007). In the copy choice model for VLR assembly proposed by Nagawa et al., a replicating DNA end 1) dissociates from the original template, 2) switches templates using short regions of identity, and 3) copies a donor sequence elsewhere in the genome (Nagawa et al, 2007). Thus the copy choice model strongly resembles the successive gene conversion model for multiple conversion tracks (Figure 34A). VLR assembly is initiated by a cytidine deaminase, a possible ancestor homologue of AID, implying a functional and evolutionary relationship between VLR assembly and Ig gene conversion.

In the current study SSBs, induced by K122I and K223I I-SceI mutants, were unable to activate the gene conversion machinery (Figure 30A, B), suggesting that SSBs do not cause gene conversion as easily or frequently as DSBs.

Although this is the first direct study of gene conversion intermediates at the Ig locus, it has been previously suggested that gene conversion could be triggered by SSBs. Nakahara et al. reported that gene conversion in DT40 is enhanced by a single-strand-specific exonuclease, *E. coli* Exo1 (SbcB), but not by a double-strand specific exonuclease, chicken Exo1, suggesting the role of SSBs in gene conversion (Nakahara et al, 2009).

Nevertheless, in the same study the authors provide evidence that also DSBs can be involved in gene conversion, since DT40 mutants deficient in key factors for DSB repair, Nbs1 or RAD54 (Nakahara et al, 2009) showed defective gene conversion.

Similarly Davis and Maizels reported that a SSB induced on the transcribed strand by an I-AniI nickase mutant can lead to homology-directed repair in a GFP reporter (Davis & Maizels, 2014), but such homology-directed repair can be several-fold more efficiently induced by a DSB (Davis & Maizels, 2014).

Moreover another study provided genetic evidence supporting the role of DSB in immunoglobulin gene conversion (Tang & Martin, 2006).

Tang and Marin found that NHEJ deficient DT40 cells had increased levels of immunoglobulin gene conversion. Since NHEJ competes with HR for the repair of DSBs, these data suggested that in the absence of NHEJ, DSB repair at the locus was directed to gene conversion.

Our results show that DSBs can activate gene conversion in the absence of AID (Figure 30A). Although we could not directly assay the presence of SSBs at the locus due to technical reasons, we confirmed by western blot the level of expression of I-SceI and the nickase mutants after dox induction (Figure 30D).

Since the protein levels were very similar, and wt I-SceI was clearly able to generate DSB at the locus, this will be likely true also for K122I and K223I I-SceI.

Anyway we cannot completely rule out that the SSB levels in our reporter system were not sufficient to cause gene conversion, and it is possible that in physiological conditions also SSBs might contribute to immunoglobulin gene conversion.

Our conclusions rather propose that a DSB arising at the Ig locus as a consequence of AID deamination, can be surely used as substrate for gene conversion.

AID appears to be dispensable for gene conversion in the presence of a DSB. Anyway we cannot rule out whether additional factors specifically expressed in DT40 cells are contributing to the process and acting downstream of AID.

Except for AID, all the known components of the Ig gene diversification machinery are enzymes hijacked from ubiquitous DNA repair, recombination, and replication machineries in the course of evolution.

DR-GFP reporter systems are commonly used in a variety of cells types to assay the HR levels by inducing DSBs with I-SceI (Nakanishi et al, 2011), and showed that gene conversion is activated at such reporters in non-B cells in the absence of AID.

Nevertheless, AID-induced lesions rarely cause immunoglobulin gene conversion in human B cells, despite the presence of multiple pseudo-V genes in humans (Darlow & Stott, 2006). One way to address the contribution of other B cell specific factors to gene conversion will be the generation of a chicken non-B cell line carrying the IgV-GFP reporter at the Ig light chain locus to perform DSB-induced Ig reversion.

Indeed, the absence of AID affects the outcome of the DSB repair.

AID-induced lesions predominantly lead to gene conversion in DT40 cells (Figure 33), thus DSBs initiated by AID are destined to a gene conversion pathway in DT40 cells. AID induces a DNA lesion as an early step of B cell-specific recombination by its cytidine deaminase activity (Di Noia & Neuberger, 2002b; Petersen-Mahrt et al, 2002b); however, as the N-terminal of AID is responsible for Ig gene conversion and somatic hypermutation and the C-terminal domain of AID is essential for switch recombination (Barreto et al, 2003; Ta et al, 2003), AID can further influence the dissected B cell-specific recombination pathways, possibly via co-factors that bind the N- or C-terminus of AID. The germinal center-associated nuclear protein (GANP) is one of the candidates, which affects the fate of DSB in Ig V regions in the presence of AID (Eid et al, 2014; Singh et al, 2013). An AID-induced DNA break is supposed to be protected by AID co-factors, which direct the DNA lesion to the gene conversion pathway and prevent undesired DNA repair pathways.

In contrast to AID-induced DNA breaks, I-SceI-induced DSBs were repaired by NHEJ in higher frequency, together with additional repair systems (Figure 38 and model in figure 39). Thus AID and its cofactors might restrict the accessibility of undesired DNA repair proteins, as NHEJ, to the Ig locus.

One intriguing hypothesis is that DNA repair behaves differently at Ig locus compare to the rest of the genome, possibly through specific recruitment of AID and its cofactors.

AID is a mutator enzyme and its deregulation is associated with cancer development and lymphomagenesis (Matsumoto et al, 2007; Okazaki et al, 2003; Ramiro et al, 2007; Ramiro et al, 2004; Robbiani et al, 2009).

AID is specifically expressed in B cells, thus these cells evolved several mechanisms to regulate AID activity (Chaudhuri et al, 2003; Larijani & Martin, 2007; Matsumoto et al, 2007; Okazaki et al, 2003; Patenaude et al, 2009). The B cell genome is rather protected from AID-induced mutagenesis, in fact, the majority of germinal center B cells, which express high levels of AID (Muramatsu et al, 2000), are not transformed to lymphoma.

Recently it was shown that AID is recruited specifically to the Ig locus by interacting with a nearby sequence, named diversification activator (DIVAC) (Blagodatski et al, 2009; Buerstedde et al, 2014). A future perspective of this study will be to address the possible role of DIVAC in the recruitment of B cell specific factors to the Ig locus together with AID to promote gene conversion versus other type of repair.

In order to protect the whole genome, evolution may have invented a system for locally restricting AID-induced DNA repair at B cells Ig loci, while the collapse of such system may represent one of the mechanisms promoting carcinogenesis.

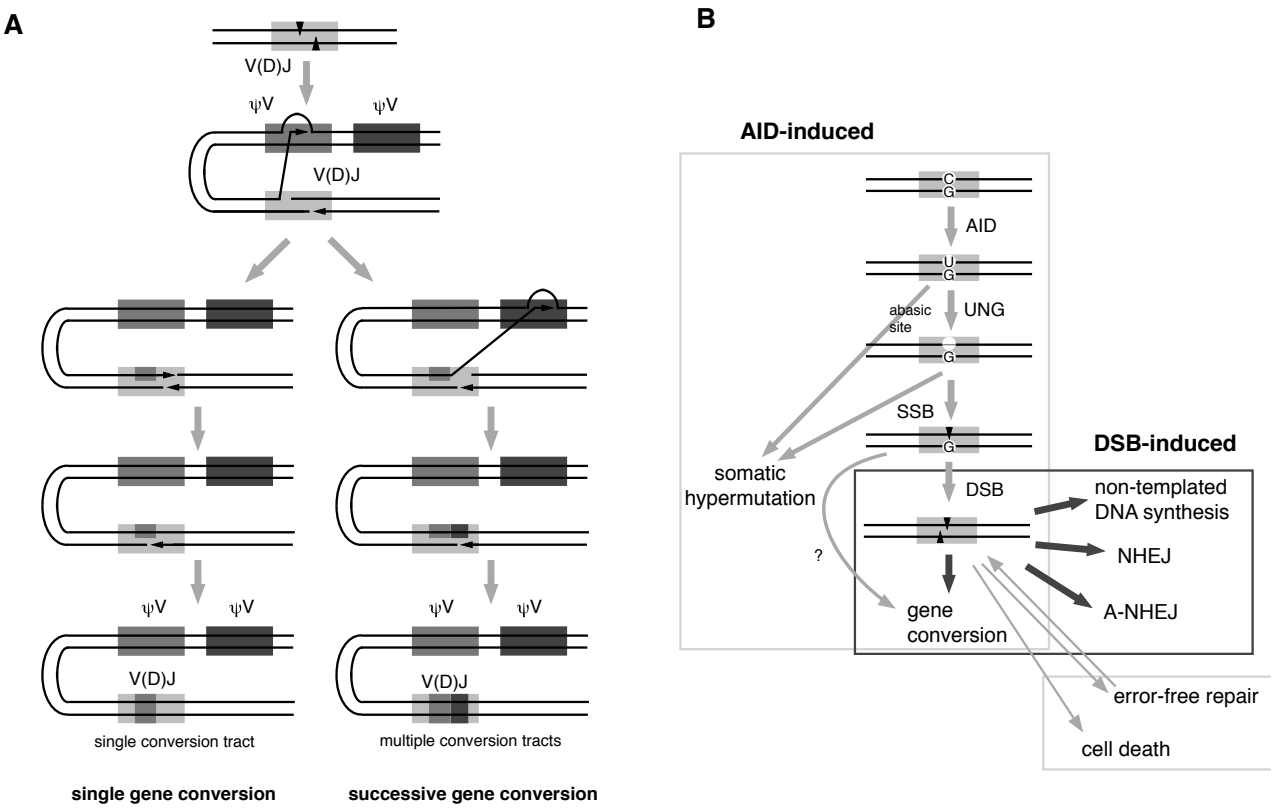


Figure 39. Models for successive immunoglobulin gene conversion and DSB induced gene conversion.
(A) Model for immunoglobulin gene conversion and successive gene conversion. (B) DNA editing model for AID-mediated gene conversion and DSB-induced gene conversion.

8.6 REFERENCES

Abe T, Branzei D (2014) High levels of BRC4 induced by a Tet-On 3G system suppress DNA repair and impair cell proliferation in vertebrate cells. *DNA Repair (Amst)* **22:** 153-164

Arakawa H (2006) Immunoglobulin gene conversion and hypermutation assay by FACS. *Subcell Biochem* **40:** 351-352

Arakawa H, Buerstedde JM (2004) Immunoglobulin gene conversion: insights from bursal B cells and the DT40 cell line. *Dev Dyn* **229:** 458-464

Arakawa H, Furusawa S, Ekino S, Yamagishi H (1996) Immunoglobulin gene hyperconversion ongoing in chicken splenic germinal centers. *EMBO J* **15:** 2540-2546

Arakawa H, Hauschild J, Buerstedde JM (2002) Requirement of the activation-induced deaminase (AID) gene for immunoglobulin gene conversion. *Science* **295:** 1301-1306

Arakawa H, Kudo H, Batrak V, Caldwell RB, Rieger MA, Ellwart JW, Buerstedde JM (2008) Protein evolution by hypermutation and selection in the B cell line DT40. *Nucleic Acids Res* **36:** e1

Arakawa H, Lodygin D, Buerstedde JM (2001) Mutant loxP vectors for selectable marker recycle and conditional knock-outs. *BMC Biotechnol* **1:** 7

Arakawa H, Saribasak H, Buerstedde JM (2004a) Activation-induced cytidine deaminase initiates immunoglobulin gene conversion and hypermutation by a common intermediate. *PLoS Biol* **2:** E179

Arakawa H, Saribasak H, Buerstedde JM (2004b) Activation-induced cytidine deaminase initiates immunoglobulin gene conversion and hypermutation by a common intermediate. *PLoS Biol* **2:** E179

Barreto V, Reina-San-Martin B, Ramiro AR, McBride KM, Nussenzweig MC (2003) C-Terminal Deletion of AID Uncouples Class Switch Recombination from Somatic Hypermutation and Gene Conversion. *Mol Cell* **12:** 501-508

Becker RS, Knight KL (1990) Somatic diversification of immunoglobulin heavy chain VDJ genes: evidence for somatic gene conversion in rabbits. *Cell* **63:** 987-997

Blagodatski A, Batrak V, Schmidl S, Schoetz U, Caldwell RB, Arakawa H, Buerstedde JM (2009) A cis-acting diversification activator both necessary and sufficient for AID-mediated hypermutation. *PLoS Genet* **5:** e1000332

Boothroyd CE, Dreesen O, Leonova T, Ly KI, Figueiredo LM, Cross GA, Papavasiliou FN (2009) A yeast-endonuclease-generated DNA break induces antigenic switching in Trypanosoma brucei. *Nature* **459:** 278-281

Buerstedde JM, Alinikula J, Arakawa H, McDonald JJ, Schatz DG (2014) Targeting of somatic hypermutation by immunoglobulin enhancer and enhancer-like sequences. *PLoS Biol* **12:** e1001831

Buerstedde JM, Reynaud CA, Humphries EH, Olson W, Ewert DL, Weill JC (1990a) Light chain gene conversion continues at high rate in an ALV-induced cell line. *EMBO J* **9:** 921-927

Buerstedde JM, Reynaud CA, Humphries EH, Olson W, Ewert DL, Weill JC (1990b) Light chain gene conversion continues at high rate in an ALV-induced cell line. *EMBO J* **9:** 921-927

Buerstedde JM, Takeda S (1991) Increased ratio of targeted to random integration after transfection of chicken B cell lines. *Cell* **67:** 179-188

Butler JE (1998) Immunoglobulin diversity, B-cell and antibody repertoire development in large farm animals. *Rev Sci Tech* **17:** 43-70

Chaudhuri J, Tian M, Khuong C, Chua K, Pinaud E, Alt FW (2003) Transcription-targeted DNA deamination by the AID antibody diversification enzyme. *Nature* **422:** 726-730

Darlow JM, Stott DI (2006) Gene conversion in human rearranged immunoglobulin genes. *Immunogenetics* **58:** 511-522

Davis L, Maizels N (2014) Homology-directed repair of DNA nicks via pathways distinct from canonical double-strand break repair. *Proc Natl Acad Sci U S A* **111:** E924-932

Di Noia J, Neuberger MS (2002a) Altering the pathway of immunoglobulin hypermutation by inhibiting uracil-DNA glycosylase. *Nature* **419:** 43-48

Di Noia J, Neuberger MS (2002b) Altering the pathway of immunoglobulin hypermutation by inhibiting uracil-DNA glycosylase. *Nature* **419:** 43-48

Eid MM, Maeda K, Almofty SA, Singh SK, Shimoda M, Sakaguchi N (2014) GANP regulates the choice of DNA repair pathway by DNA-PKcs interaction in AID-dependent IgV region diversification. *J Immunol* **192:** 5529-5539

Guo Y, Bao Y, Meng Q, Hu X, Meng Q, Ren L, Li N, Zhao Y (2012) Immunoglobulin genomics in the guinea pig (Cavia porcellus). *PloS one* **7:** e39298

Kim S, Humphries EH, Tjoelker L, Carlson L, Thompson CB (1990) Ongoing diversification of the rearranged immunoglobulin light-chain gene in a bursal lymphoma cell line. *Mol Cell Biol* **10:** 3224-3231

Larijani M, Martin A (2007) Single-stranded DNA structure and positional context of the target cytidine determine the enzymatic efficiency of AID. *Mol Cell Biol* **27:** 8038-8048

Matsumoto Y, Marusawa H, Kinoshita K, Endo Y, Kou T, Morisawa T, Azuma T, Okazaki IM, Honjo T, Chiba T (2007) Helicobacter pylori infection triggers aberrant expression of activation-induced cytidine deaminase in gastric epithelium. *Nat Med* **13:** 470-476

Matthews AG, Oettinger MA (2009) RAG: a recombinase diversified. *Nat Immunol* **10:** 817-821

McCormack WT, Hurley EA, Thompson CB (1993) Germ line maintenance of the pseudogene donor pool for somatic immunoglobulin gene conversion in chickens. *Mol Cell Biol* **13:** 821-830

McCormack WT, Thompson CB (1990) Chicken IgL variable region gene conversions display pseudogene donor preference and 5' to 3' polarity. *Genes Dev* **4:** 548-558

Muramatsu M, Kinoshita K, Fagarasan S, Yamada S, Shinkai Y, Honjo T (2000) Class switch recombination and hypermutation require activation-induced cytidine deaminase (AID), a potential RNA editing enzyme. *Cell* **102:** 553-563

Nagawa F, Kishishita N, Shimizu K, Hirose S, Miyoshi M, Nezu J, Nishimura T, Nishizumi H, Takahashi Y, Hashimoto S, Takeuchi M, Miyajima A, Takemori T, Otsuka AJ, Sakano H (2007) Antigen-receptor genes of the agnathan lamprey are assembled by a process involving copy choice. *Nat Immunol* **8:** 206-213

Nakahara M, Sonoda E, Nojima K, Sale JE, Takenaka K, Kikuchi K, Taniguchi Y, Nakamura K, Sumitomo Y, Bree RT, Lowndes NF, Takeda S (2009) Genetic evidence for single-strand lesions initiating Nbs1-dependent homologous recombination in diversification of Ig v in chicken B lymphocytes. *PLoS Genet* **5:** e1000356

Nakanishi K, Cavallo F, Brunet E, Jasin M (2011) Homologous recombination assay for interstrand cross-link repair. *Methods Mol Biol* **745:** 283-291

Niu Y, Tenney K, Li H, Gimble FS (2008) Engineering variants of the I-SceI homing endonuclease with strand-specific and site-specific DNA-nicking activity. *J Mol Biol* **382:** 188-202

Okazaki IM, Hiai H, Kakazu N, Yamada S, Muramatsu M, Kinoshita K, Honjo T (2003) Constitutive expression of AID leads to tumorigenesis. *J Exp Med* **197:** 1173-1181

Parkin J, Cohen B (2001) An overview of the immune system. *Lancet* **357:** 1777-1789

Patenaude AM, Orthwein A, Hu Y, Campo VA, Kavli B, Buschiazzo A, Di Noia JM (2009) Active nuclear import and cytoplasmic retention of activation-induced deaminase. *Nat Struct Mol Biol* **16:** 517-527

Paul K, Wang M, Mladenov E, Bencsik-Theilen A, Bednar T, Wu W, Arakawa H, Iliakis G (2013) DNA ligases I and III cooperate in alternative non-homologous end-joining in vertebrates. *PLoS One* **8:** e59505

Petersen-Mahrt SK, Harris RS, Neuberger MS (2002a) AID mutates E. coli suggesting a DNA deamination mechanism for antibody diversification. *Nature* **418:** 99-103

Petersen-Mahrt SK, Harris RS, Neuberger MS (2002b) AID mutates E. coli suggesting a DNA deamination mechanism for antibody diversification. *Nature* **418:** 99-103

Puchta H, Dujon B, Hohn B (1993) Homologous recombination in plant cells is enhanced by in vivo induction of double strand breaks into DNA by a site-specific endonuclease. *Nucleic Acids Res* **21:** 5034-5040

Qin T, Zhao H, Zhu H, Wang D, Du W, Hao H (2015a) Immunoglobulin genomics in the prairie vole (Microtus ochrogaster). *Immunol Lett* **166:** 79-86

Qin T, Zhao H, Zhu H, Wang D, Du W, Hao H (2015b) Immunoglobulin genomics in the prairie vole (Microtus ochrogaster). *Immunol Lett* **166:** 79-86

Ramiro A, Reina San-Martin B, McBride K, Jankovic M, Barreto V, Nussenzweig A, Nussenzweig MC (2007) The role of activation-induced deaminase in antibody diversification and chromosome translocations. *Adv Immunol* **94:** 75-107

Ramiro AR, Jankovic M, Eisenreich T, Difilippantonio S, Chen-Kiang S, Muramatsu M, Honjo T, Nussenzweig A, Nussenzweig MC (2004) AID is required for c-myc/IgH chromosome translocations in vivo. *Cell* **118:** 431-438

Reynaud CA, Anquez V, Grimal H, Weill JC (1987a) A hyperconversion mechanism generates the chicken light chain preimmune repertoire. *Cell* **48:** 379-388

Reynaud CA, Anquez V, Grimal H, Weill JC (1987b) A hyperconversion mechanism generates the chicken light chain preimmune repertoire. *Cell* **48:** 379-388

Reynaud CA, Dahan A, Anquez V, Weill JC (1989) Somatic hyperconversion diversifies the single Vh gene of the chicken with a high incidence in the D region. *Cell* **59:** 171-183

Robbiani DF, Bunting S, Feldhahn N, Bothmer A, Camps J, Deroubaix S, McBride KM, Klein IA, Stone G, Eisenreich TR, Ried T, Nussenzweig A, Nussenzweig MC (2009) AID produces DNA double-strand breaks in non-Ig genes and mature B cell lymphomas with reciprocal chromosome translocations. *Mol Cell* **36:** 631-641

Sale JE, Calandrini DM, Takata M, Takeda S, Neuberger MS (2001) Ablation of XRCC2/3 transforms immunoglobulin V gene conversion into somatic hypermutation. *Nature* **412:** 921-926

Saribasak H, Arakawa H (2006) Targeted transfection of DT40 cells. *Subcell Biochem* **40:** 419-421

Saribasak H, Saribasak NN, Ipek FM, Ellwart JW, Arakawa H, Buerstedde JM (2006) Uracil DNA glycosylase disruption blocks Ig gene conversion and induces transition mutations. *J Immunol* **176:** 365-371

Simsek D, Brunet E, Wong SY, Katyal S, Gao Y, McKinnon PJ, Lou J, Zhang L, Li J, Rebar EJ, Gregory PD, Holmes MC, Jasin M (2011) DNA ligase III promotes alternative nonhomologous end-joining during chromosomal translocation formation. *PLoS Genet* **7:** e1002080

Singh SK, Maeda K, Eid MM, Almofty SA, Ono M, Pham P, Goodman MF, Sakaguchi N (2013) GANP regulates recruitment of AID to immunoglobulin variable regions by modulating transcription and nucleosome occupancy. *Nat Commun* **4:** 1830

Ta VT, Nagaoka H, Catalan N, Durandy A, Fischer A, Imai K, Nonoyama S, Tashiro J, Ikegawa M, Ito S, Kinoshita K, Muramatsu M, Honjo T (2003) AID mutant analyses indicate requirement for class-switch-specific cofactors. *Nat Immunol* **4:** 843-848

Tang ES, Martin A (2006) NHEJ-deficient DT40 cells have increased levels of immunoglobulin gene conversion: evidence for a double strand break intermediate. *Nucleic Acids Res* **34:** 6345-6351

Ujvari B, Belov K (2015) Characterization of antibody V segment diversity in the Tasmanian devil (Sarcophilus harrisii). *Vet Immunol Immunopathol* **167:** 156-165

Winding P, Berchtold MW (2001) The chicken B cell line DT40: a novel tool for gene disruption experiments. *J Immunol Methods* **249:** 1-16

Xue K, Rada C, Neuberger MS (2006) The in vivo pattern of AID targeting to immunoglobulin switch regions deduced from mutation spectra in msh2-/- ung-/- mice. *J Exp Med* **203:** 2085-2094

Zarrin AA, Del Vecchio C, Tseng E, Gleason M, Zarin P, Tian M, Alt FW (2007) Antibody class switching mediated by yeast endonuclease-generated DNA breaks. *Science* **315:** 377-381

ACKNOWLEDGEMENTS

This work was made possible thanks to the help of several people during these four years.
Below all the people I would like to thank:

At first my boss Marco Foiani for giving me the chance to join his lab for my PhD. Thank you for the help and the support during these years, providing a wonderful atmosphere for doing research in your lab. Grazie!!

Hiroshi Arakawa, my co-supervisor, who followed me to develop one project of this work and introduced me to the laboratory work in my early education. Thank you for all the important suggestions that you have given me over these years and for showing me the incredible passion that you dedicate to science.

My internal and external supervisors, Stefano Casola and Fumiko Esashi, for the support and the help with useful discussions.

Qingsen Li, who collaborated with me for several experiments of AFM analysis shown in this work.

Matthieu Piel and Matthew Raab for the silicon mold of the micro-channel device.

Vittoria Matafora e Angela Bachi for the mass spectrometry analysis.

Galina Beznusenko and Alexandre Mironov, staff members of the EM facility, for the electron microscopy analysis.

Vincenzo Costanzo and Maria Vinciguerra, who provided the ATM KO Hela cell line.

Tony Hunter for sharing the plasmids of the ATM-reporter FRET sensors.

Domenico Delia and Alessandro Corti who gave me the 9E6 antibody and shared reagents and informations with me.

Daniele Piccini, who helped me in the production of the monoclonal antibody 9E6 for the ATM immunoprecipitation.

Paolo Maiuri, who designed the macro for nuclear shape analysis.

Libor Macůrek for the U2OS-FUCCI cell line.

Martin Kosar for the short-hairpin RNA against ATM.

Giorgio Scita for useful discussions.

A special thank to the Imaging facility people, especially Amanda Oldani, Sara Barozzi and Emanuele Martini for their sincere dedication towards our work.

I am grateful to Sergio Cattadori and the IFOM kitchen staff, and to the whole cell culture facility members for the incredible work that they do on a daily basis to help us.

All the people of the MF group, guys thank you for all the amazing moments in the lab, I am glad to be part of this group! Special thanks to my "lunch companions" Gururaj Kidiyoor, Christopher Bruhn, Ramveer Choudhary.

Ghadeer Shubassi for critical reading of this manuscript (and many others writings!!) and for her generous attitude towards science.

Gururaj Kidiyoor, with whom I share similar scientific interests, thank you for the collaborative atmosphere we created in these years.

All my friends, who supported me "outside the lab" throughout this period especially Chia, Eli, Vale, Marty.

Finally I want to thank my parents and my family. You always believed in me throughout my life, you gave me an excellent education and you put all your effort to support my goals.